LASER–BASED TECHNOLOGIES FOR TARGETED DRUG DELIVERY AND LABEL-FREE DIAGNOSTICS IN HIV-1

by

RUDZANI MALABI

Submitted in accordance with the requirements for
the degree of

DOCTOR OF PHILOSOPHY

in the subject

Physics

At the

UNIVERSITY OF SOUTH AFRICA

SUPERVISOR: DR PATIENCE MTHUNZI-KUFA

CO-SUPERVISOR: PROF MALIK MAAZA

CO-SUPERVISOR: DR SELLO LEBOHANG MANOTO

(November 2019)

Declarations

Name: **RUDZANI MALABI**

Student number: **58521984**

Degree: **DOCTOR OF PHILOSOPHY OF PHYSICS**

LASER-BASED TECHNOLOGIES FOR TARGET DRUG DELIVERY AND LABEL-FREE DIAGNOSTICS IN HIV-1

I declare that the above thesis is my own work and that all the sources that I have used or quoted have been indicated and acknowledged by means of complete references.

I further declare that I submitted the thesis to originality checking software and that it falls within the accepted requirements for originality.

I further declare that I have not previously submitted this work, or part of it, for examination at Unisa for another qualification or at any other higher education institution.

23 June 2020

SIGNATURE DATE

Abstract

Human immunodeficiency virus type 1 (HIV-1) still causes a chronic infection that affects millions of individuals worldwide. The infection remains incurable and presents a huge challenge for treatment, as it tends to disable a patient's immune system. Although the current HIV-1 treatment regime possesses the ability to reduce the viral load to undetectable limits, complete eradication of the virus cannot be achieved while latent HIV-1 reservoirs go unchallenged. These viral reservoirs are established early on during HIV-1 infection and are a major hurdle since they remain unaffected by antiretroviral drugs and have the ability to replenish systemic infections once treatment is interrupted. Further ailments with the highly active antiretroviral therapy (HAART) include issues such as the cumbersome lifelong treatment, development of drug resistant strains of HIV-1 and adverse side effects. Contrarily, early diagnosis of the HIV-1 infection and HIV-1 treatment is a major challenge in resource-limited countries. The current available diagnostic tools for HIV-1 infection have shown to be highly accurate in monitoring $CD4^+$ T lymphocyte count and viral load measurements. However, these tests such as enzyme-linked immunosorbent assay (ELISA) and polymerase chain reaction (PCR) which are highly efficient, are usually very expensive with complex operation, time consuming, require skilled personnel and training that makes them incompatible for the application in resource-limited areas. Therefore, this raises the urgent need for developing an HIV point of care (POC) diagnostic tool that is label-free, highly specific and sensitive as well as therapeutic modalities, which can be used to address the previously mentioned challenges. Much research has been conducted to resolve these problems but to date, there has not been application of laser and/or photonics in HIV research. Therefore, in this thesis a femtosecond laser was used in HIV infected cells for targeted antiretroviral drug delivery while preserving their viability. For the first time according to our knowledge, antiretrovirals (ARVs) that target all the life stages of the HIV-1 life cycle were utilized and they proved to be significant in reducing HIV-1 infection. Furthermore, through the employment of a continuous wave laser at 640 nm, for the first time, surface plasmon resonance was conducted to facilitate label-free detection of HIV-1. Success of these laser based technologies will open doors for incorporation in POC HIV diagnostic tools for the detection and treatment monitoring of HIV in resource-limited settings.

Keywords: HIV-1, HAART, laser-based technologies, surface plasmon resonance (SPR), antiretroviral drugs, femtosecond laser, Point of care diagnostics, drug delivery.

Acknowledgements

Almighty Heavenly Father, Thank you for giving me the courage, strength and wisdom throughout this research project.

I owe my sincere gratitude to my supervisors Dr. Patience Mthunzi-Kufa and Prof. Malik Maaza for opportunity, hard work, effort and the patience that made this research project successful, Thank you.

Dr. Sello Manoto and Dr. Saturnin Ombinda-Lemboumba, “thank you” just does not justify the “Ubuntu” that you gave me throughout this project. I consider myself very lucky to have grown under your different styles of leaderships and co-supervision. The potential you saw in me and your undying support got me to this end. Guys, words are just not enough. Although I felt like I had two bulls cornering me, lol, we made such a great team; more like the “three Musketeers”. You are one of a kind, thank you so much.

A special word of gratitude to my father, Nnduvheni Keith Malabi, my superhero. “Ndo vha ndi tshi dou vha ndi ngafhi are husi vhone khotsi anga”, the unconditional love, courage, believing in me, inspiration and financial support throughout my life has made the young woman I am today. In you, I have the best dad in the world and am forever grateful. My Mother, Mutondwaini Rosheen Malabi, you have been my pillar of strength through good times and those crying times, you have been an inspiration throughout and encouraged me not to give up when I felt that it was just too much. Thank you for praying for me, only the best mothers gives all the love, support, encouragement, faith and hope. I have extraordinary parents in both of you. To my siblings (Edzani, Masala, Mudinda and Rofhiwa) never a dull moment, thanks for cheering up when I needed it the most.

Dr. Thembinkosi Mabila, Sir, “that vision is now the reality of my life”, the road was not easy. Your encouragement, guidance, and unwavering support shaped and molded me. I know and understand the saying “it takes a village to raise a child” because of you, I am grateful to be one of your academia products.

My dearest friends and colleagues: Dr. Mathew Esona, Dr. Maemu Gededzha, Pleasure, Tlou, Thabo and Grace, I called, you listened, I cried, you gave me a shoulder, I laughed, and you laughed with me. Irreplaceable is what you all are and to all my friends who supported me and encouraged me throughout this journey, my warmest regards to all of you.

To my Biophotonics teammates Lebogang, Charles and Masixole, thank you for all the support and kindness throughout my studies.

I would sincerely like to acknowledge and thank the Council for Scientific and Industrial Research (CSIR) and the National Laser Centre, National Research Foundation (NRF) and the University of South Africa for giving me the financial support and opportunity to learn and conduct this research project.

Publications and intellectual patent generated during this PhD

Publications

1. Malabi, R., Manoto, S. L., Ombinda-Lemboumba, S., Maaza, M., & Mthunzi-Kufa, P. (2019). Laser enhanced drug delivery of antiretroviral drugs into HIV-1 infected TZMbl cells. Journal of biophotonics, e201800424**. (Chapter 2 in thesis)**
2. Ombinda-Lemboumba, S., Malabi, R., Lugongolo, M. Y., Thobakgale, L., Manoto, S. L., & Mthunzi-Kufa, P. (2019). Label-free differentiation of HIV-1 infected from uninfected cells using transmission measurement. Journal of biophotonics, e201800349.
3. Oluwole, D. O., Manoto, S. L., Malabi, R., Maphanga, C., Ombinda-Lemboumba, S., Mthunzi-Kufa, P., & Nyokong, T. (2018). Evaluation of the photophysicochemical properties and photodynamic therapy activity of nanoconjugates of zinc phthalocyanine linked to glutathione capped Au and Au3Ag1 nanoparticles. Dyes and Pigments, 150, 139-150.
4. Manoto, S. L., Thobakgale, L., Malabi, R., Maphanga, C., Ombinda-Lemboumba, S., & Mthunzi-Kufa, P. (2017). Therapeutic strategies to fight HIV-1 latency: progress and challenges. Biologia, 72(10), 1101-1112.

Conference proceedings

1. Malabi, R., Manoto, S., Ombinda-Lemboumba, S., Maaza, M., & Mthunzi-Kufa, P. (2019, March). Detection of biological analytes using surface plasmon resonance as a biosensing technique for possible development of a point of care diagnostic tool. In Plasmonics in Biology and Medicine XVI (Vol. 10894, p. 108940P). International Society for Optics and Photonics.(**Chapter 5 in thesis**)
2. Malabi, R., Manoto, S., Ombinda-Lemboumba, S., Khanyile, S., Khamlich, S., Maaza, M., & Mthunzi-Kufa, P. (2019, March). Growth and characterisation of gold thin film layer using an ebeam evaporation system for surface plasmon resonance applications. In Plasmonics in Biology and Medicine XVI (Vol. 10894, p. 108941E). International Society for Optics and Photonics.**(Chapter 4 in thesis)**
3. Manoto, S., Malabi, R., Ombinda-Lemboumba, S., & Mthunzi-Kufa, P. (2019, March). Biocongugation of gold nanoparticles for surface plasmon resonance sensor. In

Plasmonics in Biology and Medicine XVI (Vol. 10894, p. 108941D). International Society for Optics and Photonics.**(Chapter 5 in thesis)**

4. Manoto, S., Mabena, C., Malabi, R., Ombinda-Lemboumba, S., & Mthunzi-Kufa, P. (2019, March). Design and FDTD simulation of photonic crystal based sensor for biosensing applications. In Frontiers in Biological Detection: From Nanosensors to Systems XI (Vol. 10895, p. 1089510). International Society for Optics and Photonics.
5. Malabi, R., Manoto, S., Ombinda-Lemboumba, S., Maaza, M., & Mthunzi-Kufa, P. (2018, September). Surface Plasmon Resonance as a biosensing technique for possible development of a point of care diagnostic tool. In Laser Science (pp. JW4A-108). Optical Society of America.**(Chapter 3 in thesis)**
6. Malabi, Rudzani, Sello Manoto, Saturnin Ombinda-Lemboumba, Malik Maaza, and Patience Mthunzi-Kufa. "In-vitro photo-translocation of antiretroviral drug delivery into TZMbl cells." In Optical Interactions with Tissue and Cells XXVIII, vol. 10062, p. 1006204. International Society for Optics and Photonics, 2017 **(Chapter 2 in thesis)**
7. Ombinda-Lemboumba, S., Malabi, R., Lugongolo, M. Y., Thobakgale, S. L., Manoto, S., & Mthunzi-Kufa, P. (2017, February). Investigation of HIV-1 infected and uninfected cells using the optical trapping technique. In Biophysics, Biology and Biophotonics II: the Crossroads (Vol. 10075, p. 100750M). International Society for Optics and Photonics.
8. Maphanga, C., Malabi, R., Ombinda-Lemboumba, S., Maaza, M., & Mthunzi-Kufa, P. (2017, February). Pros and cons of characterising an optical translocation setup. In Optical Interactions with Tissue and Cells XXVIII (Vol. 10062, p. 100621A). International Society for Optics and Photonics.
9. Manoto, S. L., Oluwole, D. O., Malabi, R., Maphanga, C., Ombinda-Lemboumba, S., Nyokong, T., & Mthunzi-Kufa, P. (2017, February). Photodynamic activity of zinc monocarboxyphenoxy phthalocyane (ZnMCPPc) conjugated to gold silver (AuAg) nanoparticles in melanoma cancer cells. In Optical Methods for Tumor Treatment and Detection: Mechanisms and Techniques in Photodynamic Therapy XXVI (Vol. 10047, p. 1004716). International Society for Optics and Photonics.
10. Manoto, S. L., Oluwole, D. O., Malabi, R., Maphanga, C., Ombinda-Lemboumba, S., Nyokong, T., & Mthunzi-Kufa, P. (2017, February). Phototoxic effects of free phthalocyanine and phthalocyanine conjugated to gold nanoparticles for targeted photodynamic therapy of melanoma cancer," Proc. SPIE 10047, Optical Methods for

Tumor Treatment and Detection: Mechanisms and Techniques in Photodynamic Therapy XXVI (Vol. 10047, p100470D) International Society for Optics and Photonics.

Patents

1. Ombinda-Lemboumba, S., Malabi, R., Lugongolo, M. Y., Thobakgale, S. L., Manoto, S., & Mthunzi-Kufa, P. Investigation of HIV-1 infected and uninfected cells using the optical trapping technique.

Table of Contents

Declarations i

Abstract ii

Acknowledgements iii

List of figures xi

1. Introduction 1

1.1. Preface 1

1.1.1. Laser drug delivery system using femtosecond lasers pulses 2

1.1.2. Surface plasmon resonance 3

1.2. Synopsis of the thesis 4

References 7

Chapter 2 8

Laser enhanced drug delivery of antiretrovirals into HIV-1 infected TZM-bl cells 8

2.1. Introduction 8

2.1.1. HIV classification and literature 10

2.1.2. HIV treatment 10

2.1.3. ARV drug delivery 12

2.2. Overview of lasers and their literature 12

2.2.1. Laser light properties 13

2.2.1.1 Laser coherence 13

2.2.1.2. Laser brightness or intensity 13

2.2.1.3. Laser monochromaticity and directionality 13

2.2.2. Principles of Lasers 14

2.2.3. Elements of lasers 16

2.2.4. Laser modes 17

2.2.5. Laser interaction with tissues 18

2.2.6. Laser light delivery system 19

2.3. Experimental Methods 20

2.3.1. Cell culture 21

2.3.2 Pseudovirus production and *in vitro* infection 21

2.3.3. Optical setup 21

2.3.4 Photo-translocation of ARVs into TZM-bl cells 23

2.3.5 Cellular viability 23

2.3.6 Cellular cytotoxicity 23

2.3.7 Luciferase assay 24

2.3.8 Data analysis 24
2.4. Results and Discussion 24
2.4.1 Cellular Morphology 26
2.4.2 Cellular viability assay 27
2.4.3 Cytotoxicity Assay 28
2.4.4 HIV-1 Inhibition Luciferase Assay. 30
2.5. Conclusions 31
References 33
Chapter 3 39
Development and characterisation of the surface plasmon resonance system 39
3.1. Introduction 39
3.2. History of surface plasmon resonance (SPR) 40
3.2.1. Plasma frequency/ electron oscillation 41
3.2.2. Evanescent waves and surface waves 42
3.3. Surface plasmon resonance 44
3.4. Types of SPR sensors 46
3.4.1. SPR sensor coupling with a prism 47
3.4.2. SPR sensors coupling with diffraction gratings 48
3.4.3. SPR sensors coupling with waveguides 48
3.5. Experimental methods 49
3.5.1. Custom made SPR Set up 49
3.5.1.1. Light source 51
3.5.1.2 The prism and the gold thin film 51
3.5.1.3. Detector 52
3.5.1.4. Angular measurements 52
3.6. Results and discussion 52
3.7. Conclusion 55
References 57
Chapter 4 60
Growth and characterization of the gold thin film layers for SPR setup using the electron beam evaporation system. 60
4.1. Introduction 60
4.1.1. Electron beam evaporation system 62
4.1.2. Characterization of thin films 64
4.2. Experimental methods 68

4.2.1. Sample preparation 68
4.2.2. Characterization techniques. 70
4.2.2.1. Analysis using X-ray diffraction. 70
4.2.2.2 Analysis using scanning electron microscope 71
4.3. Results and Discussion 72
4.3.1. Characterization using X-ray diffraction (XRD) Spectroscopy 72
4.3.2. Surface morphology using Scanning electron Microscope 74
4.4.3. UV-Vis Characterization 75
4.4.4. SPR signaling 76
4.5. Conclusion 79
References 81
Chapter 5 84
Detection of biological analytes and HIV-1 using SPR as a biosensing technique for possible development of a POC diagnostics tool. 84
5.1. Introduction 84
5.1.1. Applications of SPR sensors 85
5.1.2. Characteristics of SPR sensors 86
5.1.2.1. Sensitivity 86
5.1.2.2 Resolution 86
5.1.2.3. Limit of detection 87
5.2. Experimental methods 87
5.2.1. Gold nanoparticle (AuNP)-goat anti mouse IgG conjugation 87
5.2.2. Immobilization of primary and secondary antibodies. 87
5.2.3. SPR sensing of the functionalized substrates on the custom made SPR system 88
5.2.4. Structural analysis of the substrates using scanning electron microscopy (SEM) 89
5.2.5. SPR sensing on the custom made SPR system 89
5.3. Results and Discussion 90
5.3.1. UV-Vis spectroscopy 90
5.3.2. Immobilisation of antibodies and structural analysis using scanning electron microscopy 92
5.3.3. Detection of biological analytes using SPR sensor 93
5.3.4. Immobilization of HIV-1 antibodies and structural analysis using SEM. 95
5.3.5. Detection of HIV-1 using the SPR sensing system 97
5.4. Conclusion 99
References 100
Chapter 6 103

Conclusion 103
Appendix... 108

List of figures

Figure 1:	Illustration of a typical SPR sensing	4
Figure 2.1:	Illustration of laser emission before and after absorption	15
Figure 2.2	An image illustrating the basic components of a laser	17
Figure 2.3:	An illustration of a non-invasive translocation optical setup	22
Figure 2.4:	An image showing the action sites of different ARV classes of HIV cycle	25
Figure 2.5:	An image showing the changes in cellular morphology	26
Figure 2.6:	ATP assay measuring the viability	28
Figure 2.7:	Graph showing LDH assay assessing cell membrane damage	29
Figure 2.8:	Graph showing luciferase activity assay as a measure of HIV infection	30
Figure 3.1:	The diffraction spectrum showing Wood's anomalies	40
Figure 3.2:	Illustration of total internal reflection (TIR)	43
Figure 3.3:	Illustration of the structure of an evanescent wave	43
Figure 3.4:	Illustration of SPR sensing based on the Kretschmann configuration	45
Figure 3.5:	Diagram representing SPR sensor coupling with a prism	47
Figure 3.6:	Diagram showing the SPR sensors coupling with diffraction gratings	48
Figure 3.7:	Diagram showing the SPR sensors coupling with waveguides	49
Figure 3.8:	Schematic representation of the custom made SPR rig based on the Kretschmann configuration	50
Figure 3.9:	Schematic illustration that shows the gold film placed on the prism	51
Figure 3.10:	A graph illustrating surface plasmon resonance excitation	53
Figure 3.11:	Graphs illustrating surface plasmon resonance excitation sensing	54
Figure 4.1:	An image showing the three crucibles and the tungsten filament of the e-beam system	62
Figure 4.2:	Images showing (A) the glass substrates mounted on the aluminium holders and (B) the aluminium holders placed on the six holder sample changer for e-beam deposition	63
Figure 4.3:	Diagram that depicts the experimental setup of the e-beam	64
Figure 4.4:	Basic features of a typical XRD experiment	65
Figure 4.5:	Schematic diagrams showing the Miller indices of atomic planes in a simple cubic crystal	66
Figure 4.6:	Titanium and gold pellets put on individual e-beam crucibles before evaporation	68
Figure 4.7:	An image showing cleaned glass substrates	69
Figure 4.8:	E-beam deposited substrates with 5 nm Ti and 40 nm Au	70
Figure 4.9:	A labelled image of the X-ray diffraction machine	71
Figure 4.10:	Raw data of gold synthesis using the X-ray diffraction for phase identification.	72
Figure 4.11:	X-ray diffraction pattern of the gold coated thin film	73
Figure 4.12:	Depicts SEM images of the e-beam deposited samples	74
Figure 4.13:	A Graph showing the transmittance spectra of different gold thickness	75
Figure 4.14:	A Graph showing the absorption spectra of different thickness	76
Figure 4.15:	Graphs showing shifts of SPR curve of resonance using the prism with different gold (Au) thickness	77

Figure 4.16:	Graphs showing shifts of SPR curve of resonance using the prism with different gold (Au) thickness	79
Figure 5.1:	Setup of SPR spectroscopy with the sample	88
Figure 5.2:	Schematic representation of the SPR setup with the 40nm gold substrate functionalised with antibodies	89
Figure 5.3:	UV-Vis absorption spectra of Gold (AuNPs) nanoparticle	91
Figure 5.4:	SEM images of the functionalised gold coated substrate	92
Figure 5.5:	A graph showing shifts of SPR curve of resonance of the bare gold coated slide	93
Figure 5.6:	(A) Schematic representation of the gold sensor chips coated with GP41 antibodies and HIV-1 pseudovirus for capturing GP41 antibody conjugated to AuNPs	96
Figure 5.7:	A Graph showing Shifts of the SPR curve by absorbing HIV-1 virus concentrations binding onto the GP41-AuNPs conjugates bound to the gold sensor chip	97

Abbreviations

ARVs	Antiretrovirals
ART	Antiretroviral therapy
ASSURED	Affordable, sensitive, specific, user-friendly, rapid & robust, equipment free, and deliverable to end users
ATP	Adenosine triphosphate
AFM	Atomic force microscope
ATR	Attenuated total reflection
AIDS	Acquire Immunodeficiency Syndrome
Au	Gold
AuNPs	Gold nanoparticles
Å	Angstrom
BK7	Borkron (borosilicate crown glass)
CD4+	Cluster differentiation 4
CNS	Central nervous system
CW	Continuous Wave
CCD	Charged coupled device
Cu	Copper
CO_2	Carbon dioxide
cm	Centimeters
DNA	Deoxyribonucleic Acid
DMEM	Dulbecco's minimal essential medium
ELISA	Enzyme-linked immunosorbent assay
Env	Envelope
EDTA	Ethylenediamine tetraacetic acid
EM	Electromagnetic wave
EDC	N-ethyl-N'-(3-dimethyiamino-propyl) carbodiimide hydrochloride

fs	Femtosecond
GP41	Glycoprotein 41
HIV-1	Human Immunodeficiency Virus 1
HAART	Highly active antiretroviral therapy
H_2O_2	Hydrogen peroxide
IgG	Immunoglobulin G
kW	Kilowatts
KHz	Kilohertz
LTR	long terminal repeats
LDH	Lactate dehydrogenase
LED	Light emitting diode
mW	milliwatts
mm	millimetres
ms	milliseconds
ml	millilitres
NA	Numerical aperture
NNRTI	Non-nucleoside reverse transcriptase inhibitors
NRTI	Nucleoside reverse transcriptase inhibitors
nm	nanometers
NHS	N-hydroxysuccinimide
PBS	Phosphate buffer saline
PCR	Polymerase chain reaction
POC	Point of care
PI	Protease inhibitors
PVD	Physical vapor deposition
PEG	Polyethylene glycol
pg/ml	picogram per millilitres

RNA	Ribonucleic acid
ROS	Reactive oxygen species
RLUs	Relative light units
RI	Refractive index
SPR	Surface plasmon resonance
SEM	Scanning electron microscope
SP	Surface plasmon
SPP	Surface plasmon polaritons
TIR	Total internal reflection
TEM	Transverse Electromagnetic Mode
Ti	Titanium
UV	Ultra Violet
V	Volts
XRD	X-ray diffraction

Chapter 1

1. Introduction

1.1. Preface

Human Immunodeficiency Virus (HIV-1) mortality rate has decreased tremendously since the institution of highly active antiretroviral therapy (HAART) worldwide. With the expansion to access antiretroviral therapy and it effectiveness program to monitor HIV control and management, HIV diseases is still monitored by $CD4^+$ T lymphocyte count and viral load measurements. These two measurement approaches can only indicate the strength of the individual's immune system and the viral replication of the virus in the plasma. Rapid point of care (POC) HIV testing for viral load measurement and $CD4^+$ T cell count can facilitate timeous initiation of antiretroviral therapy (ART) and dose monitoring of treatment efficacy [1]. Without proper monitoring of the therapy, adverse side effects, poor availability of the drugs and lack of patient compliance may lead to viral replication and emergence of drug resistance. Therefore, point of care diagnostic tools which are affordable, sensitive, specific, user-friendly, rapid and robust, equipment free, and deliverable to end users (ASSURED) and can regularly do viral load testing to effectively monitor antiretroviral therapy (ART) efficiency and detect treatment failure are highly required. Meanwhile there is a need to explore therapeutic targeting of HIV-1 to try and eradiate HIV-1. Biosensors have portrayed to be a great potential tool for analysis as they can be integrate within microprocessor-based electronics and allows for easy computation of signals in diagnosis of some diseases. The surface plasmon resonance (SPR) biosensors are label free, real-time, highly sensitive and portable immunosensors. They are cost effective, consume little reagents and can be performed without any complex sample purification. It is for these reasons, this PhD study has focused on the design and development of a highly sensitive SPR system that can detect and quantify HIV-1 in real time. SPR biosensors not only provide alternative ways of excitation of surface plasmons to capture viruses, but they can also enable the advance detection and quantification of the virus. Meanwhile, optical drug delivery using ultrafast laser pulses with extremely high peak powers that can precisely disrupt the cell membrane is a unique tool that allow immediate transportation and expression of exogenous material in live mammalian cells. These has shown benefits of efficiently being therapeutic to tissues and cells without causing toxicity and

damage [2, 3]. This targeted drug delivery technique will, open doors to minimize drug resistance and combat the toxic side effects of the orally administered antiretrovirals (ARVs).

For PhD research purposes, the aim of this study was to optically deliver ARVs into HIV-1 infected cells using femtosecond laser pulses *in vitro*. Here, a custom made photo-translocation system was constructed, characterized and optimized for optical drug delivery parameters. In order to exploit the benefits of non-invasive, sterile and non-toxic therapy delivery to the cells, biological assays such as cellular viability, cellular cytotoxicity and luciferase assay were performed to assess cellular responses after laser treatment. The assays facilitated the analysis of the efficiency of the laser assisted drug delivery system on the HIV infection.

Given the major challenges in early HIV-1 diagnosis and treatment, this thesis introduces and outlines the two optical methods namely: surface plasmon resonance and laser enhanced drug delivery using femtosecond laser pulses to address the diagnosis and treatment of HIV-1 infection respectively.

1.1.1. Laser drug delivery system using femtosecond lasers pulses

A laser is a device that stimulates atoms or molecules to emit light at a particular wavelength. It amplifies the light by typically producing a very narrow beam of radiation. There are various types of lasers that have been developed over the past years with highly varied characteristics, which are dependent on the applications such as cladding industrial settings and eye surgery in medical applications [2, 3]. Most lasers have wavelengths in the visible and near-infrared regions. To date, lasers have become standard tools in diverse applications such as laser pointer highlighters for presentation for educational purposes, writing of patterns on objects without touching them and removal of unwanted hair in humans. For medical applications, lasers are used as delivery systems because of their minimal invasive nature. Microscopic delivery i.e. introduction of drugs into a single cell by increasing plasma membrane permeability and macroscopic delivery i.e. releasing of drugs within groups of cells or tissues at a targeted location in the body. These two key drug delivery systems have shown tremendous success in effectively being therapeutic to tissue and cells without causing toxicity and damage [2]. Laser aided transfection has demonstrated high operational efficiency when conducting transfection experiments, with the benefit of non-invasive, sterile and non-toxic treatment of cells [3, 4]. The acceptance of foreign genes, medications and other macromolecules into active mammalian cells have been promoted by using various developed methods such as chemical cationic polymers and lipids, virus-related or physical methods. However, each of these

delivery schemes translates to detailed limitations such as low levels of biodegradability and subsequent toxicity. Nonetheless, a drug delivery scheme possessing minimum cytotoxicity for both *in vitro* and *in vivo* techniques that can be functional under sterile tissue culture protocols and can offer targeted management of a great number of individual cells is highly required. Optical drug delivery procedures using a femtosecond (fs) laser light sources satisfy these criteria. The fs laser is the most commonly used light source in the area of laser facilitated drug delivery because it produces very short pulses and has comprehensive spectral range in the near infrared regime ranging within the 700-1000 nm region [5]. Femtosecond laser pulses have high peak powers and adequate photon density to activate non-linear effects such as multi-photon absorption confined at laser beam focus. Therefore, the use of fs laser pulses for optical drug delivery in HIV-1 infected cells offers a high degree of longitudinal confinement of the deposited pulsations leading to native disruptive effects at the targeted area and minimal collateral destruction.

In this thesis, the use of femtosecond laser pulses as a drug delivery sub-system in a photo-translocation system to deliver ARVs that target different life stages of the HIV-1 life cycle, into HIV-1 infected cells is explored.

1.1.2. Surface plasmon resonance

Optical sensors are sensing devices, which converts the quantity of the molecule being measured to another quantity in a form of mass, which is normally encoded into one of the characteristics of the light wave. Surface plasmon resonance (SPR) is an optical sensing technique whereby there is a charged density oscillation of electromagnetic waves through a dielectric media and a metal surface. This technique has been used in various disciplines such as biochemistry, chemistry, biology and biomedicine. This is because, for the most part, SPR spectroscopy is a technique used to detect biomolecular binding interactions. In SPR, one molecular partner is immobilized on a metallic film. Light excites surface plasmons in the metal when the binding partner binds to the immobilized molecule. This causes a detectable change in the surface plasmon signal resulting in a shift in the reflected angle as depicted figure 1 below.

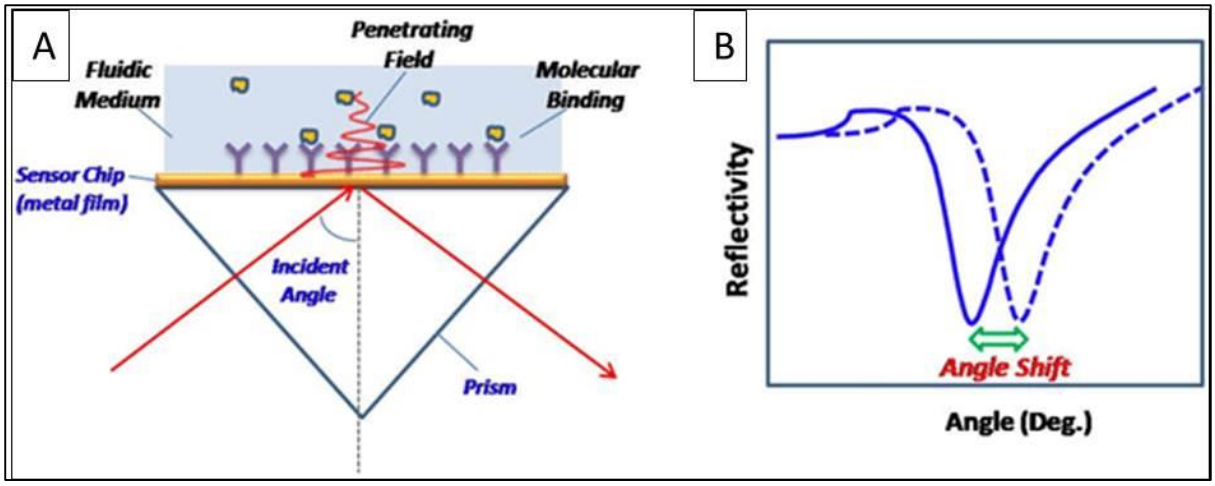

Figure 1: Diagram illustrating a typical SPR sensing technique. An incident light is directed onto a SPR sensor chip via a glass prism and the reflected beam is detected via a photodetector. At an appropriate angle (resonance angle), the incident light excites the surface plasmons in the sensor chip (metal film) and the intensity of the reflected light drops to a minimum. The electromagnetic field created by SPR penetrates the fluidic medium and probes molecular binding processes taking place on the surface and the refractive index changes in the fluidic medium. In image B, the reflectivity vs. incident angle plot shows a sharp drop in the reflection intensity due to SPR, also referred to as the SPR "dip" [6].

It is known that the use of optical biosensors to study molecular interactions is a well-accepted method [6]. This technology has been used to measure in real time the binding kinetics between a macromolecule in solution and an immobilized receptor. The advantage of the SPR biosensing method versus other optical biosensors is that the entire interaction between the analytes and the ligand is monitored in real time, without any molecule labelling; moreover, reduced analysis time and simple procedures for sample preparation are added advantages when compared with traditional analytical methods. In this study, the surface plasmon resonance sensing technique is used to facilitate label-free detection of HIV.

1.2. Synopsis of the thesis

This thesis consists of six chapters. Chapter 1, briefly describes and summaries the challenges of HIV-1 diagnosis and treatment and the purpose of the study. The chapter further outlines targeted laser drug delivery and surface plasmon resonance techniques.

In Chapter 2, focus is placed on details behind the laser drug delivery system. This chapter begins with the introduction to lasers, types of lasers and how they are employed as drug delivery systems. It also details the different conventional delivery systems that have been used for the delivery of ARVs. In this chapter, photo-translocation, a photonics based

macromolecule delivery methodology is also outlined. Experimental results demonstrated that the successful use of femtosecond laser pulses for photo-translocation of ARVs into infected cells using different ARVs that target all the life stages of the HIV-1 virus. Lastly, laboratory data displaying cellular response of the cells following laser treatment via biological assays was presented.

Chapter 3 discusses the development and characterization of the SPR setup. This chapter begins with a brief history of SPR and its phenomenon. It then concentrates on how the SPR system was designed based on the Kretschmanns geometry of SPR, and built using a 640 nm continuous laser with different optics such as mirrors for the optical train, the glass prism as the heart of the setup and the photodiode as the detection system. It further details the essential components that are used to the SPR system. The system was characterized by measuring the reflected intensity of light using the photodiode, as a function of the external angle being measured. As an experimental technique, angular measurements were explored and used to optimize the SPR system.

Chapter 4 explores growth and characterization of gold thin film layers using an e-beam evaporation system for SPR applications. In this chapter, gold thin film layers with adhesion layers of titanium was coated on multiple glass slides using the e-beam technique. Following that, the structural and morphological investigations of the thin film layer coating were investigated using the X-ray diffraction system (XRD) while the scanning electron microscope (SEM) was utilized to investigate the morphology of the thin film layer coating. The optical analysis using absorption and transmission spectra technique was utilized in determining the appropriate layer to use for SPR. Initially, the slides were coated with gold using the sputtering method and a challenge of the gold peeling off from the slides was encountered. However, the e-beam method proved otherwise to be highly efficient with controlled structural processes for the gold thin film layer.

Chapter 5 concentrates on the detection of biological analytes and HIV-1 using SPR as a biosensing technique for possible development of a POC diagnostics tool. Firstly, immobilization of biomolecules and signal amplification of the SPR system using the gold thin layer from chapter 4 are outlined. The gold coated slides were functionalized and bioconjugation was achieved by covalently attaching antibodies to gold nanoparticles. The sensor chips were used on the SPR sensor system built in Chapter 3 for biosensing applications, which in this case was the detection of biological analytes and the HIV. Gold nanoparticles

were used to improve the sensitivity of the SPR system, for signal enhancement. The angular interrogation and spectral experiment before and after conjugation were performed to clearly distinguish the difference in shifts of the analytes that have bound to the surface of the sensor chips and the HIV virus respectively. Using the Origin software data analysis on the collected data in a form of graphs was completed.

Additionally, structural morphology changes of the sensor chips were observed through employment of SEM, analysis not only emphasized the novelty in the functionalization protocol used, but also proved that the protocol was efficient for the bioconjugation of antibodies and nanoparticles to the sensor chips. Lastly, Chapter 6 concludes on the content of the thesis, displays limitations and transcribes future aspects of the work concerning HIV treatment and diagnostics.

References

1. Mauk M, Song J, Bau HH, Gross R, Bushman FD, Collman RG, Liu C. Miniaturized devices for point of care molecular detection of HIV. Lab on a Chip. 2017; 17(3):382-94.
2. Terakawa M, Mitsuhashi T, Shinohara T, Shimizu H. Near-infrared femtosecond laser-triggered nanoperforation of hollow microcapsules. Optics Express. 2013 May 20; 21(10):12604-10.
3. Antkowiak M, Torres-Mapa ML, Gunn-Moore F, Dholakia K. Application of dynamic diffractive optics for enhanced femtosecond laser based cell transfection. Journal of Biophotonics. 2010 Oct; 3 (10-11):696-705.
4. Tsampoula X, Garces-Chavez V, Comrie M, Stevenson DJ, Agate B, Brown CT, Gunn-Moore F, Dholakia K. Femtosecond cellular transfection using a nondiffracting light beam. Applied Physics Letters. 2007 Jul 30; 91(5):053902.
5. Brown CT, Stevenson DJ, Tsampoula X, McDougall C, Lagatsky AA, Sibbett W, Gunn-Moore FJ, Dholakia K. Enhanced operation of femtosecond lasers and applications in cell transfection. Journal of Biophotonics. 2008 Aug;1(3):183-99.
6. http://biosensingusa.com/technical-notes/technical-note-102-spr-sensitivity-detection-limit/

Chapter 2

Laser enhanced drug delivery of antiretrovirals into HIV-1 infected TZM-bl cells

In this chapter, the introduction summaries the importance of conducting the current study in an attempt to potentially create a new treatment regime. A brief overview on HIV and it's literature including; classification, treatment, and antiretroviral drug delivery methods are described. In sections 2.1.2 and 2.1.3, the challenges encountered with the current treatment regime of HIV were clearly stipulated as well as the reason for exploring a laser based delivery method. Furthermore, a summary on laser light properties and radiation were described with emphasis on the laser interaction with tissues and cells in medical applications. In this chapter it is shown for the first time that the laser based HIV-ARV drug delivery technique using femtosecond laser pulses is able to significantly reduce HIV-1 infection. A custom made photo-translocation system was constructed and optimised for the efficient photo-translocation of the ARVs into the HIV-1 infected TZM-bl cells. The use of tightly focused femtosecond laser beam pulses to precisely perforate the cell membrane and allow ARVs for their targeted delivery in the infected cells was demonstrated. Employment of biological assays to access cellular responses after laser treatment was explored. Finally, the results obtained not only demonstrated that femtosecond laser pulses were highly effective in delivering ARVs into HIV-1 infected TZM-bl cells, but also displayed a significant reduction in HIV-1 infection post laser manipulation.

2.1. Introduction

The HIV-1 morbidity and mortality rate has dramatically decreased across the globe since the introduction of highly active antiretroviral therapy (HAART) [1, 2]. It is estimated that approximately 36.7 million people are infected and living with HIV-1 disease worldwide [3] and as from June 2016, 18.2 million of these cases were accessing antiretroviral therapy globally [4]. HAART can suppress viral replication and restore immune response in HIV-1 infected patients [5, 6], nonetheless, the treatment fails to completely eliminate HIV-1 infection. The HIV virus stays hidden in the sanctuary sites known as the physiological reservoirs, and remains a chronic and life-long infection [7-9]. The presences of viral reservoir

sites that are inaccessible by the existing treatment contribute to the ineffectiveness of HAART. These reservoirs can be defined as anatomical and cellular reservoirs. Cells such as microglia, astrocytes and macrophages are the main cellular reservoirs, as the virus therein is of archival nature and persevere for extensive eras. Lymphoid organs, genitourinary tract and the central nervous system are the major anatomical reservoirs, as these sites immunologically shelter the virus at the early phase of infection [8, 9]. The early establishment of these viral reservoirs during primary infection is the major contributor of antiretroviral drugs (ARVs) failing to completely eradicate the virus [9, 10]. The current available therapies are unable to access HIV-1 reservoirs in which the proliferation of the HIV virus, regulated by several enzymes and biochemical processes occur at cellular and molecular levels [10].

Drug delivery systems that can deliver ARVs into sub epithelial layers, penetrate the target cells, maintain therapeutic concentrations of the drugs in systemic circulation and cross the physiological barriers to viral sanctuary sites such as the lymphatic system, central nervous system (CNS) and macrophages are essential in treating and eradicating the HIV-1 infection[10,11,12]. To date a range of novel efficient antiretroviral drug delivery systems that include the use of ceramic implants [13], liposomes [14, 15], solid colloidal nanoparticles [16, 17], nanopowders and bio adhesive coated matrix tablets [5, 13] have been explored with partial success. Therefore, further research and investigation of novel ARV delivery systems is critical.

Lately, the introduction of drugs into a single cell by increasing plasma membrane permeability using laser sources have shown tremendous success in being therapeutic to the cells without causing any toxicity and damage [18, 19]. This laser assisted drug delivery system can be applied under sterile tissue culture protocols and can offer targeted treatment of a large number of individual cells. When it comes to immediate transportation of exogenous matter into cells; femtosecond lasers operating in the near infrared region of the light spectrum have shown striking benefits compared to using ultraviolet lasers [20]. Femtosecond (fs) laser sources emit extremely short pulses with high peak powers that trigger non-linear effects such as multi-photon absorption [20, 21]. Their ability to precisely disrupt the cell membrane to enable the immediate transportation of exogenous matter into live mammalian cells [22-24], makes them the most powerful tool for photo-translocation and transfection techniques. In addition, the use of fs laser pulses assisted drug delivery elicits benefits of non-invasive, sterile and non-toxic therapy to the cells [18, 25-27]. The primary aim of this study was to optically deliver ARVs into HIV-1 infected TZM-bl cells and to use different biological assays to evaluate cellular

responses post laser poration. Furthermore, this study also investigated the effects of this laser assisted drug delivery system on HIV-1 infection.

2.1.1. HIV classification and literature

HIV-1 was first identified as the leading cause of death in 1983 [28]. HIV-1 is a single stranded positive sense enveloped RNA virus, a member of the genus *lentivirus,* family of *Retroviridae* and subfamily *Orthoretrovirinae.* HIV-1 and HIV-2 are the two types of the virus that have been characterised, with HIV-1 causing majority of the infections globally due to its virulent and infective nature [29]. HIV hijacks white blood cells in the immune system and forces them to make copies of the virus. When HIV enters the body, it mainly targets the $CD4^+$ lymphocyte cells. After $CD4^+$ cell infection, it undergoes a series of stage processes whereby it replicates itself creating many copies of the virus, thus resulting in HIV replication or life cycle [30]. During infection, HIV attaches to a precise type of receptor ($CD4^+$ receptor) and co-receptor (CCR5) on the surface of the $CD4^+$ lymphocyte cell, where it fuses with the host cell and discharges its genomic material into the cell [30]. The reverse transcriptase enzyme will change the genomic material of the virus to enable it to integrate into the host DNA. The virus novel genomic material then enters the nucleus of the $CD4^+$ cell using the enzyme named integrase to assimilate itself into the host genomic material where it lies dormant for years [31, 32]. Upon activation of the host cell, the virus uses the hosts' enzyme to make more of its genomic material, which are highly specialised, and it makes longer proteins [30]. The longer proteins are cut into individual proteins by an enzyme called protease; these individual proteins will come and assemble collectively together with the virus hereditary material forming a novel virion [30]. After this, the virus will push itself out of the host cell in a process known as budding, taking part of the membrane of the host cell and completing the life cycle of the HIV virus [30- 32].

2.1.2. HIV treatment

The use of antiretroviral therapy and HAART has improved the quality of lifespan and has increased survival of HIV-infected individuals [28]. Combination of three or more ARVs was introduced to help combat the fight against HIV-1 disease [33]. Studies done have shown that in 1996 a daily dosage of drugs of more than 20 pills were taken, nonetheless, recently, this dosage was reduced to a single pill a day [33]. For example, tenofovir, emtricitabine and efavirenz are combined together to make a single pill [33]. Of note, drug resistance is often seen in patients that are taking HIV medication. There are so many factors that can cause drug resistance in HIV positive individuals. Literature has documented that these resistances can

occur when there are interactions between two or more medications that a person might be taking together with the antiretrovirals [28, 34]. For example, in the case where the patient has diabetes, changes in the virus itself makes it unable to respond to the medication that the patient is taking [28]. Some patients tend not to take the medicine as prescribed by the doctor, which also results in drug-resistance, for some patients it might be that the patient has been infected with the HIV drug resistant strain [28].

Due to its ability to stay concealed within the diseased blood cells, HIV remains a chronic and life-long infection, it stays hidden against the body's immune defences in what is called reservoirs and these sites are not sensitive to anti-HIV drugs. Cells such as microglia, macrophages and astrocytes are the main cellular reservoirs because the virus within these cells is replication-competent, is of archival nature and continues for longer periods of time [35]. Anatomical reservoirs are sanctuary sites that immunologically shelter the virus and this is where drug penetration is reduced. Lymphoid organs (spleen, lymph nodes), genitourinary tract and the central nervous system (brain) are the major anatomical reservoirs. These HIV-1 reservoirs are established early during primary infection and creates a major difficulty for virus eradication [35, 36].

2.1.3. ARV drug delivery

The development of effective drug delivery approaches for the treatment of HIV-1 remains a global challenge. Shortcomings such as drug resistance, drug-drug interactions and biological barriers that prevent the drug to access the potential target site are some of these challenges. Drug related challenges such as low solubility, bioavailability, premature elimination, short shelf life and off target side effects make a significant contribution to these problems [37]. While plasma drug concentrations in therapeutic dose ranges makes it more difficult due to the short half-life of these ARVs. By improving the delivery of the current available molecules, several novel drug delivery systems have been trialled for delivering ARVs. For example, the use of pre-exposure prophylaxis to prevent the establishment of chronic infection and cell specific targeting of efficacious drug concentrations by using nanomaterials such as liposomes in HIV reservoirs [38].

However, none of them has been able to address these challenges in a satisfactory manner. Although these methods are promising to a certain extent, however, alternative therapeutic modalities that can help eradicate HIV reservoirs need to be explored. To date, not much has been documented on the use lasers as drug delivery system in HIV research. Drug delivery system regulates the behaviour of medication in tissues and cells with minimal adverse side effects. Macroscopic delivery and microscopic delivery have been shown and proven to be highly effective for smart delivery systems. Lasers can be easily interfaced with microscope systems allowing single cells and sub cellular organelles to be transfected using a multitude of wavelengths and laser modalities [38]. During laser-assisted delivery of exogenous matter, the laser can be easily directed to target the desired area on the cell with very high spatial precision [39]. Since femtosecond lasers, have ultrashort pulses and high peak powers, they have been extensively used for specific excision of cell organelles and tissues. Due to nonlinear optical interaction fs lasers enable peripheral particles into a single cell without inflicting significant damage to the cell [40]. This research will therefore focus on using fs laser pulses to directly deliver ARVs *in vitro*. The next section will give an overview of lasers and their literature.

2.2. Overview of lasers and their literature

Laser is the type of light that occupies one region of the electromagnetic spectrum. The dual nature of light can make it behave as both an electromagnetic wave, or as a particle like a photon. Laser beams can have varying degrees of monochromaticity, can be temporally and spatially coherent and may propagate with a variety of irradiance profiles. It is important to

have knowledge of these characteristics to be able to predict transportation of the beam through various optical elements and to analyse the subsequent interaction with materials.

2.2.1. Laser light properties

The laser is a source of electromagnetic radiation with particular properties such as coherence, brightness or intensity, monochromaticity and directionality. These phenomena are described in detail on sections 2.2.1.1 to 2.2.1.3 below.

2.2.1.1 Laser coherence

This concept speaks to the electromagnetic waves of light rays that are in phase with each other in both space and time. For a laser, the coherent nature is derived from its generation by stimulated emission that means the emitted photon is exactly in phase with the stimulating photon [41]. There are two types of coherence i.e. spatial and temporal coherence. Spatial coherence is when the crest and the troughs of all the waves coincide along lines perpendicular to the rays. Temporal coherence, the frequency of the wavelength and speed of travel are all constant [41, 42]. Coherence plays a vital role in lasers as it distinguishes it from the other light sources, which lack this special feature.

2.2.1.2. Laser brightness or intensity

The intensity of a laser is generated from the collimation of laser light as it moves through space maintaining its concentration thus brings about the characteristics of brightness. On the other side, brightness translates to the high concentrations of energy when the laser is focused on a small spot. This is because the light spreads in small region of space and in a small wavelength range. Measuring the brightness of a light source such as a laser, would firstly help to characterize such a monochromatic, coherent, and unidirectional light but also help in accurate measure of the power intensity emitted by the light source [42].

2.2.1.3. Laser monochromaticity and directionality

Monochrome refers to all the photons that have the same wavelength, the light produced by a particular laser will be of a characteristics wavelength or wavelengths. For example, a typical incandescent light bulb emits wavelengths of the entire spectrum usually from ultraviolet through the entire visible range and then into the infrared range. While when it comes to directionality, the phenomenon speaks to little divergence of the laser beam as it exits the laser device [41]. This means the beam can travel a considerable distance with very little movement away from parallelism and if there is no divergence the laser retains its brightness.

2.2.2. Principles of Lasers

Electrons in an atom and molecules exist in very specific energy levels which are called states. In these states, the atoms possess electrons that are a characteristic to the specific element or combination of elements. The transition of an atom or molecules from one state to another can occur, such state is called quantum transition [41]. Quantum transition results when atoms interact with optical radiation. If an atom on the upper state transitions to the lower state, then the energy as a photon electromagnetic radiation can be emitted with a frequency given by the following equations:

$$V = E_2 - E_1 /h \qquad (2.1)$$

$$E_2 - E_1 = hV \qquad (2.2)$$

and

$$E = \frac{hc}{\lambda} \qquad (2.3.)$$

Where, $\mathbf{E_2\text{-}E_1}$ is the energy difference between the two levels **E2** and **E1**, which is E. h, is planks constant (6.625×10^{-34} J sec^{-1}), c is the speed of light (3×10^8 m sec^{-1}), *V* is the frequency and λ is the wavelength in (m).

On the other hand, if the atom is initially in the lower energy state and makes a transition to the higher state, then the energy is absorbed (figure 2.1(a)). By absorbing a photon, that has the energy equal to the difference between the lower state and a higher one. The electrons then move to the more energetic state, called the excited state. This state is less stable than the lower state or ground state, thus the electrons tend to give up energy by radiating the photon of energy equal to the energy difference between the two states and returning to some lower state, this transition triggers emission.

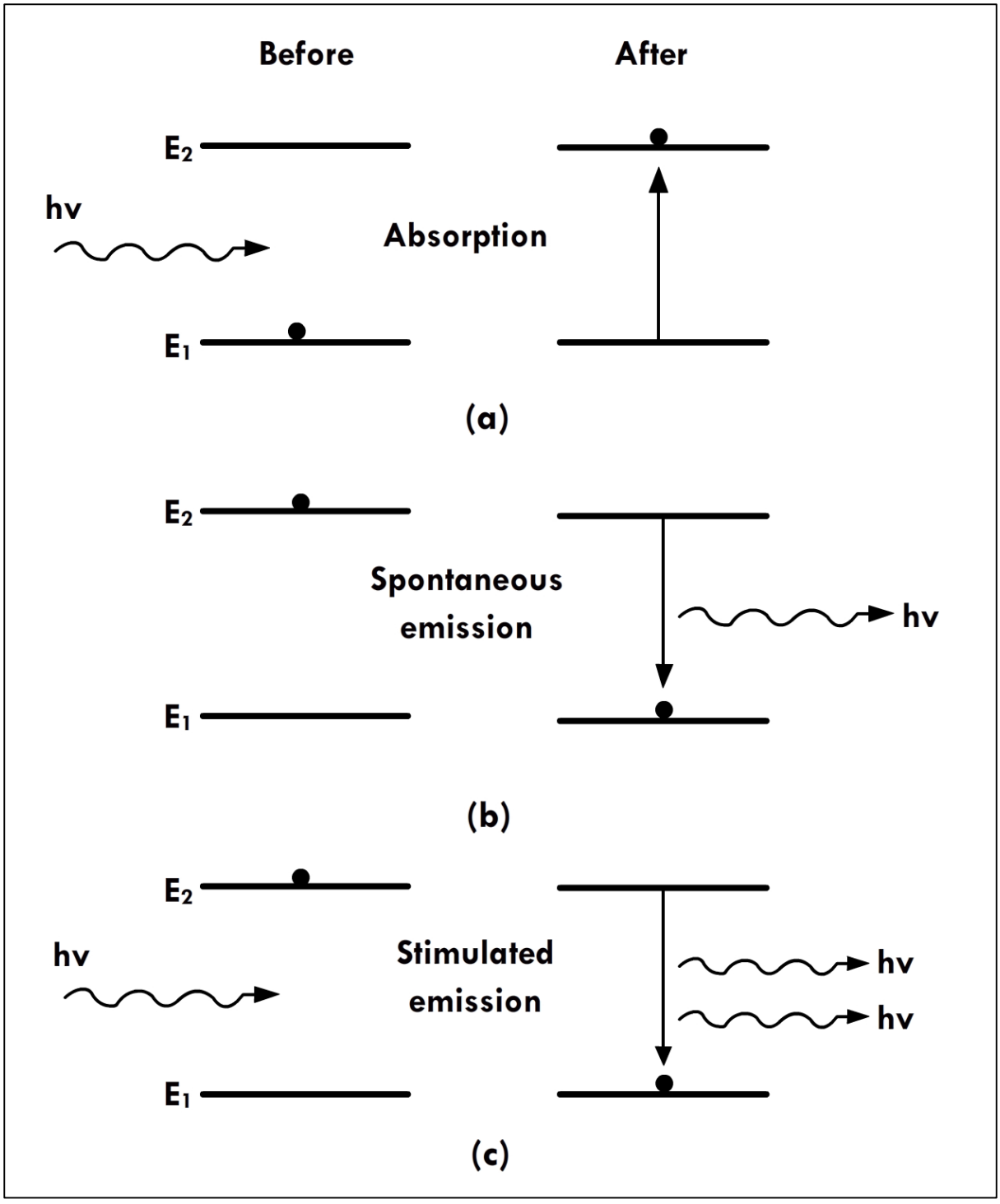

Figure 2.1: Illustration of laser emissions before and after photon absorption. (a), an electron (●) occupying the lower energy state (E1) in the presence of photon energy(hv) can be excited to higher energy level (E2) absorbing the energy of the photon. (b) An electron occupying E2 decays to E1 releasing the energy difference as photon energy, in a process is called spontaneous emission.(c) An electron occupying E2 decays to E1 releasing the energy difference as a photon energy but stimulated by the presence of a photon, the process is known as stimulated emission.[42] .

There are two ways of photon emission namely; spontaneous emission and stimulated emission. In spontaneous emission (figure 2.1.(b)), atoms at the energy level E2 decay to the level of E1 spontaneously without any stimulus, in this instance, decay of atoms, transition, direction of the emitted photons and their polarisation are all at random. On the other hand, in stimulated emission (figure 2.1.(c)), atoms lies in the upper energy level then the same incident photon may play the role of a trigger and induce the transition from E2 to E1, the transition causes an emission of a photon. This means that, the photons emitted by the electrons of laser are in same phase and move in the same direction [41, 42].

With the above mentioned emission processes, laser action is preceded by absorption of energy to populate higher levels , spontaneous emission to produce initial photons for stimulation and lastly stimulation emission for the generation of coherent output or laser. In the next section 2.2.3, elements of lasers highlighting the essential components for its operation are transcribed and discussed

2.2.3. Elements of lasers

There are three basic conditions that must be satisfied for the operation of most laser devices, the first one is the active medium which is a collection of atoms, molecules or ions that can be solid, liquid or gas states. The composition of the medium determines the wavelength, power output and name of a particular laser. Then there is the pumping source, this is the source of energy to pump the laser medium. A laser beam is generated when a laser medium is pumped in the optical cavity. The beam then leaves the cavity through the partially transmissive mirror by which the population inversion is created inside the active medium. Finally is the optical resonator, these consist of two mirrors where the laser medium is placed in the optical cavity and its axis made to coincide with common axis of the mirrors. One mirror is generally fully reflective for wavelength of operation of the laser, the other is partially transmissive, by selection of some photon states, and the suppression of the other states can be realised. The image in figure 2.2 below illustrates the basic component of the laser mentioned in section 2.2.3 above.

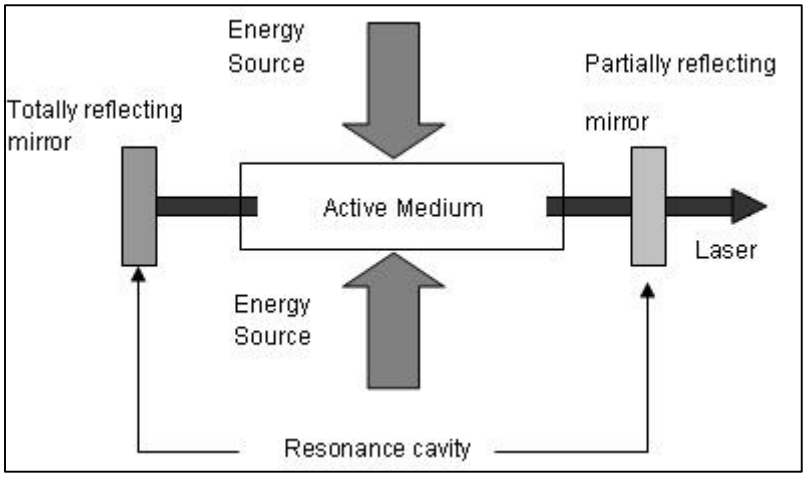

Figure 2.2: The basic components of a laser. The resonance cavity consisting of two mirrors (reflectors) totally reflective mirror (100% reflective) and the other is partially transmissive mirror (99% reflective). For light amplification and active medium consist of the pump source that adds energy to the lasing material [42].

Given these basic components, it is easier to distinguish lasers from ordinary light sources such as a tube light or incandescent lamp. To understand more about the operation of lasers, different laser modes are transcribed in the next section 2.2.4.

2.2.4. Laser modes

The distance between the resonating mirrors that determine photon wavelength is known as the longitudinal mode of a laser. The optical cavity is structured to optimize the amplification of only one frequency in order to maintain monochromaticity [43]. On the other hand, the transverse electromagnetic mode (TEM) is defined as the distinctive energy distribution pattern across the face of the beam. For example, when we have a Gaussian or a normal distribution of energy across the beam, the highest power intensity occurs with a TEM beam. Furthermore, lasers can operate in the following modes; the continuous wave mode (CW), these lasers emit beams in an uninterrupted continuous manner. They usually employ gas as their lasing medium. In this CW mode, the partially transmitting end of the optical cavity allows a fraction of the light energy to escape, and the energy that is pumped in the lasing medium to be maintained without any interruptions. Described secondly are the pulsed mode lasers, where, pulses are a temporal sequence of laser beams that have an on and off cycle. These cycles are either gated or pulsed electronically. The gating allows the duration of the pulses to be compressed, thus, allowing the production of a corresponding increase in peak power that is much higher than what was observed with the continuous mode. Then there are Q-switched lasers, this mode allows the generation of laser pulses of short duration from few nanoseconds to few tens of nanoseconds and high peak power. The q-switched mode is achieved by introducing a shutter

into the optical cavity of the laser, the energy in the active medium is raised to the level far above such that there is an obstruction in the system. Then, when the shutter is opened to permit light in the cavity, all the stored energy is released in an extremely short period [42, 43].

Given that, light in a laser beam can be either continuous or pulsed, and is usually coherent unlike other light beams, they have numerous distinct applications. The coherence of laser's light differ resulting in modes of operation mentioned above that optimize a laser's performance for various applications. For the purpose of this study, a pulsed laser was utilized. In the next section 2.2.5 laser interaction with tissues is described in detail with relevance to the study.

2.2.5. Laser interaction with tissues

Laser light is the kind of energy that can be directed to the tissue surface, where it can be either reflected and refracted, scattered, absorbed or transmitted in order to achieve an anticipated effect [43]. Depending on the optical properties of the tissue like its reflectivity, scattering and absorption coefficients, parameters such as wavelength, energy, pulse duration, operation mode and output spectral profile play a crucial role when it comes to the fractional intensity absorbed by the tissues and its processes.

In medicine, lasers have been used for surgery, whereby they are used to monitor and control the tissue response. In eye surgery for instance, the laser can be used for measuring of blood velocity as well as laser fluorescence bronchoscope to detect tumors in early phases. Lasers offer high precision, the possibility of operating in inaccessible areas and limited damage to blood vessels and surrounding tissues [43, 44]. Nonetheless, lasers can also be used in delivery to introduce foreign material into tissues of interest by improving cell membrane permeability allowing transportation of substances to enter into the cytoplasm without damaging the cell membrane.

Of note, in the optical properties that govern the laser interaction with tissues; refraction plays a role when irradiating transparent media like corneal tissue. Laser light passing through the tissues, undergoes multiple scattering processes, and transformed from a narrow collimated beam into a broad diffuse beam. When it comes to scattering, the scattering coefficient increases with the increase in the wavelength, however, during absorption, the intensity of an incident light is attenuated by passing through the medium due to partial conversion of light energy to heat energy of the absorbing material. The ability of a medium to absorb electromagnetic radiation depends on factors such as electronics constitution of its atoms and

molecules, wavelength of radiation, the thickness of the absorbing layer and the parameters temperature and concentration [43]. The most important laser property that decides the suitability for surgical procedure is the penetration depth of its radiation in the tissue this property changes significantly with the wavelength of the laser radiation.

In biological tissue, water molecules or macromolecules such as proteins and pigments can cause absorption. Absorption of infrared light can be attributed to water molecules, while proteins and pigments absorb UV and visible light. The absorbed portion of the laser radiation can produce photochemical or photothermal effects depending on the wavelength of the laser radiation and nature of the tissue [43, 44, and 45]. It can also produce fluorescence based on the emission. When applying laser light to biological tissue, a variety of interaction mechanisms may occur due to the specific tissue characteristics and laser parameters. In this study, only the interaction of light with biological tissue using the wavelength independent mechanism highlighted. Tissue interaction with laser light depends on power density and pulse duration. It is known that when using power densities that exceeds 10^{11} W cm^{-2} or 10^{14} W cm^{-2}, where pulse duration is in picoseconds or femtosecond range, multiphoton ionization of atoms and molecules may occur, this phenomenon is called optical breakdown [46]. Optical breakdown is associated with physical effects such as plasma formation and shockwave generation where there will be a breakdown of the plasma membrane with a significant reduction of plasma energy and disruptive effects. This is ideal for the treatment of cells with minimal damage that the study is exploring. Cavitation and jet formation take place when this breakdown occurs in soft tissues [44, 45]. Furthermore, clean and well defined removal of tissue without any thermal or mechanical damage can be achieved given that the laser parameters are well suited for the application [44, 45, and 46].

2.2.6. Laser light delivery system

Over the years, we have seen lasers evolving in the medical field where the development of minimally invasive techniques and surgery has escalated the need for small efficient energy delivery system [45, 47]. Laser light delivery systems can be defined as the controlled transport of light between a light source and a target tissue. This light source can be anything from a light bulb emitting broadband incoherent spectrum or coherent monochromatic laser. Lasers can be used for both therapeutic and diagnostic applications. Ultra-fast lasers such as femtosecond lasers in particular have been seen to have developed over the years and play a vital role in the field of biomedicine [45]. An example includes the non-invasive therapy involving femtosecond laser pulses in a two photon based procedure for the reversal of

cataracts on human eye lenses [45]. Furthermore, in cell biology, the exposure of cells to high intensity ultrashort optical pulses has shown to improve localized cell membrane permeability when using a femtosecond laser during laser cell interaction studies [45, 47]. That is, when a beam of fs laser pulses is tightly focused on the mammalian cell membrane, the membrane is induced which results in the increased permeability through a multi-photon poration process. Such cell perforation leads to the uptake of various biological media within the vicinity of the cell before the cell membrane can self-heal [45, 47]. Photoporation is a photonics based technique where ultrafast laser pulses are employed to disrupt the cellular membrane, allowing membrane-impermeable substances passage into the cytoplasm. Optically assisted transfection is the process in which a highly localised laser beam alters the permeability of the plasma membrane of the cell, thereby allowing the entry of the extracellular nucleic acids [48]. Using different light sources such as continuous wave lasers and femtosecond lasers optical transfection has shown to be a promising non-viral method that has benefits of spatially targeted therapy because of its ability to permeate the lipid bi-layer cell membrane in a sterile and relatively non-invasive environment [48, 49].

Although transfection efficiencies differ from the application of different laser types, femtosecond laser irradiation provides a transient permeability of the cell membrane through a multiphoton process [49]. This technique also allows selective dosing in a population of cells. Different studies have reported that femtosecond laser pulses enable the creation of spatially confined chemical, thermal and mechanical effects in biological media [49, 50, 51]. The membrane permeation mechanism varies depending on the laser wavelength and the pulse duration [49]. To date there is a lot of improvement on the optical transfection technique, the use of focused laser beam pulses to transiently perforate the cell membrane in order to allow exogenous material into the cell offers numerous rewards over traditional methods. Femtosecond laser pulses have been the most efficient photo-translocation tool to date, which also offers single cell selectivity [49, 50, 51, 52]. In this chapter, the use of femtosecond laser pulses in a photo-translocation system to deliver ARVs into HIV-1 infected TZM-bl cells was explored. In addition, the influence of ARVs and lasers on cellular processes after photo-translocation using different biological assays was investigated.

2.3. Experimental Methods

Sections 2.3.1 to 2.3.8.details the experimental methodology of how fs laser pulses promotes ARVs targeted delivery in HIV-1 infected TZM-bl cells.

2.3.1. Cell culture

The adherent TZM-bl (ATCC, PTA-5659) and 293T/17 (ATCC, CRL, 11268) cell lines (Sigma-Aldrich, South Africa) were used for this study. TZM-bl cells were maintained in Dulbecco's minimal essential medium (DMEM) growth medium (Sigma-Aldrich, D5796) containing 10% fetal bovine serum and 1% L-Glutamine-Penicillin-Streptomycin (Sigma-Aldrich, G6784). The cells were harvested using trypsin/EDTA solution (Sigma-Aldrich, T4049) and placed at 37^0C incubator with 5% CO_2 and 85% humidity. The adherent 293T/17 cells were used to produce pseudoviruses, which were used to infect TZM-bl cells.

2.3.2 Pseudovirus production and *in vitro* infection

HIV-1 Env pseudoviruses were produced by transfecting 293T/17 cells using the superfect transfection reagent, following protocol by Li *et al,* 2005 [53]. A total volume of 3 x 10^6 cells/ml were seeded in a T75 flask with 4 µg of HIV-1 plasmid and 8 µg of env HIV-1 plasmid backbone. The supernatant containing pseudoviruses was harvested after 48 hours and filtered with a 0.45 µm filtration system. The 50% tissue infectious dose ($TCID_{50}$) assay was used to determine pseudovirus infectious titre. A fivefold serial dilution of pseudoviruses was added in each well of the 96 well plate and then freshly trypsinised TZM-bl cells (2 x10^5) containing 25 µg/ml of dextran (Sigma-Aldrich, D9885) was added to each well. The plate was incubated at 37^0C in a humidified 5% CO_2 and 85% humidity. After 48 hours incubation, 100 µl of the culture media was removed from each well and 100 µl of the luciferase reagent was added to the cells. After 2 minutes incubation at room temperature, 150 µl of the cell lysate was transferred to a 96 well plate and luminescence was measured using the Glomax®Discover System.

2.3.3. Optical setup

A custom made inverted microscope photo-translocation setup was assembled together by combining a 60X objective lens of 0.8 numerical aperture (NA) and Gaussian laser beam at 800 nm from a coherent regenerative Titanium Ti:sapphire femtosecond amplifier with a repetition rate of 1 KHz (Kilohertz) and producing 130 fs pulses of up to 1 watts (W) average power. As shown in figure 2.3, the optical train of the laser output was sent through the half wave ($\lambda/2$) plate and a polarising beam splitter (PBS) in order to attenuate and control the laser beam power at the sample stage, thereby preventing damage to the cell membrane. The half wave plate was set at an angle relative to normal that produces approximately 80% laser power reduction after the PBS. For this work, the output power of the femtosecond laser was around 720 mW and the measured power after the PBS was about 140 mW. In addition, a neutral

density filter was inserted on the beam path to further reduce and obtain the desired photoporation laser power at the sample stage.

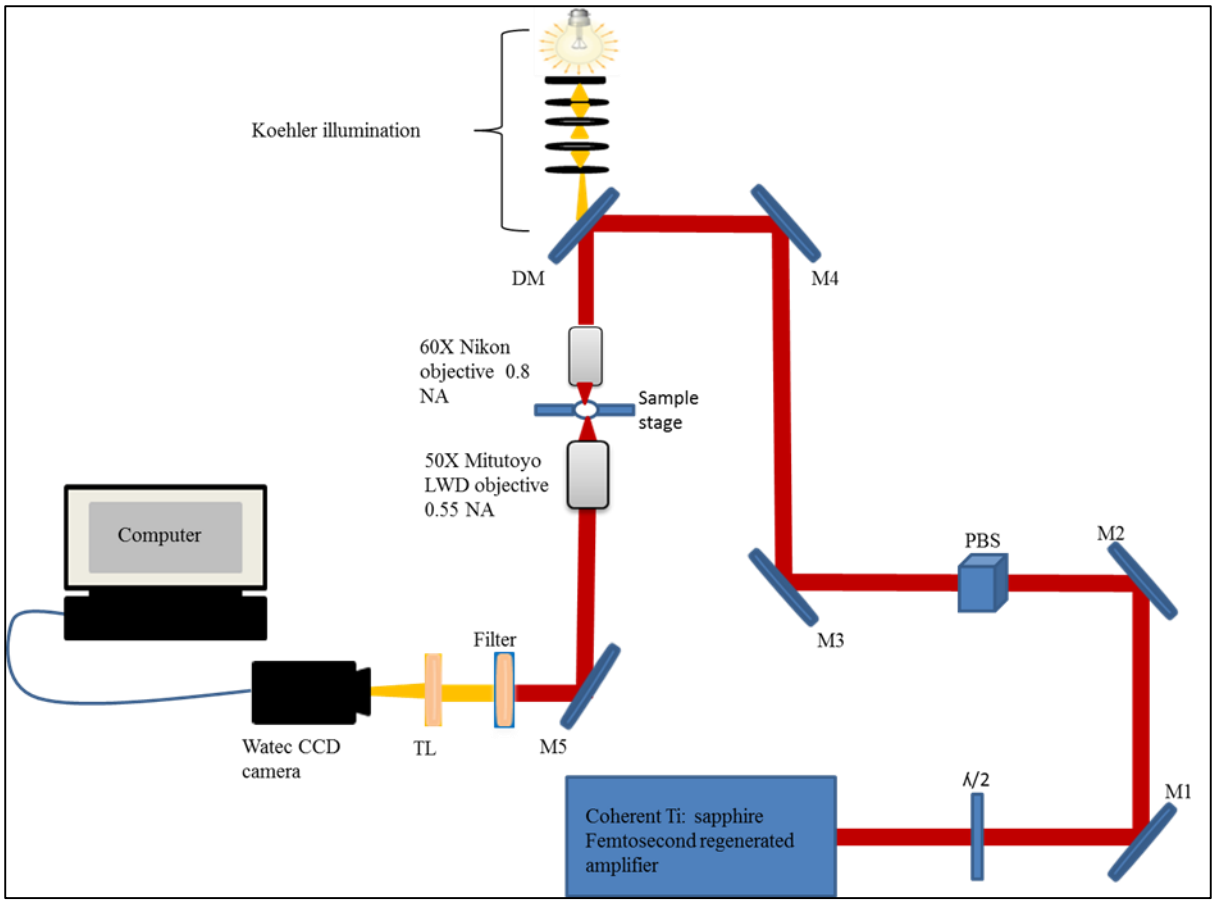

Figure 2.3: An illustration of a non-invasive translocation optical setup used to deliver ARVs into HIV-1 infected TZMbl cells. Koehler illumination provides light to the sample stage through a light emitting diode (LED). Mirrors (M1-M4) were used to direct the beam to the sample stage. The dichroic mirror (DM) was used to reflect the beam via Mirror 5 and transmit the white light to overfill the back aperture of the 60X air objective. The imaging system consisted of the long working distance Mitutoyo 50X objective together with a tube lens that transmits the image to the charged couple device (CCD) camera

A dichroic mirror (DM) was used to reflect the 800 nm laser beam and transmit the white light toward the back aperture of the 60 X objective lens of numerical aperture 0.8 (Nikon MRP 01902). This short working distance 60 X objective lens was utilised to focus and deliver the laser beam with a spot size of 1.22 µm at the sample stage. An automated shutter (Uniblitz electronics LS652ZMI) was aligned on the optical path to control the number of the laser pulses on the cells at the sample stage. An imaging system consisted of Koehler illumination, a long working distance 50 X Mitutoyo objective together with a tube lens, which transmits the image

to the charged couple device (CCD) camera (Watec W96N15832), was used to visualise the photoporated cells. The optimum power for the translocation studies was determined by performing trypan blue studies into TZM-bl cells and it was adjusted to 4 µW with the beam exposure time set to 10 ms at the focus, this is performed in order to preserve cell viability

2.3.4 Photo-translocation of ARVs into TZM-bl cells

Translocation of antiretroviral drugs; nevirapine, efavirenz, ritonavir and raltegravir into HIV infected TZM-bl cells was performed via a femtosecond laser of wavelength 800 nm at one dose of 4 µW and 10 ms laser to cell exposure time . Adherent TZM-bl cells were cultured in a 35 mm glass bottom petri dish with a 23 mm diameter coated with poly-d-lysine (World Precision Instruments, FD35PDL-100). Prior the addition of drugs, the cells were washed with 1 ml of 1X Hanks Balanced Salt Solution (HBSS, Gibco, 14170-088) and then immersed in 20 µl of neat growth media containing a final concentration of 10 µg/ml of each drug. To observe the difference between laser treated drug delivery and the innate uptake of the drugs by the cells, control dishes with the same conditions were also prepared. The plates were washed with 1X HBSS after laser treatment, covered in 2 ml growth media and incubated overnight before assessing biological responses. Cellular morphology was performed using a bright field microscope before assessing biological responses using biological assays.

2.3.5 Cellular viability

Following laser treatment, the CellTiter-Glo®luminescent assay (Anatech, Promega, G7573) was used to determine viable cells by quantifying adenosine triphosphate (ATP) present in metabolically active cells. During the experiment, 50 µl of the substrate reagent and the cell suspension was added to the plate and the solution was mixed on an orbital shaker for 2 minutes to lyse the cells. For the signal to stabilize, the plate was incubated for 10 minutes in the dark at room temperature. Luminescence was read in relative light units (RLUs) using the Glomax®Discover System.

2.3.6 Cellular cytotoxicity

Cell cytotoxicity was evaluated by using the non-radioactive CytoTox96® assay (Anatech, Promega, G1780) which measures the amount of cytoplasmic lactate dehydrogenase (LDH) that is released by the cells into the medium when there is cell membrane damage. The supernatant was removed from the plates and transferred into 2 ml Eppendorf tubes. Before, the tubes were spun down at 2200 rpm (rotations per minute). Then, 50 µl of the cell supernatant was added to each well of the 96 well plate and an equal volume of the LDH

substrate mix was added. The plate was incubated for 30 minutes in the dark at room temperature; thereafter 50 µl of the stop solution was added to each well. Absorbance was read at a wavelength of 490 nm using the Glomax®Discover System.

2.3.7 Luciferase assay

To determine the infection efficiency of the virus in the cells, the luciferase activity was assessed using the Bright Glo™luciferase assay. Here, TZM-bl cells expressing the luciferase reporter gene under the control of HIV-1 long terminal repeats (LTR); when exposed to HIV-1 infection, the luciferase gene will be expressed. During the assay, 100 µl of the cell suspension was added to an equal volume of luciferase reagent and incubated for 2 minutes in the dark. Quantification of luciferase activity was read using the Glomax®Discover System. The RLUs are directly proportional to the number of infectious virus particles present in the initial inoculum.

2.3.8 Data analysis

In this study, the experiments were performed in duplicates and repeated four times (n = 4). Microsoft Excel was used as a data analysis tool where averages, standard deviations and standard errors were calculated to denote the results. The T-test was used to determine the statistical significance between the controls and the experimental groups. The results were considered significantly different at $P < 0.05$. The statistical differences between the controls and the experiment groups are represented on the graphs for all the assays performed as; (*) = $P < 0.05$, (**) = $P < 0.01$ and (***) = $P < 0.001$.

2.4. Results and Discussion

Although the current human immunodeficiency virus (HIV-1) treatment regime possesses the ability to reduce the viral load to undetectable levels; complete eradication of the virus cannot be achieved while latent HIV-1 reservoirs go unchallenged. The antiretroviral drugs (ARVs) used for the treatment of HIV-1 infection were designed based on the five major stages of the virus life cycle namely, the nucleoside reverse transcriptase inhibitors (NRTIs), non-nucleoside reverse transcriptase inhibitors (NNRTIs), protease inhibitors (PI), integrase inhibitors and entry inhibitors.

The HIV-1 virus infection cycle is shown in the figure 2.4 below. After the virus enters the cell, the NRTIs (2) and NNRTIs (2) are responsible for blocking and interfering with the virus, making it difficult for the virus to replicate, the PIs (3) prevents the virus from making copies

of itself, while Integrase inhibitors (4) blocks the integrase enzyme that is needed for the virus to infect the T lymphocyte cells.

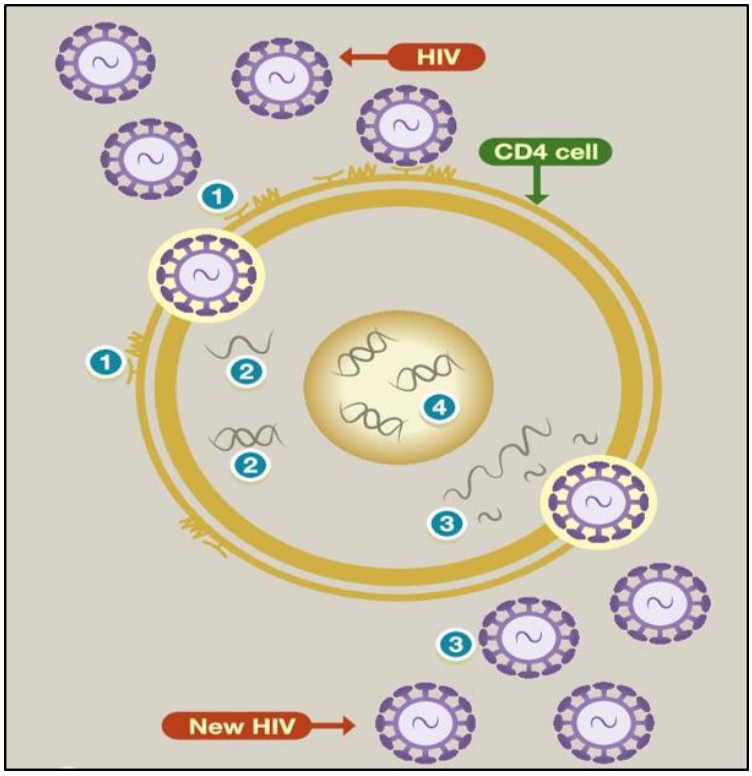

Figure 2.4: An image that shows the action sites of different ARV classes of the HIV cycle. 1 shows entry inhibitors that prevent virus from entering the cell. 2 shows the NRTIs and NNRTIs which prevents the production of DNA to RNA. 3 show protease inhibitors that disrupt the production of the new HIV virus and 4 integrase inhibitors that prevent the virus from integrating on the host cell DNA. Reproduced with permission from reference [26].Copyright (2018) Elsevier.

With the advent of highly active antiretroviral therapy (HAART), the prognosis of HIV-1 has improved significantly. However, HAART has issues such as the cumbersome lifelong treatment, development of drug resistant strains of HIV-1 and unavoidable side effects [10, 27] Therapeutic targeting of HIV-1 therefore requires further investigation and current therapies need modification in order to address this challenges. This situation therefore deflected research towards investigating the potential of novel antiretroviral drug delivery systems. One such approach involves the use of femtosecond laser pulses in promoting targeted delivery of ARVs in an *in vitro* proof of concept study. The idea behind the optical drug delivery revolves around using ultrafast laser pulses with extremely high peak powers to precisely disrupt the cell plasma membrane, in order to allow immediate transportation and expression of exogenous matter into live mammalian cells. The use of lasers for the introduction of exogenous material

in the cells has shown to be a robust tool that not only provides sterility, but is also non-invasive, beneficial and non-toxic to the cells [27, 54]. In the current study the use of femtosecond pulses as a drug delivery system to deliver ARVs into HIV-1 infected TZM-bl cells was demonstrated. Additionally, following laser treatment, cellular responses such as changes in ATP, LDH and the luciferase enzyme were evaluated. In sections 2.4.1 to 2.4.5 my results are presented and discussed.

2.4.1 Cellular Morphology

A bright field light microscope was used to evaluate cellular morphology. This was done to assess the structural changes and form of the cells (Figure 2.5).

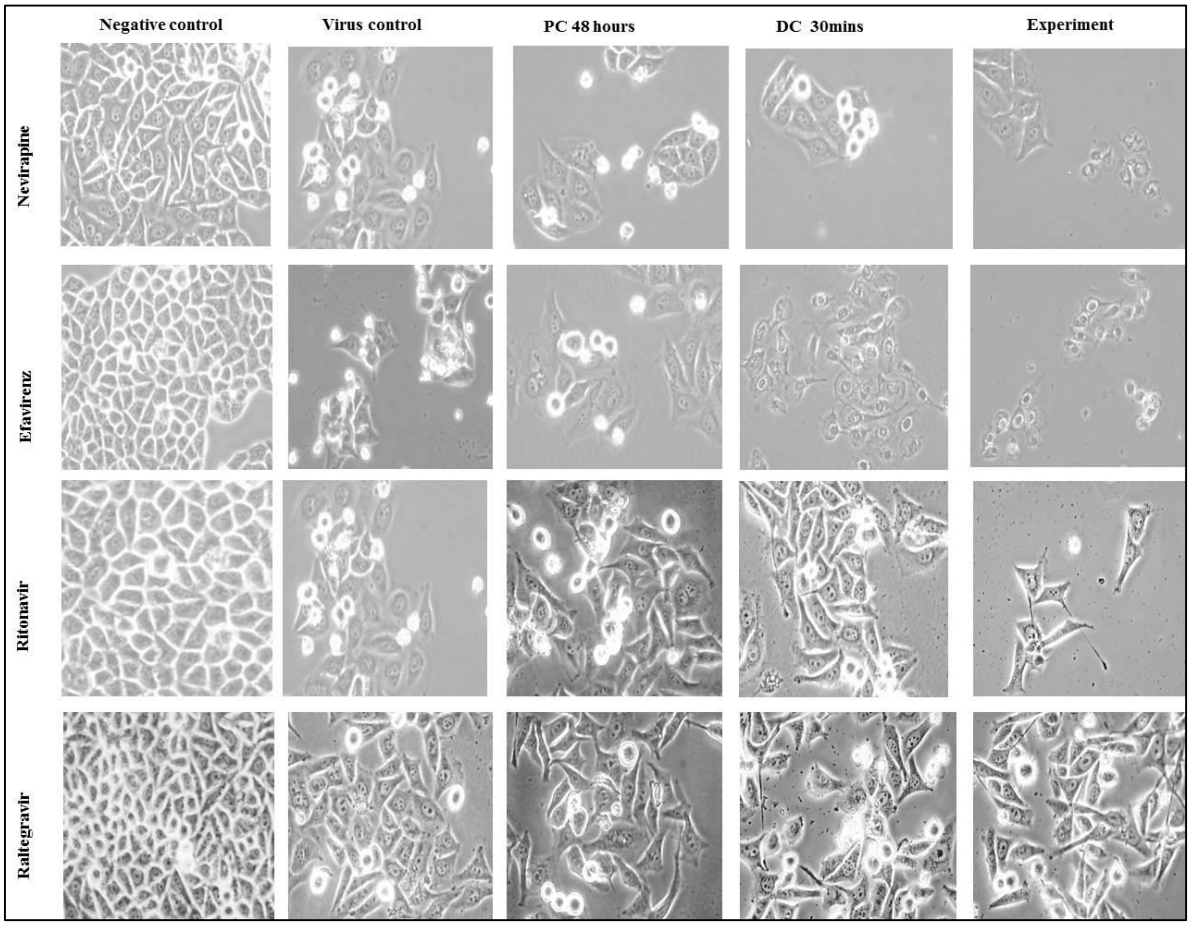

Figure 2.5: An image showing the changes in cellular morphology of the negative control (NC=uninfected non-irradiated cells with no ARVs), virus control (VC=non-irradiated infected cells), positive control (PC 48 hours=non-irradiated infected cells incubated with ARVs for 48 hours), drug control (DC 30 mins =non irradiated infected cells incubated with ARVs for 30 minutes) and the experiment (EXP=irradiated infected cells incubated with ARVs for 30 minutes Antiretroviral drugs applied included nevirapine, efavirnez, ritonavir and raltegravir.

The negative control (NC = uninfected non-irradiated cells with no ARVs) showed no changes in cellular morphology and the cells grew as a monolayer sheet of cells. On the contrary, the virus control (VC = non-irradiated infected cells) showed changes in cellular morphology where cells rounded up and some detached from the culture dish as an indication of cells undergoing stress. These changes in cellular morphology correlate with that of cells undergoing cell death after exposure to HIV-1 [55]. The positive control (PC = non-irradiated infected cells incubated with ARV's for 48 hours) also showed changes in cellular morphology when compared to NC and these changes were similar to that of VC with efavirenz and nevaripine showing the most damage to TZM-bl cells. These results suggest that a combination of ARVs and HIV-1 is toxic to TZM-bl cells. Similarly to VC and PC, the drug control (DC = non irradiated infected cells incubated with ARVs for 30 minutes) also showed changes in cellular morphology. The same changes in cellular morphology were noted in the experiment (EXP = irradiated infected cells incubated with ARVs for 30 minutes). The cell damage noted in all the HIV infected cells is due to the HIV-1 inducing cytopathic effects on the cells. These can cause them to round up and fuse with adjacent cells, which can in turn result in the formation of syncytia and the appearance of cytoplasmic or nuclear inclusion bodies [34].

2.4.2 Cellular viability assay

The ATP assay was used to assess cellular viability. The virus control (VC), showed a significant decrease in cellular viability when compared to the negative control, (NC) $P < 0.05$ (Figure 2.5). A similar decrease in cellular viability was seen in the positive control (PC), drug control (DC) and the experiment (EXP), except in the case of the drug control using nevirapine and raltegravir. The PC showed more reduction in cellular viability as compared to the VC and this suggests that the ARVs used in this study were toxic to the TZM-bl cells, which is in agreement with what was observed in the cellular morphology study. In the PC, cells were exposed to ARVs for a prolonged period (48 hours) of time than any other group and hence a reduced ATP content than the other groups (Figure 2.6).

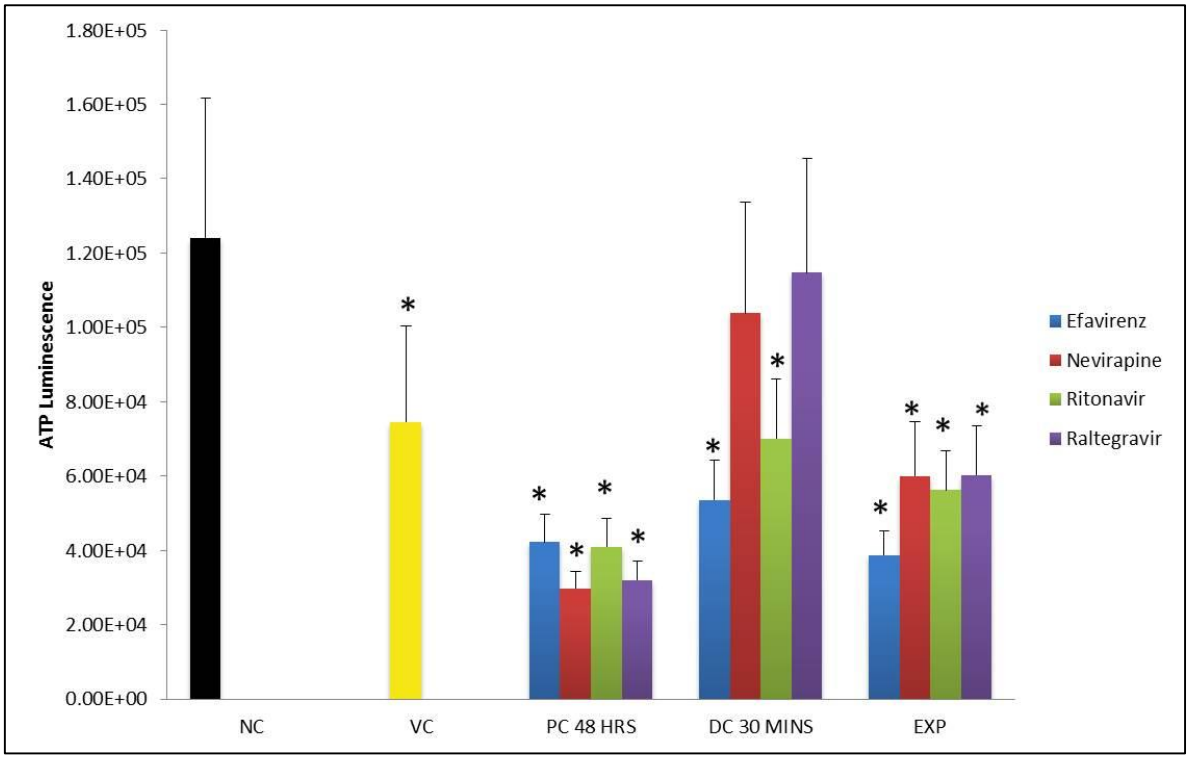

Figure 2.6: ATP assay measuring the viability of the NC,VC, PC, DC and EXP. Significant differences between the NC and all the other groups are represented in the graph as (*) = $P < 0.05$. Error bars represents the standard error of the mean where n = 4.

In literature, the reactive oxygen species (ROS) generated during HIV infection have been shown to be responsible for many aspects of the HIV-1 pathogenesis which includes; increased viral replication, reduced cell proliferation and viability, loss of immune function and excessive weight loss [57]. Of note, ARVs have also been shown to induce ROS production, therefore, the reduced cellular viability after HIV-1 infection and administration of ARVs could be attributed to the generation of ROS. The ROS produced during HIV-1 infection and ARVs administration can be hydrogen peroxide (H_2O_2), singlet oxygen (O_2), hydroxyl free radicals (OH) or superoxide anions ($O2^-$) which results in oxidative damage to cellular components or cell death [58].

Previous studies have shown that ARVs induces toxicity in many cell lines. Robertson *et al*, 2012 [59] demonstrated the first evidence for ARV induced toxicity in primary rat neurons.

2.4.3 Cytotoxicity Assay

The LDH assay was used to evaluate cell membrane damage and the results obtained are presented in Figure 2.7 below.

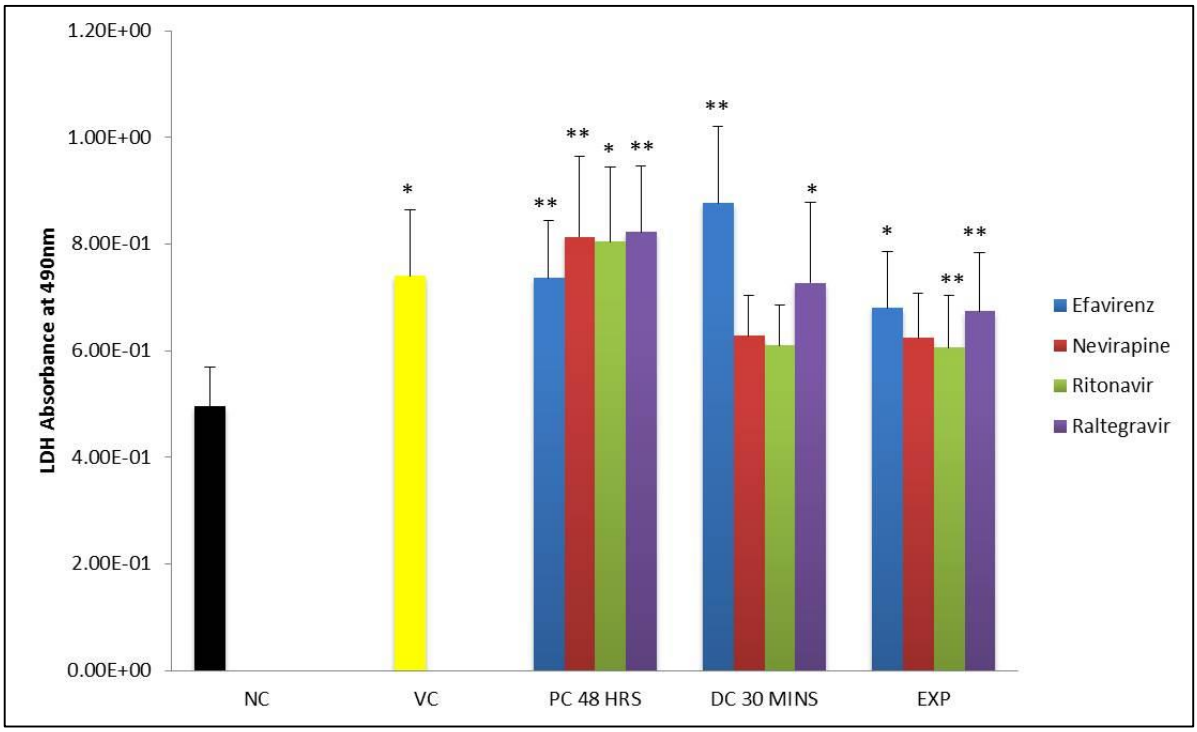

Figure 2.7: LDH assay assessing cell membrane damage of NC, VC, PC, DC and EXP. Significant differences between the NC and all the other groups are represented in the graph as (*) = P <0.05 and (**) = P <0.01. Error bars represents the standard error mean where n=4.

Here, the VC showed a significant increase in the amount of LDH released by the cells when compared to the NC, $P < 0.05$. A similar trend was seen in the PC, DC and EXP. There were no statistically significant differences noted in the amount of LDH released by the cells when the NC was compared to the DC and EXP exposed to nevirapine. This correlates with the data of the ATP assay where cells in which DC was exposed to nevirapine in the assay showed a similar cellular viability to that of the negative control.

An increase in the LDH was noted in the HIV-1 infected cells in the absence or presence of ARVs indicates that HIV-1 infection together with the addition of ARVs induces cellular membrane damage. The interaction of the virus with the cell membrane induce alterations of the cells such as appearance of cytoplasmic inclusion bodies, formation of secondary messengers and movement of ions which leads to changes in cellular activities [60, 61]. A study by Cohen, 2010 [62] noted that HIV-1 interacts with the host cell membranes within minutes of adsorption of the virus and causes changes in intracellular ion concentrations, osmotic driven fluid entry and swelling of the cells and eventually cell death. In general, the PC group which were cells exposed to ARVs for 48 hours showed the greatest cell membrane

damage than the other groups suggesting that prolonged exposure of cells to ARVs could be toxic.

2.4.4 HIV-1 Inhibition Luciferase Assay.

HIV infection was measured using the luciferase assay in the TZM-bl cells, here, the VC showed a significant increase in the luciferase activity when compared to the negative control NC, $P < 0.01$ (Figure 2.8). This result shows that HIV-1 infection took place after introduction of the pseudovirus since luciferase activity is expected to increase after HIV-1 infection due to the expression of the luciferase gene in the TZM-bl cells. On the contrary, PC showed a reduction in luciferase activity when compared to VC and for this group; the luciferase activity was similar to that of the NC. These results were expected, since ARVs are known to reduce HIV infection and in this study, exposure of infected cells to ARVs for 48 hours was adequate to reduce the luciferase activity. The DC showed a significant increase in the luciferase activity when compared to the NC. The statistical difference for efavirenz, nevirapine, ritonavir and raltegravir were $P < 0.01$; $P < 0.001$; $P < 0.001$ and $P < 0.01$ respectively, see Figure 2.8.

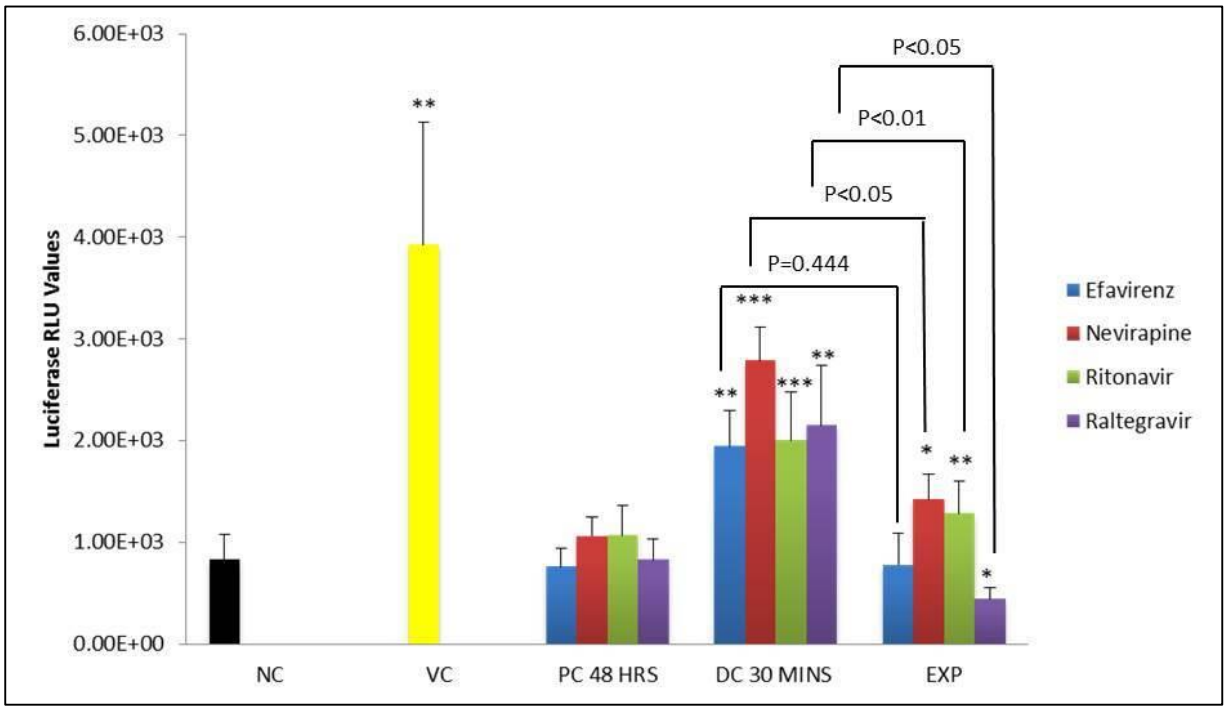

Figure 2.8: Graph showing luciferase activity assay as a measure of HIV infection in the NC,VC, PC,DC and EXP. Significant differences between the NC and all the other groups are represented in the graph as (*) =P<0.05, (**) = P<0.01 and (***) = P<0.001. Error bars represents the standard error mean where n=4.

On the contrary, when the VC was compared to the DC, there was a decrease in the luciferase activity. ARVs reduces HIV-1 infection and hence the reduction in the luciferase activity in

the DC. Since TZM-bl cells in the DC were exposed to ARVs for only 30 minutes, the reduction in luciferase activity was not lower than that of the PC, where HIV-1 infected cells were exposed to ARVs for 48 hours. In the EXP group, there was a further reduction in luciferase activity as compared to the DC. The statistical difference for efavirenz, nevirapine, ritonavir and raltegravir were $P = 0.444$; $P < 0.05$; $P < 0.001$ and $P < 0.05$ respectively. These results show that drug delivery of ARVs using the femtosecond laser pulses was much more effective in reducing the HIV-1 than the passive diffusion of ARVs in the DC.

Raltegravir, which is an integrase inhibitor, showed the highest reduction in luciferase activity in the EXP group. Raltegravir inhibits the HIV-1 integrase enzyme that is responsible for the transfer of virally encoded DNA into the host chromosome, which is a vital step in HIV-1 replication [63]. Raltegravir was followed by efavirenz, which is a non-nucleoside reverse transcriptase inhibitor (NNRTI) in reducing HIV-1 infection. Efavirenz has been shown to be as effective as Raltegravir in reducing viral infection and is included in the initial regimen in developing countries due to its low costs, efficacy and convenient dosage schedule [64]. In reducing HIV-1 infection, Efavirenz was followed by ritonavir, which is a protease inhibitor (PI), and nevirapine, which is a NNRTI. The targeting of protease enzyme by the PI during HIV-1 infection is important in disrupting the viral replication resulting into immature and defective virus [65].

2.5. Conclusions

The development of HAART has improved the quality of life and increased survival of HIV-1 infected individuals, but shortcomings such as poor bioavailability, drug toxicity, viral reservoirs and drug resistance strains have been the major obstacle for the complete eradication of the disease. Majority of the ARVs used for the treatment of HIV-1 cannot reach the inaccessible HIV viral reservoirs. Promising drug delivery systems such as the use of pre-exposure prophylaxis to prevent the establishment of chronic infection and cell specific targeting of efficacious drug concentrations in the HIV reservoirs have been explored, however the inability of the ARVs to cross the blood brain barrier makes the eradication of the virus in the reservoir impossible. To date there is still no cure for HIV-1 and the vaccines attempts have been unfeasible. With its benefits of non-invasive and non-toxic therapeutic treatment to cells, femtosecond lasers pulses have proven to be the most powerful tool as a photo-translocation technique. This study successfully demonstrated the use of fs laser pulses in promoting targeted

optical drug delivery of ARVs into HIV-1 infected TZM- bl cells and that this laser aided drug delivery system efficiently reduces HIV-1 viral infectivity *in vitro*. Further work will involve the integration of an endoscope-like optical fibre to these optical drug delivery system *in vivo* applications.

References

1. Bazzoli C, Jullien V, Le Tiec C, Rey E, Mentré F, Taburet AM. Intracellular pharmacokinetics of antiretroviral drugs in HIV-infected patients, and their correlation with drug action. Clinical pharmacokinetics. 2010 Jan 1;49(1):17-45.

2. Ramana LN, Anand AR, Sethuraman S, Krishnan UM. Targeting strategies for delivery of anti-HIV drugs. Journal of Controlled Release. 2014 Oct 28;192:271-83.

3. Who UN, Unicef. Global report: UNAIDS report on the global AIDS epidemic 2013. Geneva: UNAIDS. 2013:3-5

4. Http://www.unaids.org/sites/default/files/media_asset/UNAIDS_FactSheet_en.pdf

5. Ramana LN, Sethuraman S, Ranga U, Krishnan UM. Development of a liposomal nanodelivery system for nevirapine. Journal of biomedical science. 2010 Dec;17(1):57C.

6. Hammer SM, Saag MS, Schechter M, Montaner JS, Schooley RT, Jacobsen DM, Thompson MA, Carpenter CC, Fischl MA, Gazzard BG, Gatell JM. Treatment for adult HIV infection: 2006 recommendations of the International AIDS Society–USA panel. Jama. 2006 Aug 16;296(7):827-43

7. A. Mandas, E.L. Iorio, M.G. Congiu, C. Balestrieri, A. Mereu, D. Cau , S. Dessì and N. Curreli. *J Biomed Biotechnol*. **2009**,*749*, 575.

8. Malim MH, Cullen BR. HIV-1 structural gene expression requires the binding of multiple Rev monomers to the viral RRE: implications for HIV-1 latency. Cell. 1991 Apr 19;65(2):241-8.
9. Vyas TK, Shah L, Amiji MM. Nanoparticulate drug carriers for delivery of HIV/AIDS therapy to viral reservoir sites. Expert opinion on drug delivery. 2006 Sep 1;3(5):613-28.
10. Mallipeddi R, Rohan LC. Progress in antiretroviral drug delivery using nanotechnology. International journal of nanomedicine. 2010;5:533
11. Alexaki A, Liu Y, Wigdahl B. Cellular reservoirs of HIV-1 and their role in viral persistence. Current HIV research. 2008 Sep 1;6(5):388-400.
12. Rizvi SA, Saleh AM. Applications of nanoparticle systems in drug delivery technology. Saudi Pharm J 26: 64–70.

13. Betageri GV, Deshmukh DV, Gupta RB. Oral sustained-release bioadhesive tablet formulation of didanosine. Drug development and industrial pharmacy. 2001 Jan 1;27(2):129-36.
14. Désormeaux A, Bergeron MG. Liposomes as drug delivery system: a strategic approach for the treatment of HIV infection. Journal of drug targeting. 1998 Jan 1;6(1):1-5.
15. Iannazzo D, Pistone A, Romeo R, Giofrè SV. Nanotechnology approaches for antiretroviral drugs delivery. J Aids Hiv Infec. 2015;1(2):1-3.
16. Chattopadhyay N, Zastre J, Wong HL, Wu XY, Bendayan R. Solid lipid nanoparticles enhance the delivery of the HIV protease inhibitor, atazanavir, by a human brain endothelial cell line. Pharmaceutical research. 2008 Oct 1;25(10):2262-71.
17. Mamo T, Moseman EA, Kolishetti N, Salvador-Morales C, Shi J, Kuritzkes DR, Langer R, Andrian UV, Farokhzad OC. Emerging nanotechnology approaches for HIV/AIDS treatment and prevention. Nanomedicine. 2010 Feb;5(2):269-85.
18. Terakawa M, Tsunoi Y, Mitsuhashi T. In vitro perforation of human epithelial carcinoma cell with antibody-conjugated biodegradable microspheres illuminated by a single 80 femtosecond near-infrared laser pulse. International journal of nanomedicine. 2012;7:2653.
19. Breunig HG, Sauer B, Batista A, König K. Rapid vertical tissue imaging with clinical multiphoton tomography. InOptics, Photonics, and Digital Technologies for Imaging Applications V 2018 May 24 (Vol. 10679, p. 106790N). International Society for Optics and Photonics.
20. Denk W, Strickler JH, Webb WW. Two-photon laser scanning fluorescence microscopy. Science. 1990 Apr 6;248(4951):73-6.
21. Brown CT, Stevenson DJ, Tsampoula X, McDougall C, Lagatsky AA, Sibbett W, Gunn-Moore FJ, Dholakia K. Enhanced operation of femtosecond lasers and applications in cell transfection. Journal of Biophotonics. 2008 Aug;1(3):183-99.
22. Stevenson DJ, Gunn-Moore FJ, Campbell P, Dholakia K. Single cell optical transfection. Journal of the Royal Society Interface. 2010 Jun 6;7(47):863-71.
23. Stevenson D, Agate B, Tsampoula X, Fischer P, Brown CT, Sibbett W, Riches A, Gunn-Moore F, Dholakia K. Femtosecond optical transfection of cells: viability and efficiency. Optics express. 2006 Aug 7;14(16):7125-33.
24. Antkowiak M, Torres-Mapa ML, Stevenson DJ, Dholakia K, Gunn-Moore FJ. Femtosecond optical transfection of individual mammalian cells. Nature Protocols. 2013 Jun;8(6):1216.

25. Davis AA, Farrar MJ, Nishimura N, Jin MM, Schaffer CB. Optoporation and genetic manipulation of cells using femtosecond laser pulses. Biophysical journal. 2013 Aug 20; 105(4):862-71.
26. Page M, Taylor S. Amtiretroviral pharmacology. Medicine.2018 May 1;46 (5) : 287-92.
27. Tirlapur UK, König K. Targeted transfection by femtosecond laser. Nature. 2002 Jul;418(6895):290-1
28. Gallant JE. Initial therapy of HIV infection. Journal of Clinical Virology. 2002 Dec 1;25(3):317-33.
29. Gallo RC. The early years of HIV/AIDS. Science. 2002 Nov 29;298(5599):1728-30.
30. Sharp PM, Hahn BH. Origins of HIV and the AIDS pandemic. Cold Spring Harbor perspectives in medicine. 2011 Sep 1;1(1):a006841.
31. Engelman A, Cherepanov P. The structural biology of HIV-1: mechanistic and therapeutic insights. Nature Reviews Microbiology. 2012 Apr;10(4):279-90.
32. Siliciano JD, Siliciano RF. Latency and viral persistence in HIV-1 infection. The Journal of clinical investigation. 2000 Oct 1;106(7):823-5.
33. Trkola A. HIV–host interactions: vital to the virus and key to its inhibition. Current opinion in microbiology. 2004 Aug 1;7(4):407-11.
34. De Clercq E. Anti-HIV drugs: 25 compounds approved within 25 years after the discovery of HIV. International journal of antimicrobial agents. 2009 Apr 1;33(4):307-20
35. Lee J. The non-nukes. Sustiva. Viramune. The two major players. Positively aware: the monthly journal of the Test Positive Aware Network. 2005:12.
36. Alexaki A, Liu Y, Wigdahl B. Cellular reservoirs of HIV-1 and their role in viral persistence. Current HIV research. 2008 Sep 1;6(5):388-400.
37. Malim MH, Cullen BR. HIV-1 structural gene expression requires the binding of multiple Rev monomers to the viral RRE: implications for HIV-1 latency. Cell. 1991 Apr 19;65(2):241-8.
38. Maphanga C, Ombinda-Lemboumba S, Manoto S, Maaza M, Mthunzi-Kufa P. Targeted femtosecond laser driven drug delivery within HIV-1 infected cells: in-vitro studies. In Optical Interactions with Tissue and Cells XXVIII 2017 Feb 15 (Vol. 10062, p. 1006205). International Society for Optics and Photonics.

39. Yavuz B, Morgan JL, Showalter L, Horng KR, Dandekar S, Herrera C, LiWang P, Kaplan DL. Pharmaceutical approaches to HIV treatment and prevention. Advanced Therapeutics. 2018 Oct;1(6):1800054.
40. Mthunzi P, Dholakia K, Gunn-Moore FJ. Phototransfection of mammalian cells using femtosecond laser pulses: optimization and applicability to stem cell differentiation. Journal of biomedical optics. 2010 Jul;15(4):041507.
41. Tsampoula X, Taguchi K, Čižmár T, Garces-Chavez V, Ma N, Mohanty S, Mohanty K, Gunn-Moore F, Dholakia K. Fibre based cellular transfection. Optics express. 2008 Oct 13;16(21):17007-13.
42. Terakawa M, Mitsuhashi T, Shinohara T, Shimizu H. Near-infrared femtosecond laser-triggered nanoperforation of hollow microcapsules. Optics Express. 2013 May 20;21(10):12604-10.
43. Ellliot D.J Academic Press USA 1995.
44. Sze SM. Semiconductor devices: physics and technology. John wiley & sons; 2008.
45. Jawad MM, Qader ST, Zaidan A, Zaidan B, Naji A, Qader IT. An overview of laser principle, laser-tissue interaction mechanisms and laser safety precautions for medical laser users. Int J Pharmacol. 2011 Feb 15;7(2):149-60.
46. Serebryakov VA, Boĭko ÉV, Petrishchev NN, Yan AV. Medical applications of mid-IR lasers. Problems and prospects. Journal of Optical Technology. 2010 Jan 1;77(1):6-17.
47. Vogel A, Venugopalan V. Mechanisms of pulsed laser ablation of biological tissues. Chemical reviews. 2003 Feb 12;103(2):577-644.
48. Noack J, Vogel A. Laser-induced plasma formation in water at nanosecond to femtosecond time scales: calculation of thresholds, absorption coefficients, and energy density. IEEE journal of quantum electronics. 1999 Aug;35(8):1156-67.
49. Praveen BB, Stevenson DJ, Antkowiak M, Dholakia K, Gunn-Moore FJ. Enhancement and optimization of plasmid expression in femtosecond optical transfection. Journal of biophotonics. 2011 Apr;4(4):229-35.
50. Stevenson DJ, Gunn-Moore FJ, Campbell P, Dholakia K. Single cell optical transfection. Journal of the Royal Society Interface. 2010 Jun 6;7(47):863-71
51. Antkowiak M, Torres-Mapa ML, Stevenson DJ, Dholakia K, Gunn-Moore FJ. Femtosecond optical transfection of individual mammalian cells. Nature Protocols. 2013 Jun;8(6):1216.

52. Vogel A, Venugopalan V. Mechanisms of pulsed laser ablation of biological tissues. Chemical reviews. 2003 Feb 12;103(2):577-644
53. Tirlapur UK, König K. Targeted transfection by femtosecond laser. Nature. 2002 Jul;418(6895):290-1.
54. Soman P, Zhang W, Umeda A, Zhang ZJ, Chen S. Femtosecond laser-assisted optoporation for drug and gene delivery into single mammalian cells. Journal of biomedical nanotechnology. 2011 Jun 1;7(3):334-41.
55. Li M, Gao F, Mascola JR, Stamatatos L, Polonis VR, Koutsoukos M, Voss G, Goepfert P, Gilbert P, Greene KM, Bilska M. Human immunodeficiency virus type 1 env clones from acute and early subtype B infections for standardized assessments of vaccine-elicited neutralizing antibodies. Journal of virology. 2005 Aug 15;79(16):10108-25.
56. Soman P, Zhang W, Umeda A, Zhang ZJ, Chen S. Femtosecond laser-assisted optoporation for drug and gene delivery into single mammalian cells. Journal of biomedical nanotechnology. 2011 Jun 1;7(3):334-41.
57. Doitsh G, Galloway NL, Geng X, Yang Z, Monroe KM, Zepeda O, Hunt PW, Hatano H, Sowinski S, Muñoz-Arias I, Greene WC. Cell death by pyroptosis drives CD4 T-cell depletion in HIV-1 infection. Nature. 2014 Jan;505(7484):509-14.
58. Ogawa M, Takemoto Y, Sumi S, Inoue D, Kishimoto N, Takamune N, Shoji S, Suzu S, Misumi S. ATP generation in a host cell in early-phase infection is increased by upregulation of cytochrome c oxidase activity via the p2 peptide from human immunodeficiency virus type 1 Gag. Retrovirology. 2015 Dec 1;12(1):97.
59. Dumais N, editor. HIV and AIDS: Updates on Biology, Immunology, Epidemiology and Treatment Strategies. BoD–Books on Demand; 2011 Oct 26
60. Sharma B. Oxidative stress in HIV patients receiving antiretroviral therapy. Current HIV research. 2014 Jan 1;12(1):13-21
61. Robertson K, Liner J, Meeker RB. Antiretroviral neurotoxicity. Journal of neurovirology. 2012 Oct 1;18(5):388-99.
62. Ando T, Imamura H, Suzuki R, Aizaki H, Watanabe T, Wakita T, Suzuki T. Visualization and measurement of ATP levels in living cells replicating hepatitis C virus genome RNA. PLoS pathogens. 2012 Mar;8(3).
63. Palmer CS, Cherry CL, Sada-Ovalle I, Singh A, Crowe SM. Glucose metabolism in T cells and monocytes: new perspectives in HIV pathogenesis. EBioMedicine. 2016; 6: 31–41. PubMed Abstract Publisher Full Text| Free Full Text.

64. Cohen BE. Amphotericin B membrane action: role for two types of ion channels in eliciting cell survival and lethal effects. The Journal of membrane biology. 2010 Dec 1; 238(1-3):1-20.

65. Hicks C, Gulick RM. Raltegravir: the first HIV type 1 integrase inhibitor. Clinical Infectious Diseases. 2009 Apr 1;48 (7):931-9.

66. Lalezari JP, Bellos NC, Sathasivam K, Richmond GJ, Cohen CJ, Myers Jr RA, Henry DH, Raskino C, Melby T, Murchison H, Zhang Y. T-1249 retains potent antiretroviral activity in patients who had experienced virological failure while on an enfuvirtide-containing treatment regimen. The Journal of infectious diseases. 2005 Apr 1;191(7):1155-63.

Chapter 3

Development and characterisation of the surface plasmon resonance system

In this chapter, a brief history of SPR, and principles such as plasma frequency and evanescent waves (surface plasmon wave) that govern SPR as a physical method are described. Subsequently, the different types of SPR sensors based on the coupling and excitation methods are detailed. Then, I detailed the different components that are essential in building an SPR sensing system that is ideal for sensing applications. Next, the assembly of the SPR system using a coherent cube laser (640 nm with output power 60 mW) is transcribed. Following this, angular measurements using the custom made SPR system was achieved. Of note, different laser sources can be used for building an SPR system, in this case the laser light in the visible region was able to create plasmons required for sensing applications. Particularly the 640 nm laser was able to create a plasmon when using gold as the sensing material for these applications.

3.1. Introduction

Briefly, SPR is the resonance oscillation of electrons at the interface between a negative and a positive permittivity material excited by an electromagnetic radiation, e.g., light. The surface plasmon polaritons (SPPs) launched upon the radiation can be propagating along the metal-dielectric interface and decay evanescently at the normal direction for a flat surface [1, 2]. Surface plasmons (SPs) are very sensitive to the near surface refractive index (RI) changes and well suited to the detection of surface-binding events [2-4]. The basic methodology of SPR sensing is based on the Kretschmann configuration, where a prism is used for the light-SP coupling at the surface of a thin metal film [3]. The probe light undergoes total internal reflection on the inner surface of the prism. At a defined SPR angle, an evanescent light field travels through the thin gold film and excites SPs at the metal-dielectric interface [3-5], reducing the intensity of the reflected light at the resonance wavelength or changing the phase of the incident light [4].

In section 3.2, the history of SPR and the principles such as plasma frequency and evanescent waves that govern surface plasmon resonance as a physical method are described. Since the introduction of SPR is already stipulated in chapter 1, in this chapter, a summary intro of SPR was described above, before focusing on the main objective of the study, which was to build

and characterise a SPR system that can excite plasmon resonance using the Kretschmann configuration for sensing applications.

3.2. History of surface plasmon resonance (SPR)

The spectrum of a continuous source of white light using diffraction grating in reflection was first observed by Wood in 1902 [5]. He noticed that when polarised light is shone on a mirror grating, there were bright and thin dark bands in the diffracted spectrum (figure 3.1 below). These were then referred to as Wood's anomalies.

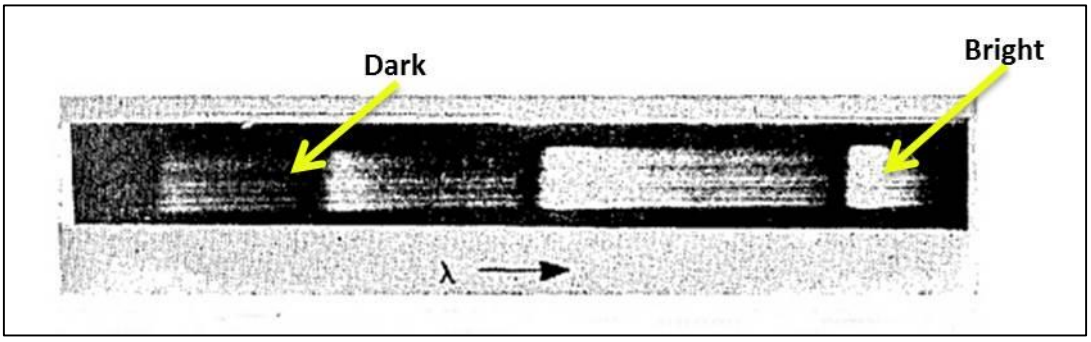

Figure 3.1: A photograph image showing the diffraction spectrum showing Wood's anomalies of bright and dark bands [5]

Since Wood could not explain how the light, gratings and metal interacted, in 1907 Rayleigh theoretically treated these anomalies [6]. He based it on the expansion of the scattered electromagnetic field of outgoing waves [6]. He discovered that the scattered field was singular at wavelengths, which one of the spectral orders came from the grazing angle from the gratings. [6]. Given that, he then concluded that the wavelength corresponds to the Wood's anomalies. With further theoretical analysis, in 1941, Fano concluded that the anomalies that Wood observed were due to the excitation of surface waves on the surface grating [7]. When Pines and Bohm did their experiments on gasses and foils in the fifties, they observed energy losses in gasses [8, 9. 10]. Then concluded that the energy losses are due to the excitation of conducting electrons forming plasma oscillations or plasmons [8,9, 10] they also realized that the excitation of the plasma oscillations on the surface leads to some of the electric field being extended beyond the surface of the dielectric field. These lead to the formation of electromagnetic waves at the surface of the metal. As years went by with the growing interest to the anomalies, in the late sixties, Kretschmann and Otto demonstrated that these surface waves can be excited by using attenuated total reflection (ATR) [11,12]. ATR is the

electromagnetic waves (evanescent waves) that decay exponentially with distance from the interface after the light that penetrates the boundary of a medium with the angle of incidence greater than the critical angle is totally reflected [13]. Within the same year, Kretschmann and Raether decided to put the experiment to test and obtained the same results from a different configuration of the attenuated total reflection method [12]. These configurations lead to the used of prism coupler based structures and diffraction at diffraction gratings as the major approaches for the optical excitation of surface plasma waves or surface plasmon waves. Given this approaches, the excitation of surface plasmon waves by using ATR method was the used for thin film metal characterisation , sensing and biochemical sensing, while the diffraction grating method was used as an alternative to the prism based method.

Following, all this theoretical and experiment investigations by these different scientists and its relative simplicity with thin films, SPR became a biosensing technique to use for biological and chemical interaction after it was exploited through evanescent waves in the characterisation of thin films. In this study, SPR was used as an optical sensing technique using the prism coupler based method for biosensing applications due to its ability to create longer evanescent waves (surface plasmon wave) that can promote biological and chemical interactions. In the next subsection 3.2.1 and 3.2.2., is a detailed narrative of the two most important features that constitutes SPR.

3.2.1. Plasma frequency/ electron oscillation

In order to get excitation of SPR, plasma free electrons play a significant role in the metal surface. Plasma is an electrically neutral medium of unbound positive and negative particles. These particles are unbound on the metal surface, but they can still experience different electrical forces. Any moving charged particles generate an electric current within a magnetic field, and any movement of a charged plasma particle affects and is affected by the fields created by the other charges [14, 15]. This then results in natural vibrations of the plasm particles Optical characteristics of the metal based on the natural vibrations of a free electron plasma need to be explored. Solid state plasma is a combination of movable charged particles in the solid state, described by characteristics of gas discharged plasma [14, 15]. Since the plasma is linked to a collection of charged particles, the energy of the electric field is drawn from the kinetic energy of the thermal wave of the gas particles. For metals, any changes in the position of electrons in relation to fixed ions on the crystal lattice (which can be gold or silver) gives rise to the forces of electrostatic nature leading to the electroneutrality of the whole metal

[13]. For example, bulk free electrons can waver with an eigenfrequency given by the plasma frequency:

$$\omega^2 p = \frac{ne^2}{e_0 m} \qquad (3.1)$$

Where *n* is the number density of electrons, *e* is the electric charge, *m* is the mass of the electrons and $\boldsymbol{\varepsilon}_0$ is the permittivity of free space.

However close to the metallic surface, this wave occurs with lower energy and gives rise to longitudinal charged density wave disseminating along the interface [15, 16, 17]. This charged density wave is called a plasmon polariton. This plasmon polariton wave is the electron oscillations coupled with electromagnetic field that result in a formation of an optical wave known as the surface plasmon wave.

Knowing that, plasmon polaritons leads to the formation of surface plasmon wave, subsection 3.2.2.describes on how surface plasmon waves interact with the metal

3.2.2. Evanescent waves and surface waves

When the angle of incidence, θ of the light ray is greater than the critical angle, θ_c, where

$$\sin\theta_c = n_2/n_1 \qquad (3.2)$$

No refraction takes place, instead all the light is reflected back into the denser material, this is known as total internal reflection (TIR). In this situation, light travels from the higher refractive index medium 1 to a lower refractive index medium 2 as a result TIR takes place within medium 1 (figure 3.2 below).

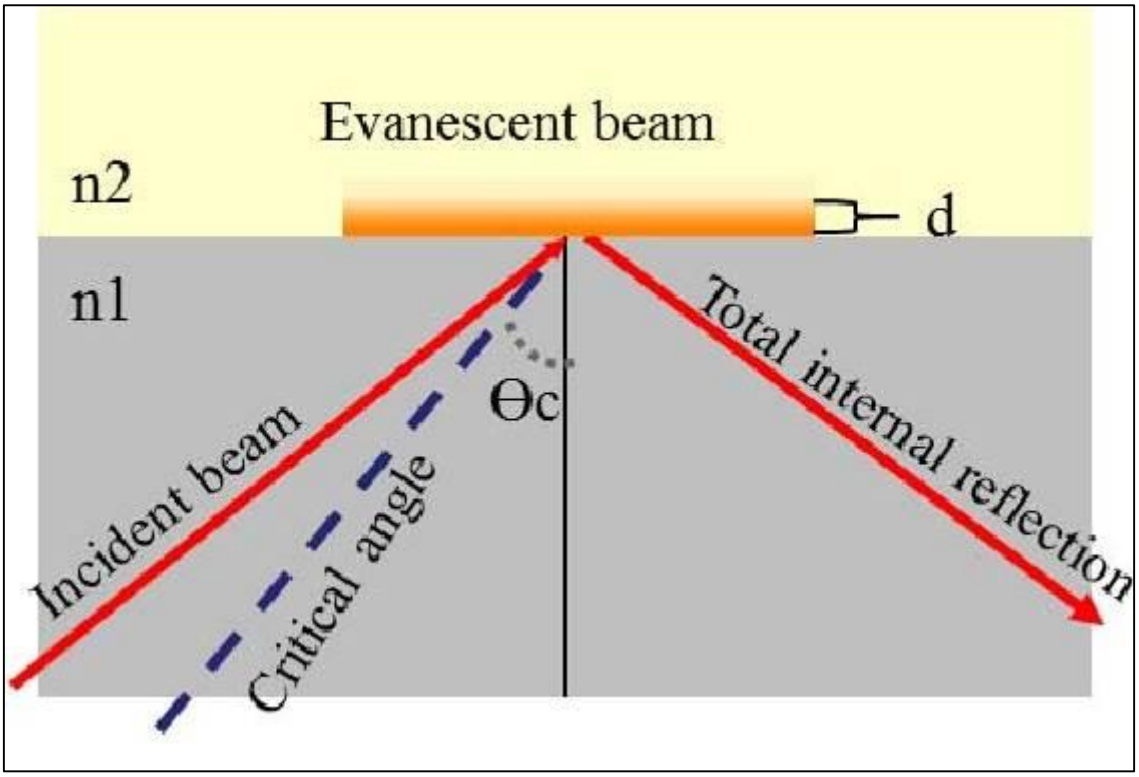

Figure 3.2: Illustration of total internal reflection (TIR). Light moves from a higher refractive index medium (n1) to a lower refractive index medium (n2) given the condition that the incident angle,θ (incident beam), is greater than the critical angle given by θ_c , then TIR occurs at medium 1.

Under the conditions of TIR, in the lower refractive index medium there will be a formation of evanescent waves (figure 3.3 below).

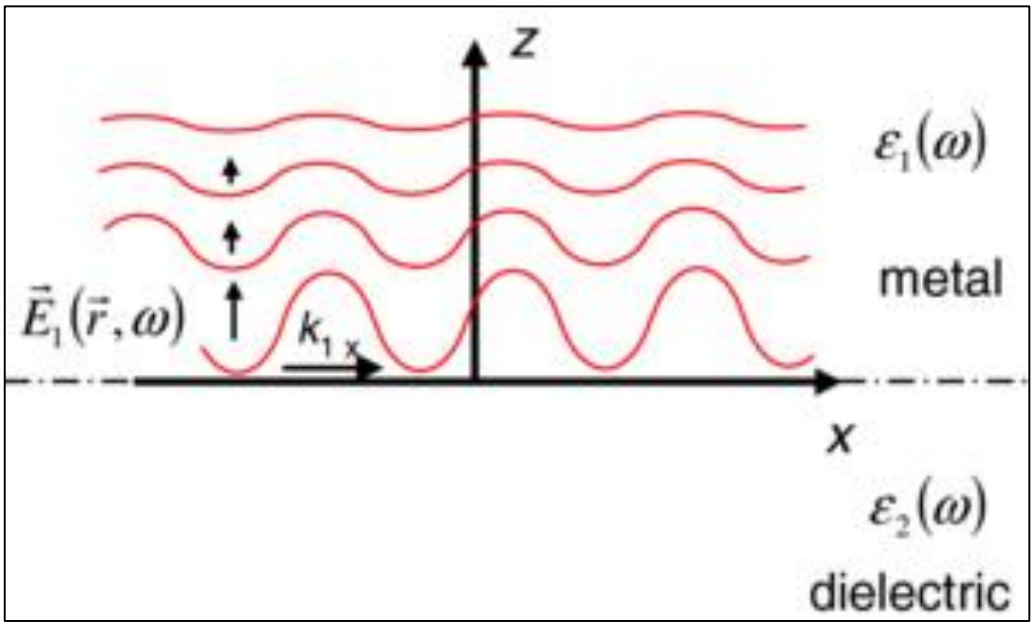

Figure 3.3: Illustration of the structure of an evanescent wave. The wave propagates along the *x* direction with the wave vector k_{1x}. It has an exponentially wave moving in the direction normal to the interface (*z*), where the decay length is given by $1/k_z$ and there is no propagation but an oscillation of the electric field [24].

This waves decay exponentially with the distance to the interface of the two media (1 and 2). When a gold thin film is placed on the interface, there, an evanescent wave is heightened, penetrating through to gold film and now occurring in the second medium [14, 15]. The changes of this parallel evanescent wave are expressed as:

$$K_{evan,II} = \frac{2\pi}{\lambda} n_1 \sin\theta \qquad (3.3)$$

Where $K_{evan,II}$ is the evanescent wave , λ_0 is the wavelength of the incident light, n_1 is the refractive index of the higher refractive index medium 1 and θ is the incident angle.

3.3. Surface plasmon resonance

Surface plasmons are collective coherent oscillations of delocalized electrons that are stimulated by the incident illumination at the interface between a metal and the dielectric medium [15]. SPR is generated by surface plasmons that can strengthen the electromagnetic field. SPR is very sensitive to the refractive index that is attached to the surface of the metal film.

Additionally, changes in the condition of the medium have a high influence in the resonance spectral responses [16, 17]. Specifically, SPR sensors are used to sense molecular information in the enhanced contained electromagnetic field. They are also perceived as thin-film optical refractometers by measuring the variation of the refractive index on the surface of the metal film [19]. The mechanism of SPR sensors includes both the electromagnetic and chemical enhancement. Localized surface plasmon is caused by the former, which can enhance the spectra over a large frequency range while the latter can selectively enhance molecule signals that are absorbed at the surface of the metal [20-23]. In the initial phase of SPR, there is an evanescent field that does not propagate as an electromagnetic wave; however, its energy is spatially concentrated in the surrounding of oscillating charges.

Theoretically, SPR is the communication between the incident electromagnetic waves and free electrons in a metal [20]. At the interface amongst a semi-infinite metal layer with a complex permittivity denoted by:

$$\varepsilon_m = \varepsilon'_m + i\varepsilon''_m \qquad (3.4)$$

together with dielectric medium with a complex permittivity denoted by:

$$\varepsilon_d = \varepsilon'_d + i\varepsilon''_d \qquad (3.5)$$

where ε'_m and ε'_d have different signs and $\varepsilon'_m < \varepsilon'_d$, an incident electromagnetic wave can be joined or put together with the free electron gas and energize the free electrons to spread evenly [24]. As a result, the conduct of the free electrons is mostly the same to that of plasma; the collective spread is known as the surface plasma wave [6, 20, and 21]. As based on Maxwell's equation with suitable conditions, the wave quantity can be shown as:

$$K_{sp} = \frac{2\pi}{\lambda}\frac{\sqrt{\varepsilon\,\mathrm{m}\,\varepsilon\,\mathrm{d}}}{\varepsilon\,\mathrm{m}+\varepsilon\,\mathrm{d}} \qquad (3.6.)$$

Where *Ksp*, is the surface wave quantity, λ represents the wavelength of the light in space, $\boldsymbol{\varepsilon}$ is the dielectric permittivity and the subscript *m* and *d* refer to the metal and the contacting dielectric medium.

The SPR event occurs when the wave quantity of the surface plasmon wave (K*sp*) matches the parts of the incident light wave quantity in the direction parallel to the interface. In general, SPR sensation is the idea on the Kretschmann configuration, which contains a high refractive index prism (figure 3.2 below).

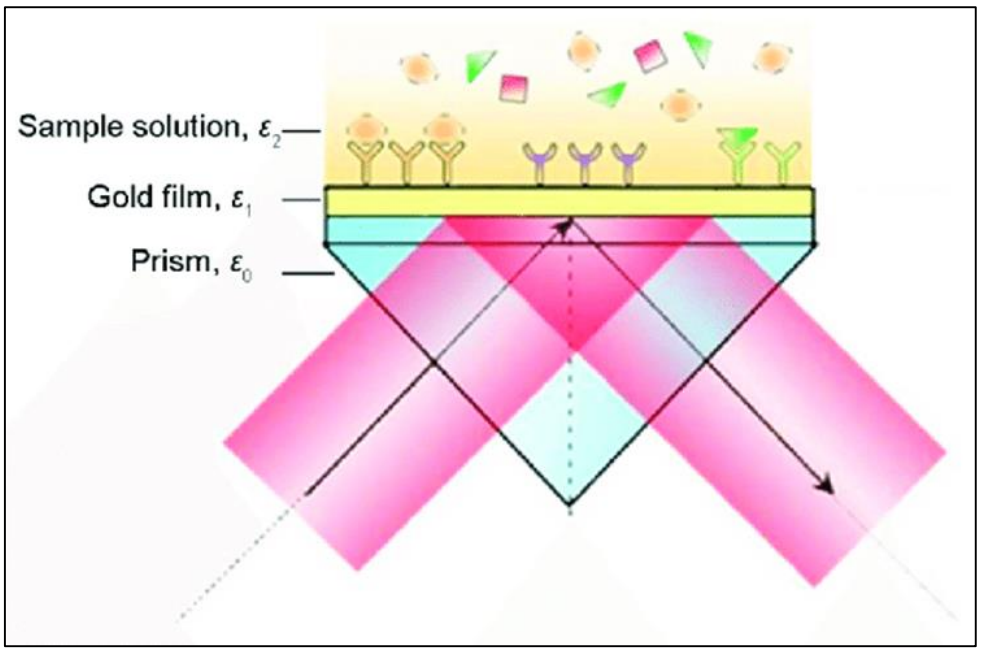

Figure 3.4: Illustration of SPR sensing based on the Kretschmann configuration, which consist of a high refractive index prism, a gold thin film and sample solution. [23].

Based on a mixture of the Fresnel equation and the interference theory, the intensity and the changing of the light sent back is determined by the use of complex reflection that measures the multi-layer medium structure [22].The intensity of the reflected light is reduced as part of the energy of the incident wave is transmitted to that of the surface plasmon. The resonant excitation of the surface plasmon occurs at the specific angle of the incidence and wavelength [21, 22, and 23]. Therefore, if the incident light contains multiple wavelengths only the light with the narrow bands of the wavelength will be attenuated due to the surface plasmon excitation, producing a characteristic dip in the wavelength spectrum of the reflected light.

The spectral position of the resonant dip, in the angle or wavelength varies with the refractive index at the sensor surface. Surface plasmon polaritons are surface waves that propagate along the surface of a conductor, usually a metal. These waves are essentially light waves that are trapped on the surface because of their interaction with the free electrons of the conductor [20, 21, and 22]. In this interaction, the free electrons respond collectively by oscillating in resonance with the light wave. The resonant interaction between the surface charge oscillation and the electromagnetic field of the light constitutes the surface plasmon polariton and gives rise to its unique properties [21].

With unique properties of being able to trap light waves on the metal surface to cause a resonant excitation at specific angle of incidence and wavelength, SPR can be used to study multi-layer medium structures and the interaction of biological analytes in a solution through exploiting surface plasmon wave to promote binding interactions of the analytes. Given this, in this study, SPR sensing system is designed and developed for biosensing applications, to be discussed in chapter 5. With relevance to the current study, section 3.4, gives an insight in the different types of SPR sensors based on their configuration of optical excitation of surface plasmon waves.

3.4. Types of SPR sensors

Generally, SPR is a phenomenon whereby the electromagnetic (EM) wave with a certain energy shot at a certain angle, resulting in a resonance that occurs in the electron on the surface of metal-dielectric interfaces [17,18]. The common types of SPR sensors include using prism

couplers, optical waveguides and diffraction gratings. To achieve SPR excitation, it is important that the plasmon wave vector and projection of the exciting light vector to the surface are equal [23, 24]. Coupling devices such as prisms, wave guides, and diffraction grating are used for the purpose of SPR excitation to create the surface plasmon wave on the metal surface are described in subsections 3.4.1 to 3.4.3.

3.4.1. SPR sensor coupling with a prism

Special prisms that are made from dielectric material with high refractive index are used for the coupling of light in SPR sensors [2]. There are two types of prism coupling configurations of SPR optical excitations; namely: The Otto's geometry and the Kretchmann geometry (figure 3.5 below). In Otto's geometry, the dielectric media is placed between the prism and the metal layer (figure 3.5a).

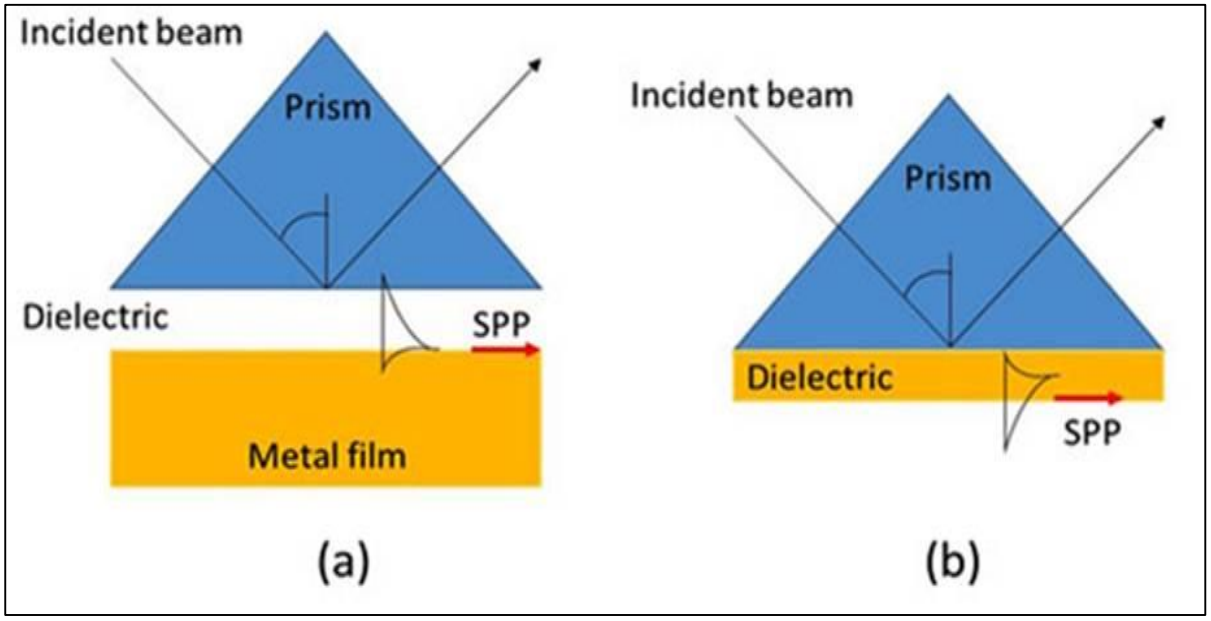

Figure 3.5: Diagram representing SPR sensor coupling with a prism based on **(a)** Otto's geometry and **(b)** Kretschmann geometry. Both geometries consist of high refractive index prism and a metal film [24].

While in the Kretschmann geometry, a metal film is placed between the prism and the dielectric media (Figure 3.5b). To date the most common used coupling method is the Kretschmann geometry whereby the thin metal film is coupled at the base of the prism made of dielectric, then the light wave passes through the prism and causes an attenuating wave on the basis of the metal surface, this wave penetrates through the metal film and excites a surface plasmon [24, 25]. A monochromatic light is used on the conducting surface with various angles of

incidence being on the range of total internal reflection. The light then goes through a detector after reflection on the metal surface.

3.4.2. SPR sensors coupling with diffraction gratings

When light falls from a dielectric media to a metal diffraction grating with a period less than the light wavelength, a possible excitation of the plasmon is generated (figure 3.6 below). This plasmon excitation happens under the light diffracted on the grating, provided that the wave vectors of the light and that of the surface plasmon are matched well [5, 6].

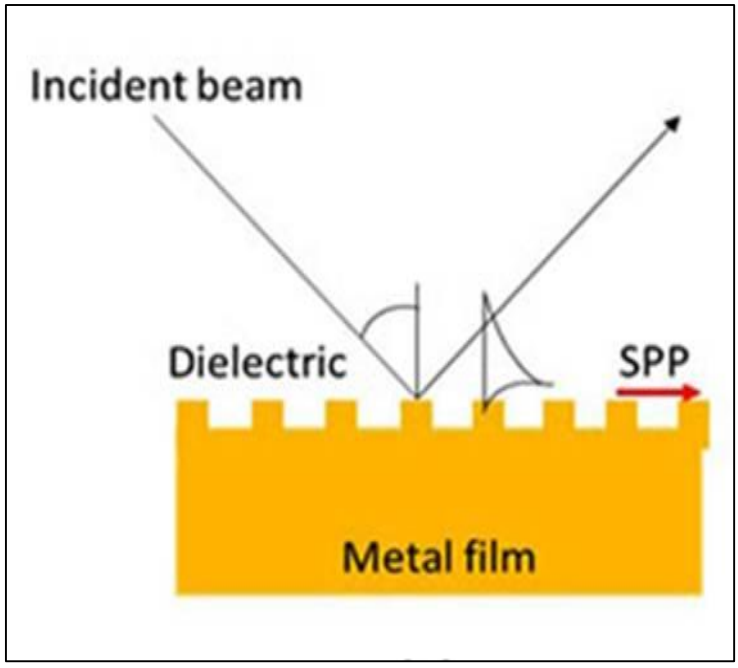

Figure3.6: Diagram showing the SPR sensors coupling with diffraction gratings. It consists of a metal film [24]

The matching wave vectors are highly dependent on the grating period and a diffraction maximum order, since SPR sensors can work in transmission mode and reflection mode. SPR sensors with this kind of diffraction gratings can be used to measure the frequency, phase, amplitude and angular characteristics.

3.4.3. SPR sensors coupling with waveguides

In this instance, a dielectric material with high refractive index is used to fabricate waveguide leading channels in which the wave propagates [2].The metal film is applied on the surface of such a channel, whereby the electromagnetic field is found to be centrally concentrated. Only a small portion of the attenuating wave penetrates into the layer with low refractive index through the metal film. This excites the surface plasmon on its exterior border as demonstrated in figure 3.7 below.

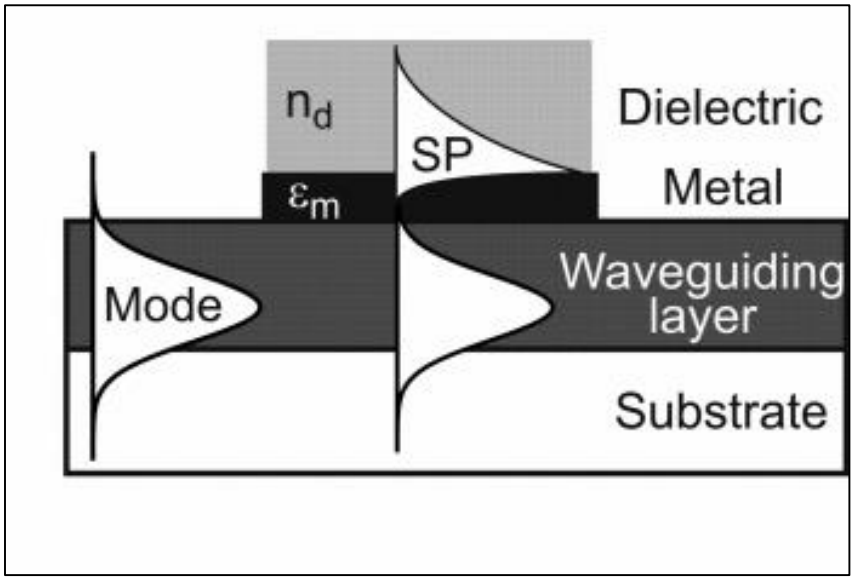

Figure 3.7: Diagram showing the SPR sensors coupling with waveguides. It consists of a substrate, waveguide layer and the metal. [2].

SPR waveguide coupled sensors can be used for signal registrations to register the following: SPR resonant frequency shift as a result of interaction of the sensor surface with the analytes, phase shift or change of the transmitted light intensity at a certain wavelength [1, 24, and 25]. In SPR sensors, refractive index directly modulates characteristics of light wave such as coupling angle, wavelength, intensity, phase and polarization. In this chapter, the measurement of the plasmon excitation in relation to angular shift using a custom made setup surface plasmon resonance setup is demonstrated. The aim of this experiment was to characterize and optimize the custom made system for applications to SPR biosensing which will be discussed in chapter 5.

3.5. Experimental methods

When designing a SPR base sensing system, laser excitation, gold film thickness and the refractive index of the dielectric material on either side of the metal film are the most crucial parameters that determine the performance of the SPR sensing system. This is as a result of having a sensing system that will be able to promote the interaction of analytes for sensing applications. In subsection 3.5.1, I present a narrative on the essential components that are used to build the SPR sensing system.

3.5.1. Custom made SPR Set up

Based on the Kretschmann configuration or geometry, the custom made SPR system composed of a light source, half wave plate, polariser, detector, prism and gold thin film (figure 3.8.

below). As a result, the main aim of the study was to design an SPR sensing system for biosensing applications as shown below. Briefly, a coherent cube laser at 640 nm with an average output power of 60 mW was used. The output beam was sent through the neutral density (ND) filter and the polarizer in order to control the power and select the p-polarisation of the laser beam on the biosensor respectively. The beam expander was used to enlarge the beam. The biosensor layer was illuminated through the BK7 equilateral prism with the refractive index n = 1.517 by the collimated p-polarized beam. A manual micrometer rotation stage with an accuracy of 0.1° was used for measuring the incident angle. The reflected beam was collected using the focusing lens and with a biased photodiode and its intensity was read with the multimeter.

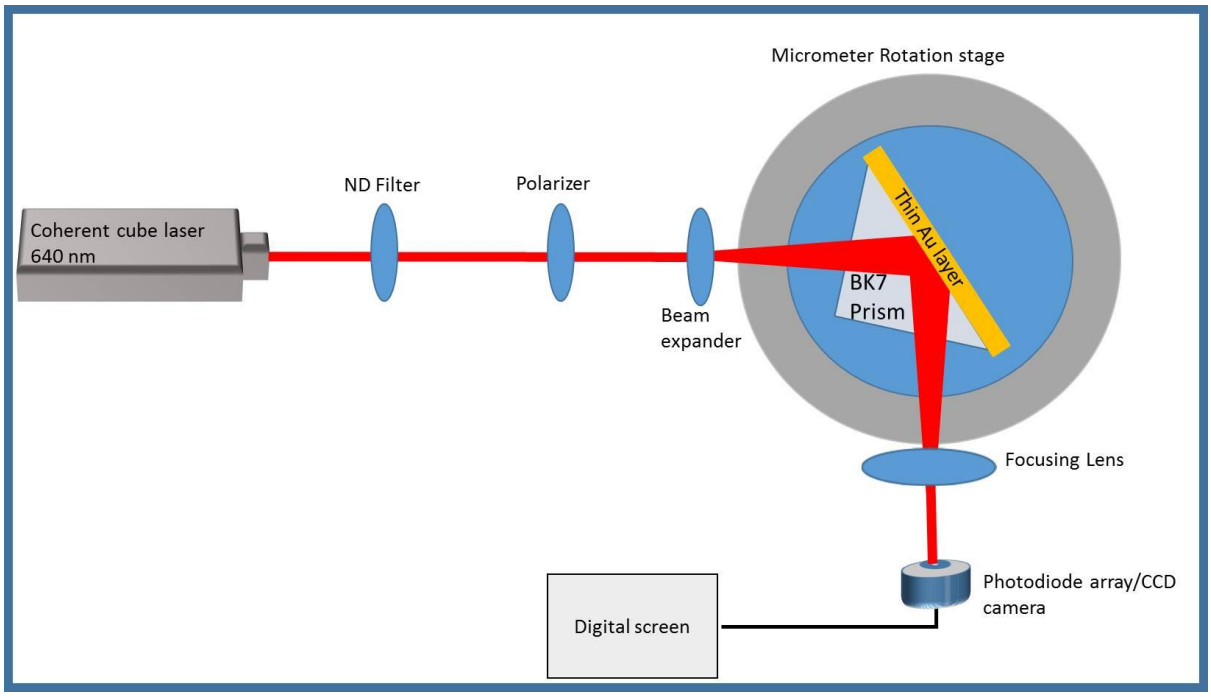

Figure 3.8: Schematic representation of the custom made SPR rig based on the Kretschmann configuration. It consists of a coherent cube laser as the light source (640nm), neutral density filter, to filter the beam. The polariser was used to attenuate the beam while the beam expander was used to enlarge the beam. The thin gold layer for was used for sensing while the focusing lens collected the beam and the photodiode measured the reflectance in the intensity.

In subsections 3.5.1.1 to 3.5.1.4, I present a narrative of the essential components that were used to build an SPR sensing system for biosensing applications that will be discussed in chapter 5.

3.5.1.1. Light source

For these SPR experiments, a p-polarised helium neon laser source emitting a wavelength of 640 nm in the visible wavelength with an average power output of 60 mW was used as the light source. The output beam was sent through the neutral density filter in order to control and neutralise the power to 5.6 mW for experimental use. The laser source was mounted on the breadboard at a height that can be adjusted for the alignment of the beam. The beam diameter was 1.31 mm and the intensity was stable. The *p*-polarised light was used as it has the ability to excite surface plasmons.

3.5.1.2 The prism and the gold thin film

A high index equilateral prism BK7 with a refractive index n = 1.517 was used with the collimated *p*-polarised beam as arranged in figure 3.9 below. SPR glass sides coated with gold were used and adapted to the prism with index matching oil (n = 1.517) that has the same refractive index as the prism.

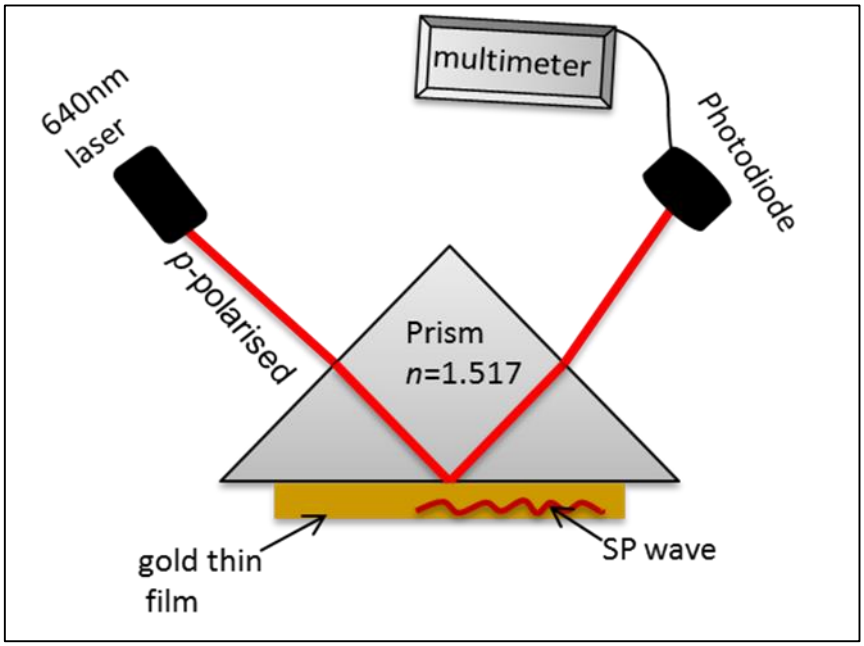

Figure 3.9: Schematic illustration that shows the gold film placed on the prism and the launch of the surface plasmon wave excitation on the gold thin film.

3.5.1.3. Detector

The reflected beam is collected with a photodiode, and its intensity can be read with the multimeter. The photodiode is chosen such that the sensor area is greater than the section of the laser, thus to ensure all the reflected light is collected and measured. The detector was moved manually to collect all the reflected light for each angle value reading that was measured. The reading on the multimeter was recorded and the data was plotted using the Origin software analysis.

3.5.1.4. Angular measurements

For the prism based experiments, angular measurements were carried out using a micrometer rotational stage that has angular resolution of 0.1^0. A photodetector was mounted on the one side of the rotation stage such that it is able to swing in the direction of the reflected light. A multimeter was connected to the photodetector in order to take a reading. The light intensity was detected by the detector corresponding to the rotation of prism for each angle measurement on the rotation stage. The rotary movement of the prism assembly was performed manually.

3.6. Results and discussion

Generally, SPR is the excitation of surface plasmons at the interface of two media with dielectric constants of opposite polarity. In a dielectric medium, the SPs have greater propagation constant than the light wave due to which they cannot be excited by direct light. Having said that, the aim of this study was to build, characterise and optimise an SPR sensing system that can excite plasmon resonance using the Kretschmann configuration for sensing applications. During data collection, the reflected intensity measured with a photodiode was manually recorded as a function of the external angle that was measured. The raw data acquired from the multimeter reading were plotted using origin software. For characterisation purposes, the following experimental conditions were setup and measurements captured; the prism with air, the prism with pristine glass and the prism with a 40 nm gold coated slide. The results shown in figure 3.10, demonstrated that there was an angular shift of the pristine slide, as compared to the prism. The same shift was also observed for the gold coated slide as compared to the prism and the uncoated slide. However, it was noted that the shift in figure 3.10 was towards the left instead of the right this could have resulted due to the weak intensity of the SPR signal or it could be the impurities found of the slides during the course of the experiments.

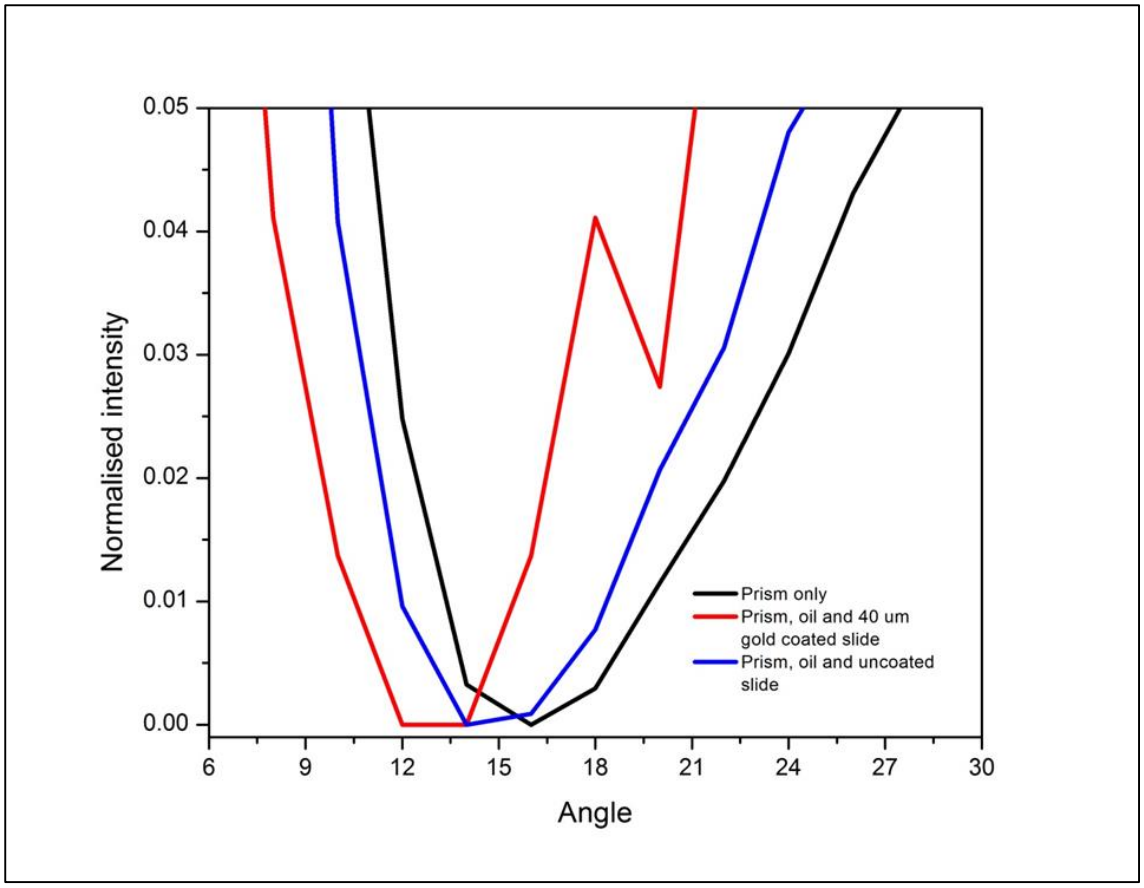

Figure 3.10: A graph illustrating surface plasmon resonance excitation sensing of the prism (black); prism oil and uncoated slide (blue) and prism oil, and gold coated thin film (red).

Figure 3.11.Shows the plotting was achieved by the normalization of the intensity by using the equation: $\theta_{int} = arcsin\frac{\sin(\theta ext - A)}{n} + A$

Where by θ_{int} is the incident angle, θ_{ext} is the external angle that is being measure after reflection, A is the angle of the prism and *n* the refractive index of the prism. With this equation normalised reflected intensity is was determined.

Given this formula, results that were analysed clearly display the shift in SPR curves to the left from the normal.

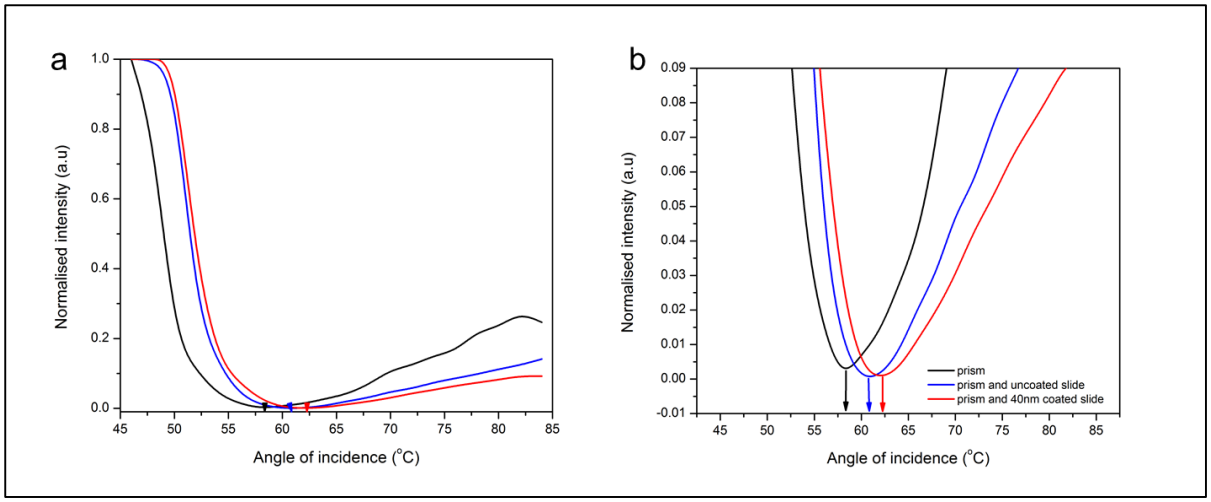

Figure 3.11: Graphs illustrating surface plasmon resonance excitation sensing of the prism (black); prism oil and uncoated slide (blue) and prism oil, and gold coated thin film (red). Values of the y-axis in **(a)** shows the normalised results before using the equation and **(b)** shows the angular shift after the application of the normalisation equation.

The results obtained clearly show the differences in the angular shift of the three scenarios, as is evident in figure 3.11 B, the prism had an angular dip at 58.36 ± 0.1^0, the combination of the prism and the uncoated slide at 60.83 ± 0.1^0 and the gold coated slide at 62.05 ± 0.1^0. The plotted data indicate that there was an angular shift of $\pm 2.47^0$ between the prism and the uncoated slide; then, $\pm 3.69^0$ between the prism and the gold coated slide; finally, ± 1.22 between the uncoated slide and the gold coated slide. These angular shifts noted in these results are as a result of the changes in the refractive index of the three materials used. These value shifts between the three materials has successfully demonstrated that the SPR rig for sensing application based on the Kretschmann geometry was successfully built, optimised and characterised.

From literature, it is known that the plasmon excitation has a sharp dip in the reflection curve around the: $\theta_{int} = \theta_{plasmon} = 41.8 \pm 0.1^0$ [18,26], in our results we noted a visible $\pm 53.8 \pm 0.1^0$, which was not too farfetched considering that the micrometer stage for each angle was manually rotated. From results obtained, the intensity of the prism, the uncoated slide and the gold coated slide nearly drops to zero, which signals that the excitation beam transfers its energy to the surface plasmon wave. This shows that indeed there was plasmon excitation by so doing, thus demonstrating that the custom made SPR system was characterised and optimised properly for angular measurements. Surface waves are confined in air layer, but when using a gold film it can be transformed to a far field propagating wave that can cause

diffusion [18, 27]. In this case, we did not notice any diffusion but reflection given shifts, translating that the gold thin used was neither damaged nor exhibited roughness.

Although the SPR shifts curves of the three materials (prism; uncoated slide and gold coated thin film) were a bit wider than the known narrower curves as stipulated in literature, this discrepancy may have resulted because the measurements were performed manually. It was also noticed that exact calculations of the reflected intensity of reproducing the plasmon excitation is possible by using the Fresnel relations applied in the three layer model. However, the glow on the surface of the metal during the experiment was evident enough that the waves were propagating causing a surface plasmon wave. This also translated that the gold surface being used is of good quality to achieve these angular measurements for SPR. Any changes in the refractive index are detected as an increase in the reflected intensity. It is known that the change in the intensity directly affects the phase of the incident light, which causes the evanescent wave (SP wave) to propagate in a parallel direction to the metal surface in a resonant mode.

Given that the aim of this study was to build and characterise and optimise a custom made SPR system based on the Kretschmann geometry for biosensing applications. The following five factors were noticed; first, the excitation beam transfers its energy to the surface plasmon wave; second, the nature of the gold film (for example roughness or reparation), plays a crucial role in terms of near and far field of the surface waves for reflection; third, the quality and cleanliness of the gold surface plays a crucial role in angular measurements of SPR; forth, that total internal reflection is critical when performing angular position of SPR especially when using the gold film; finally, the prism material is very vital for design and significant for optimizing system performance [27]. All these factors contribute to a high performance of the SPR system that can be used for biosensing, and illustrates the electromagnetic principles of SPR as a technique.

3.7. Conclusion

In this chapter, SPR system was built and characterised using the prism with air, the prism with pristine glass and the prism with a 40 nm gold coated slide. The phenomenon of SPR occurs at a certain angle, when the angle of incident light on the prism is greater than critical angle prism. When the momentum of a laser beam of the same value with momentum of electrons in the

sample, the result is the electrons separated from the sample and interact with laser light until it reaches the resonance condition. In this study, the built SPR sensing system could accurately determine angular position of the prism, the uncoated glass slide and gold coated slide. It was evident that the plasmon excitation is highly dependent on the material of excitation. Coupling of the surface plasmon wave with the gold showed a strong resonance shift in the visible region. Therefore, an SPR system that can excite plasmon resonance using the Kretschmann configuration was built and characterized for sensing applications.

References

1. Homola J, Yee SS, Gauglitz G. Surface plasmon resonance sensors. Sensors and Actuators B: Chemical. 1999 Jan 25;54(1-2):3-15.

2. Homola J. Surface plasmon resonance sensors for detection of chemical and biological species. Chemical reviews. 2008 Feb 13;108(2):462-93

3. Nguyen HH, Park J, Kang S, Kim M. Surface plasmon resonance: a versatile technique for biosensor applications. Sensors. 2015 May;15(5):10481-510.

4. Zeng S, Baillargeat D, Ho HP, Yong KT. Nanomaterials enhanced surface plasmon resonance for biological and chemical sensing applications. Chemical Society Reviews. 2014;43(10):3426-52

5. Wood RW. On a remarkable case of uneven distribution of light in a diffraction grating spectrum. Proceedings of the Physical Society of London. 1902 Jun;18(1):269.

6. Rayleigh L. On the dynamical theory of gratings. Proceedings of the Royal Society of London. Series A, Containing Papers of a Mathematical and Physical Character. 1907 Aug 2;79(532):399-416.

7. Fano U. The theory of anomalous diffraction gratings and of quasi-stationary waves on metallic surfaces (Sommerfeld's waves). JOSA. 1941 Mar 1;31(3):213-22.

8. Bohm D, Pines D. A collective description of electron interactions. I. Magnetic interactions. Physical Review. 1951 Jun 1;82(5):625.

9. Pines D, Bohm D. A collective description of electron interactions: II. Collective vs individual particle aspects of the interactions. Physical Review. 1952 Jan 15;85(2):338.

10. Bohm D, Pines D. A collective description of electron interactions: III. Coulomb interactions in a degenerate electron gas. Physical Review. 1953 Nov 1;92(3):609.

11. Kretschmann E, Raether H. Radiative decay of non radiative surface plasmons excited by light. Zeitschrift für Naturforschung A. 1968 Dec 1;23(12):2135-6.

12. Otto A. Excitation of nonradiative surface plasma waves in silver by the method of frustrated total reflection. Zeitschrift für Physik A Hadrons and nuclei. 1968 Aug 1;216(4):398-410

13. Raether H. Surface plasmons on smooth surfaces. In Surface plasmons on smooth and rough surfaces and on gratings 1988 (pp. 4-39). Springer, Berlin, Heidelberg.

14. Kretschmann E, Raether H. Radiative decay of non radiative surface plasmons excited by light. Zeitschrift für Naturforschung A. 1968 Dec 1;23(12):2135-6.

15. Klimov V. Nanoplasmonics: Fundamentals and applications. Pan Stanford, Singapore. 2012.

16. Ashcroft NW, Mermin ND. Solid state physics [by] Neil W. Ashcroft [and] N. David Mermin.1976.

17. Kedia S, Samson S, Bach L. Total internal reflection-based free space optical communication system. Journal of Microelectromechanical Systems. 2015 Jun 10;24(5):1632-41.

18. Pluchery O, Vayron R, Van KM. Laboratory experiments for exploring the surface plasmon resonance. European journal of physics. 2011 Feb 18;32(2):585.

19. Sau TK, Rogach AL, Jäckel F, Klar TA, Feldmann J. Properties and applications of colloidal nonspherical noble metal nanoparticles. Advanced Materials. 2010 Apr 22;22(16):1805-25.

20. Wang SH, Yu J. Data for peptide-binding assay with oriented immobilization of GRP78 in Biacore. Data in brief. 2016 Jun 1;7:1696-9.

21. Deng S, Yu X, Liu R, Chen W, Wang P. A two-compartment microfluidic device for long-term live cell detection based on surface plasmon resonance. Biomicrofluidics. 2016 Jul 3;10(4):044109.

22. Deng S, Wang P, Yu X. Phase-sensitive surface plasmon resonance sensors: Recent progress and future prospects. Sensors. 2017 Dec;17(12):2819

23. Liu F, Zhang J, Deng Y, Wang D, Lu Y, Yu X. Detection of EGFR on living human gastric cancer BGC823 cells using surface plasmon resonance phase sensing. Sensors and Actuators B: Chemical. 2011 Apr 20;153(2):398-403.

24. Efimov AA, Arsenov PV, Minkov KN, Ivanov VV. Fabrication of metallic lines by aerosol jet printing: Study of the effect of substrate temperature on the aspect ratio. Oriental Journal of Chemistry. 2018;34(6):2777.

25. Sotnikov DV, Zherdev AV, Dzantiev BB. Detection of intermolecular interactions based on surface plasmon resonance registration. Biochemistry (Moscow). 2015 Dec 1;80(13):1820-32

26. Otto A. Excitation of nonradiative surface plasma waves in silver by the method of frustrated total reflection. Zeitschrift für Physik A Hadrons and nuclei. 1968 Aug 1;216(4):398-410

27. Johnson PB, Christy RW. Optical constants of the noble metals. Physical review B. 1972 Dec 15;6(12):4370.

Chapter 4

Growth and characterization of the gold thin film layers for SPR setup using the electron beam evaporation system

In the previous chapter, a custom made SPR setup was introduced, described in detail and its performance explored. This chapter introduces the concept of growing gold thin films that are suitable for use in SPR sensing applications. In principle, there is no SPR sensing system without a gold thin film layer. Generally, gold thin film layers are likened to the lungs of an SPR sensing system and without use of this metal, there is no sensing of the system. Herein, firstly it outlines gold thin film as a metal; explain its characteristics and finally narrate how it relates to SPR. Then subsequently, briefly deposition methods that are relevant to date were described. In this context, the e-beam evaporation system as the preferred choice of technique was presented in detail. Then following that, a brief description of the characterization techniques that are used to typify gold thin films were outlined. Next, angular measurement of different thickness layers of gold thin films were explored, this was done to determine which thickness layers will best suit SPR sensing applications. Using the SPR system described in chapter 3, in the current chapter, angular shift in SPR curve of resonance were seen at different angular dips for all the different thickness layers of gold thin films that were explored. To end the chapter, I determine that the thickness layer of 40 nm was the appropriate to use for efficient SPR sensing applications in chapter 5. Notably, I was able to show that gold thin film layer deposition using the e-beam evaporation system is perfect for thin film layer coating for surface plasmon resonance applications.

4.1. Introduction

Gold thin metal films are required for surface plasmon research; this is due to their unique characteristics of chemical inertness, high conductivity, work function, large atomic mass and favorable optical properties [1]. These characteristics of gold seem to have sparked interests to researchers due to its potential applications in chemical and biochemical sensing [2]. In chemical and biochemical applications, gold has been used as a signal transducer based on the unique optical properties stated above [2, 3].

For example, gold thin film layers serve well as substrates in creating plasmon frequencies in SPR applications [3]. This is due to its inert character and excellent surface properties of strong scattering length, bio-conjugation and long-term stability [3, 4]. Gold is a good conductor of electrons that are capable of resonating with a suitable wavelength and produces a strong, easy to measure SPR signal in the visible light range [5]. In order to avoid losses in the metal wave guides, surface roughness and the film uniformity should be perfect at all times, these kind of challenges depend on the deposition technique that is used in order to produce ultra-smooth metallic layers [5]. One of the most common impediments in depositing smooth gold films is the high percolation threshold. The combination of high atom mobility and surface tensions effect leads to fractal-like cluster to be formed when depositing the gold [6, 7]. In order to reduce these high percolation thresholds, the most forthright technique is to deposit an adhesion layer prior to the gold layers. The adhesion layer is used to enhance the sticking of gold structures to various substrates, since it is known that gold exhibits poor adhesion to dielectric and semiconductors [7]. A standard method is to deposit a thin adhesion layer such as titanium or chromium about 2-5 nm depending on the applications of the substrate [8].

In the case of SPR, the main goal of using titanium as an adhesion layer is mainly due to its metallic properties that can be able to enhance the SPR of gold, as well as its ability to maximize SPR signals based on different thicknesses and create a smooth gold film that improves the SPR signal for plasmonic applications. For the deposited metal, the type, shape, size and the surface density of the metallic islands are the key factors affecting the electrical as well as optical properties of thin metal film including the efficiency of the plasmon-polaritons excitation [9]. The structure and properties of the metal film on a given substrate for various applications are strongly dependent on the method of deposition.

Nowadays coating by physical evaporation techniques is mostly used for optical coating of thin film for optical sensing technologies. This is because physical evaporation depositions are carried out at lower temperatures without corrosive products as compared to other deposition techniques [10, 11]. The e-beam evaporation is a physical vapor deposition (PVD) technique whereby an intense, electron beam is generated from a filament and steered via electric and magnetic fields to strike source material (e.g. pellets of gold) and vaporize it within a vacuum environment [10]. With relevance to the present work, in the next section 4.1.1 and 4.1.2, the e-beam evaporation system and characterization techniques for thin metal film are described in detail.

4.1.1. Electron beam evaporation system

The e-beam evaporator system consists of a top area with a quartz crystal monitor, an electron gun with three crucibles and a sample changer. The bottom part consists of the ion pumps, sublimation pumps and a cryopanel [11]. The top area can be shielded from the bottom chamber by means of baffle valve on to which an O-ring is fitted. This valve is usually closed, maintaining a pressure lower than 1 X 10^{-7} mbar in the bottom area. The pressure at the bottom is maintained by keeping the ions pumps. This ion pump consists of an enclosure containing one or more pumping elements that are surrounded by a strong magnetic field [11]. The pumping element consists of a multi-cell anode structure between two titanium cathode plates. When creating a vacuum pressure, the voltage of about 6000 V is maintained between the anode and cathode. The electrons attracted towards the anode are forced into a spiral path by the presence of the magnetic field. Thus, a high probability of collision between electrons and gas molecules, these collisions produces gas ions and more electrons [10, 11]. Since it consists of three crucibles, three different elements can be evaporated sequentially during each e-beam operation (figure 4.1).

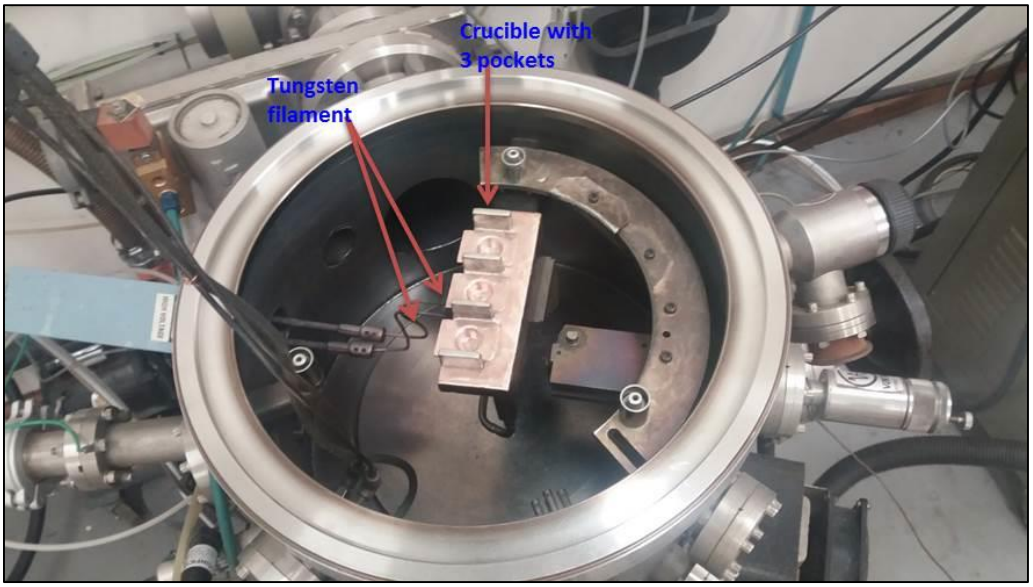

Figure 4.1: An image showing the three crucibles and the tungsten filament of the e-beam system. The crucible act as sample holders for the elements and the tungsten filament acts as the heating source.

The samples are mounted on aluminum holders, thus is to prevent the slides from falling off during deposition. They are then put in a sample changer, which can accommodate up to six holders, see figure 4.2. Once that is done, the top section of the evaporator is pumped down. The initial pumping is done with a pressure below 1 X 10^{-1} mbar, after that, the turbo pump is used to increase the vacuum.

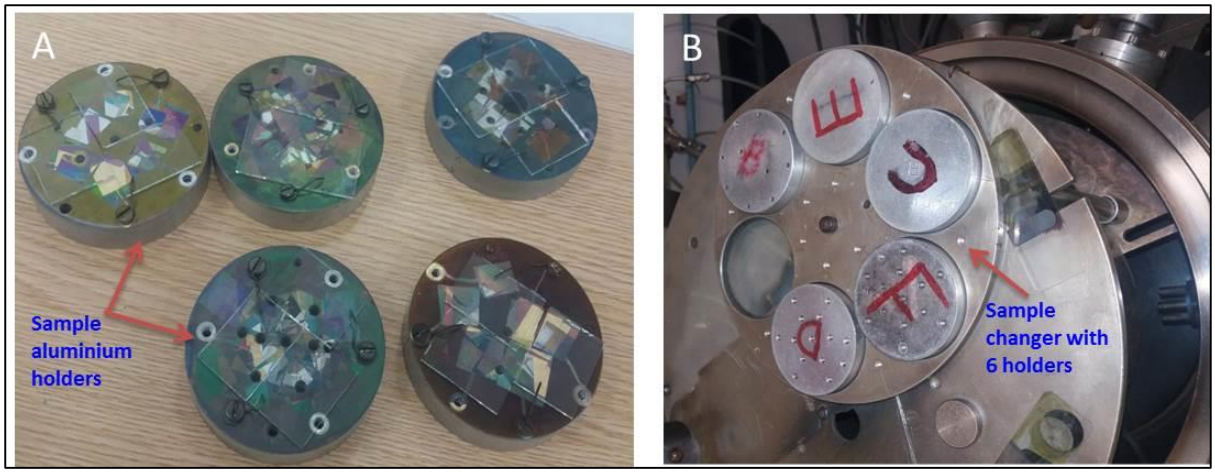

Figure 4.2: Images showing (A) the glass substrates mounted on the aluminium holders and (B) the aluminium holders placed on the six holder sample changer for e-beam deposition taken during the duration of the experiment at iThemba Labs.

After material to be evaporated has been preheated to reduce spattering and gaseous outbursts, the actual evaporation is carried out. The system is fitted with a shutter that can be opened or closed by means of magnets. The pressure during the evaporation is within the range of 1 X 10^{-7} and 3 X 10^{-6} mbar. The multilayers can be deposited sequentially without breaking the vacuum using the electron gun. This consists of the tungsten filament that produces electrons that are focused on the crucible by the magnetic field (figure 4.3).

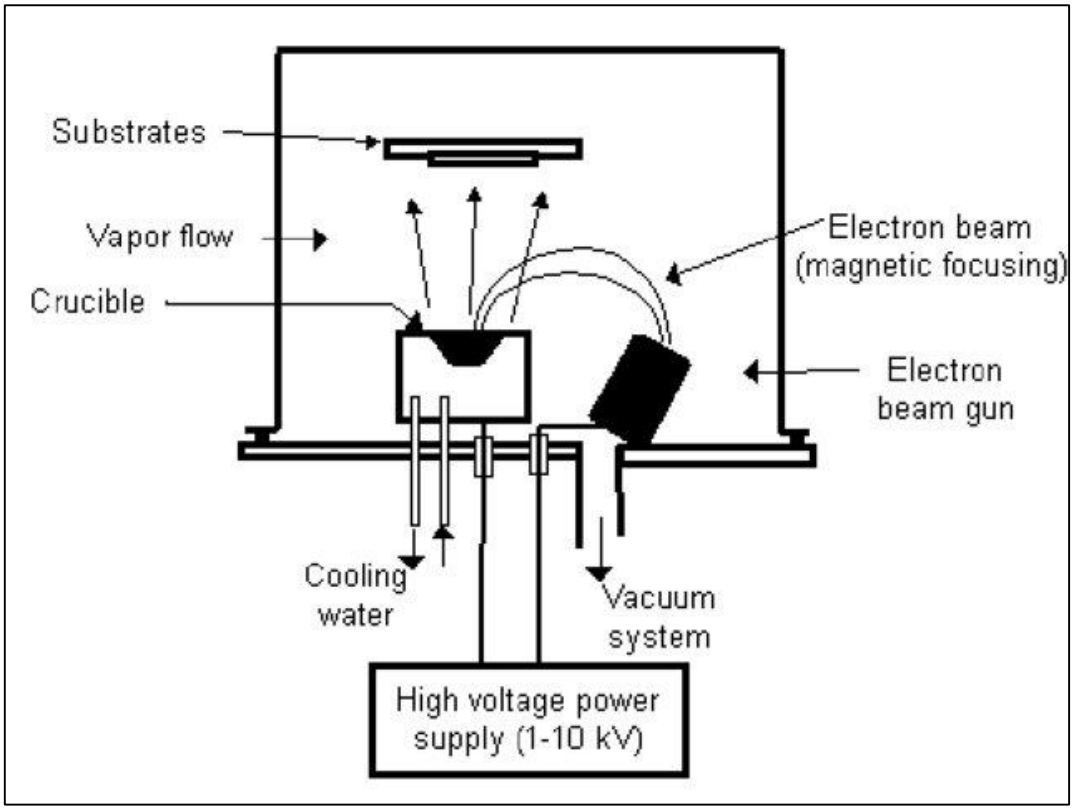

Figure 4.3: Diagram that depicts the experimental setup of the e-beam. It consists of the substrates that hold the samples facing down the crucibles, crucibles that hold the target elements, electron gun for multilayer deposition [10].

The vacuum system is advantageous, since it creates an environment where the depositions are contamination free and no impurities on the deposited layers will be observed. The film thickness is measured with a quartz monitor during evaporation. The accumulation of the material on the vibrating quartz causes frequency changes in the crystal [11, 12]. This translates into information that is fed into the microprocessor that calculates the rate of evaporation as well as the thickness of the film that is deposited. The Electron beam evaporation system offers high relative material utilization efficiency with controlled structural and morphological processes for thin metal film coatings [12].

4.1.2. Characterization of thin films

On the other hand, characterization of thin films after deposition is very essential. For this reason, structural and morphological characterization of the deposited thin films is needed since it is able to articulate more information on the deposited layers and their qualities [13]. Layer qualities such as roughness, completeness, uniformity and thickness composition are essential qualities that need to be studied after deposition [14].

Techniques such as the scanning electron microscopy (SEM), atomic force microscopy (AFM) and X-ray diffraction microscopy (XRD) are typically employed in assessing layer quality. Meanwhile, functional characterization of the deposited layers deals with the response of the layers to incoming radiation, electrical or chemical stimuli [12, 14]. This kind of characterization requires techniques such as optical absorption and transmission and surface plasmon resonance. The SEM technique offers a wide range of information about the sample and provides a high resolution image of surface of the materials [15]. Not only surface or topological information is produced through the SEM, but also information concerning the composition near the surface of material. SEM is based on the interaction of a focused electron beam with a surface of interest that is scanned by the beam [7]. During SEM imaging, a source of electrons is focused (in vacuum) into a fine probe that is scavenging over the surface of the specimen.

On the other hand, XRD is a powerful technique used to uniquely identify the crystalline phase presenting materials. Further, this method is applied to measure the structural properties of these phases such as strain state, grain size, epitaxy, phase composition, preferred orientation, and defect structure [16, 17]. It is also used to determine the thickness of thin metal films and multilayers, and atomic arrangements in amorphous materials. Additionally, it offers unparalleled accuracy in measurements of atomic spacing. The technique is also used to determine strain states in thin films [17]. Its noncontact and non-destructive nature makes it ideal to study thin metal films and multilayers since it provides quantitative, accurate data on the atomic arrangements of the films [16.17].

The basic principle of x-ray diffraction shows that x-rays are electromagnetic waves that have a short wavelength of the order 1 Angstrom (Å) which is equivalent to 10^{-10} m°. When making use of a crystal, the atoms are uniformly spaced in planes and separated by the distance of the order of 2 Å -5 Å [18]. X-ray diffraction patterns occur when the atom of the molecule in specific patterns deflects the x-ray light.

Diffraction occurs when waves travelling through an object whose dimension are order of the wavelength given by $\lambda \leq 2d$, where λ is the wavelength of the x-ray and d is the interplaner spacing The diffraction intensity is measured as a function of angle theta depending on the orientation of the sample in question which results in the diffraction pattern (figure 4.4).

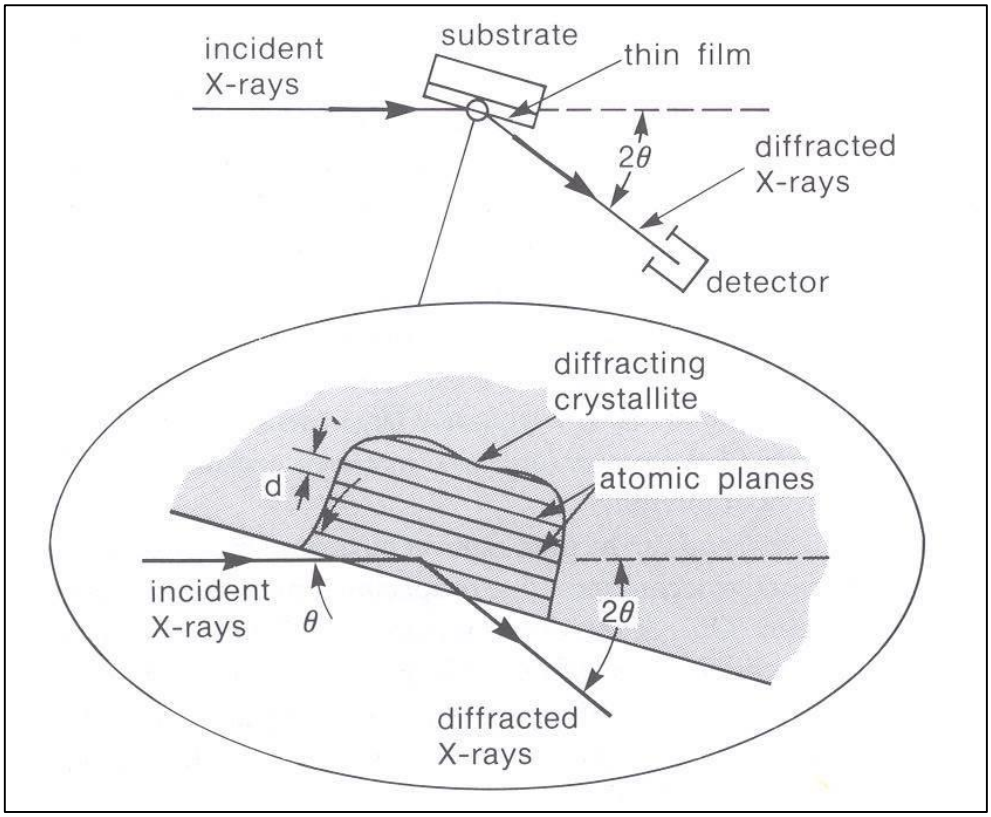

Figure 4.4: Basic features of a typical XRD experiment. In this experiment, X-rays light is shone through on the thin film substrate, causing diffracted rays when they incident on the surface of the plane. These diffracted rays are deflected in atomic planes of the molecule causing specific diffraction patterns that are transmitted to the detector [19].

In this case, the diffracted intensity is measured as a function of 2Θ according to the orientation of the specimen, which results in the diffraction pattern of the specimen. The x-ray wavelength is typically 0.7-2 Å which relates to x-ray energies (E =1 2.4 keV/λ) of 6 – 17 keV. With crystalline materials, the planes of atoms of crystals are spaced denoted **a,** distance denoted **d** apart [18, 19]. To differentiate between these spacing, coordinates system for the crystal whose unit vectors a, b, c, are the edges of the unit cell were introduced. It is known that familiar cubic crystals form an orthogonal system whereby is a coordinate system in which the coordinate lines (or surfaces) intersecting at right angles [18]. Using the Miller indices, atomic planes of crystalline materials are uniquely determined. There are three reciprocal intercepts of the planes with **a-**, **b-**, and **c-** axes [19]. They are reduced to the smallest integers having the same ratio. As a result, an (hkl) plane intercepts the crystallographic axes at a/h, b/k, and c/l [19].

In this instance, the d-spacing between the planes for a cubic crystal will be denoted by:

$$d_{hkl} = \frac{a_0}{\sqrt{h^2+k^2+l^2}}, \qquad (4.1)$$

Where a_0 is the lattice constant of the crystal (figure 4.5).

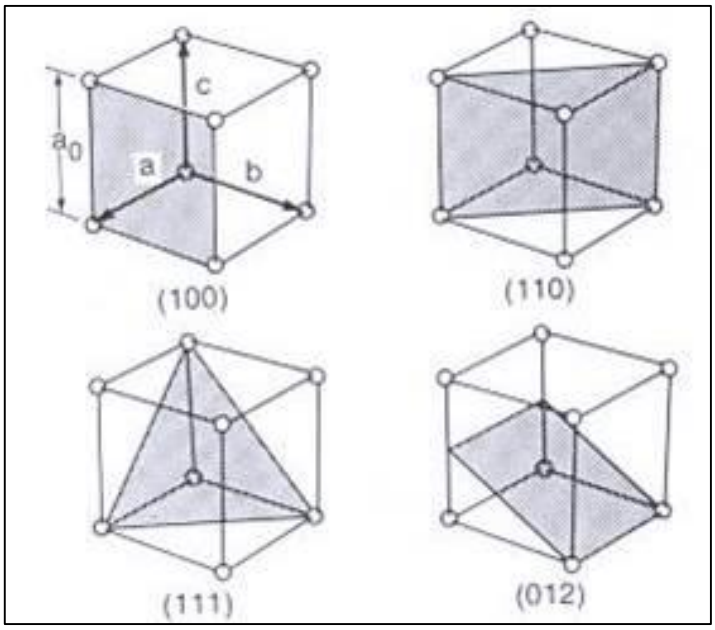

Figure 4.5: Schematic diagrams showing the Miller indices of atomic planes in a simple cubic crystal [19].

In the event that there is constructive interference from x-rays scattering by atomic planes in a crystal, diffraction peaks are observed. This is given by Bragg's law that states that x-rays reflected from different parallel planes of the crystal interfere constructively when the path difference is integral multiple of the wavelength of the x-rays [17, 18, and 19]. This is denoted by:

$$\lambda = 2d_{hkl} \sin\theta_{hkl} \qquad (4.2)$$

Where Θ_{hkl} is the angle between the atomic planes and the incident known as the Braggs angle The diffraction is recorded when the detector is positioned such that the diffraction angle is $2\Theta_{hkl}$. The crystal is orientated such that the normal and the diffraction plane is on the same plane with the incident and diffracted X-rays. Thus, is equal to the Braggs angle Θ_{hkl},

Thin films consist of many grains or crystalline that has a distribution of orientations to satisfy diffraction conditions. The diffracted X-rays emerge as cones about the incident beam with an opening angle of $2\Theta_{hkl}$ creating a diffraction pattern [19]. It is known that all the crystallites in thin films have the same atomic planes that are parallel to the substrate surface and are randomly distributed. Since they are known to have a fiber texture, face centred cubic films grow with (111) fiber texture [19]. The (111) planes runs parallel to the substrate plane and

(220) plane is perpendicular to the substrate and randomly distributed [18, 19]. As a result, the diffraction pattern will consist of rings about the film normal or (111) axis [19].

In this chapter, the main aim was to grow and characterize gold thin metal layer using the e-beam evaporation system for SPR applications.

4.2. Experimental methods

4.2.1. Sample preparation

In this study, gold (Au) was selected for the e-beam deposition based on its remarkable properties that make it compatible for SPR sensing applications. To enhance the sticking of gold on the glass substrates a 5 nm titanium (Ti) adhesion layer was deposited sequentially with 40 nm Au thin layer coating onto glass substrates using an e-beam evaporation system with a power supply of 3 kW. Ti and Au pellets with 99.9% purity were placed in the crucibles for evaporation of the Ti and Au thin films respectively, see figure 4.6.

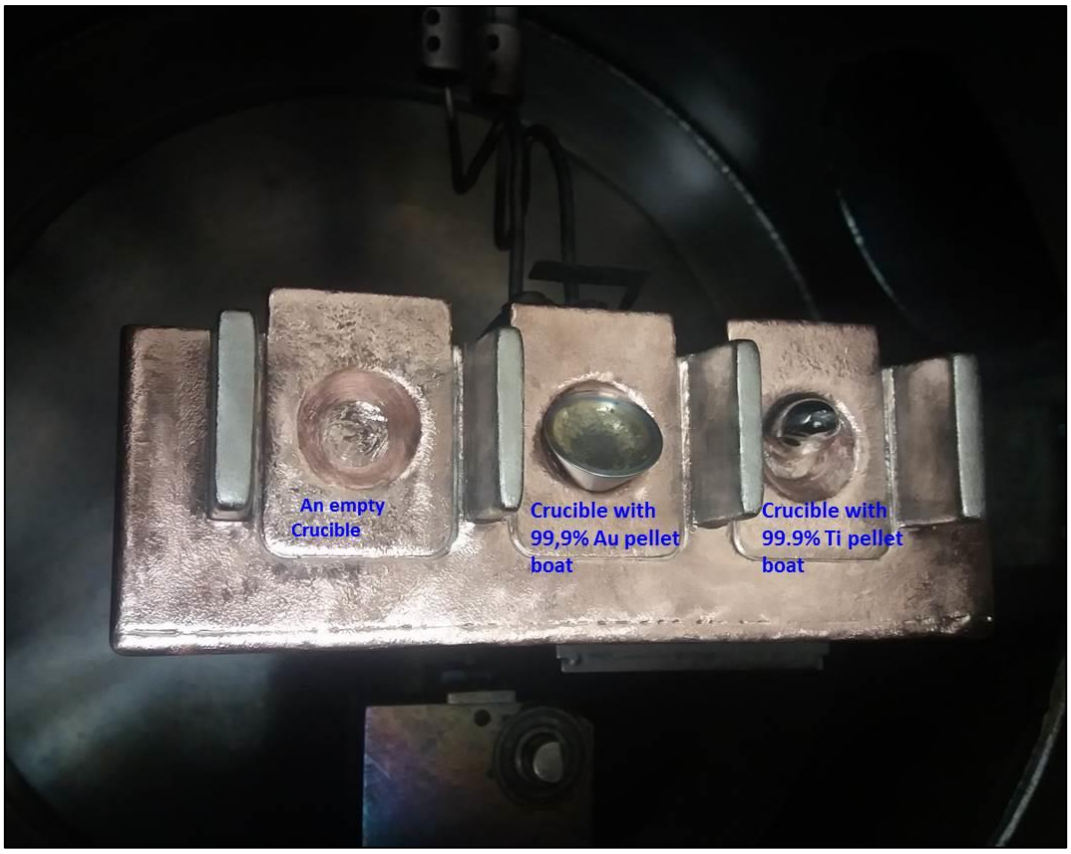

Figure 4.6: Titanium and gold pellets put on individual e-beam crucibles before evaporation.

Prior deposition, glass microscope slides of the sizes 22 mm x 22 mm and a thickness of 1mm where used as substrates. The glass substrates were cleaned by ultrasonic washing, degreased

using ethanol and acetone, and thereafter rinsed using deionized water before being mounted to the aluminum holders, as shown in figure 4.7.

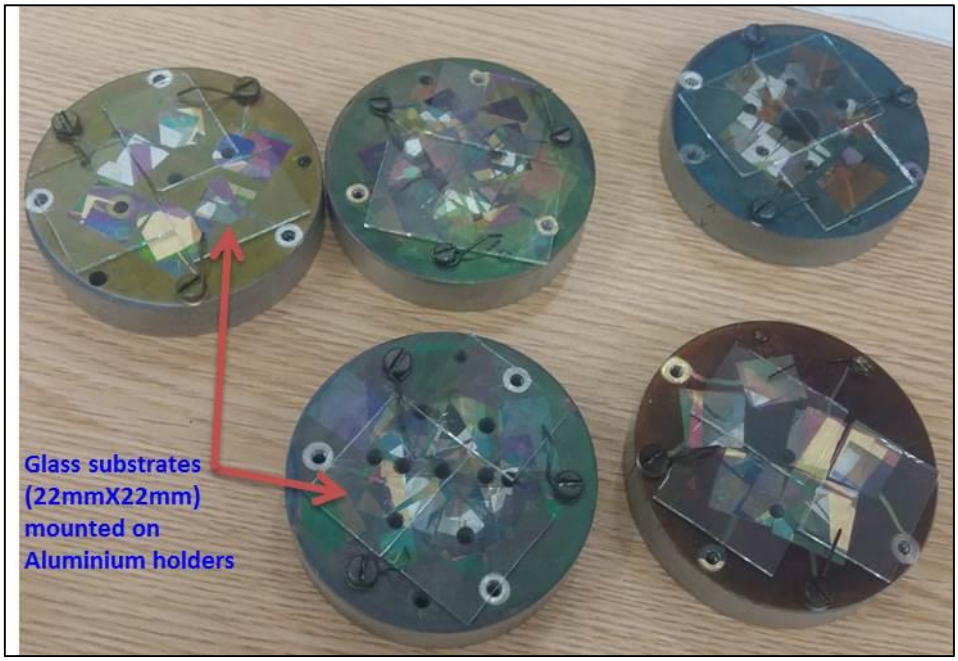

Figure 4.7: An image showing cleaned glass substrates (22 mm X 22 mm) mounted on Aluminium holders for e-beam evaporation.

The aluminum holders mounted with glass substrates were then placed into the sample changers that was assembled above the crucibles of the e-beam machine. The e-beam chamber was pumped down to a base pressure of 1 x 10^{-7} mbar. To remove atmospheric gases after pumping, degassing of the targets was done. After the pump had reached vacuum, the materials in the crucibles were preheated sequentially, to reduce spattering and gaseous outburst. Deposition was conducted using the e-gun current with the deposition chamber pressure of 1 X 10^{-6} mbar and deposition rate for the coatings of Ti and Au set at 20 MA, and 1.8 Å/s ± 0.6 Å/s used respectively. After the completion of the coating with 5 nm Ti on each of the glass substrate mounted on the aluminum holders on each sample changer period e-beam deposition, the next target, which was the gold, was indexed into position above the shutter. All these steps were repeated in all the substrates on the six sample changers with holders for the whole period of Au e-beam deposition. Once e-beam deposition was completed; the top part of the e-beam was switched off, the samples were left in the e-beam chamber until it had cooled down under vacuum for two hours. At the end, thin layer (Ti/Au) samples (shown below) were placed in petri-dishes.

Figure 4.8: E-beam deposited substrates with 5 nm titanium (Ti) and 40 nm gold (Au) taken after deposition.

4.2.2. Characterization techniques.

The optical properties of the substrates were measured using the UV-VIS-NIR spectrometer to determine the absorbance spectra of the coated thin film layer (Au) substrates. Transmission spectroscopy assessments were also run on the thin film layers using the Ocean optic 4000 + USB spectrometer. The data was analyzed using the Origin software version 8.

4.2.2.1. Analysis using X-ray diffraction.

The X-rays diffraction measurements were carried out using a BRUKER D8-ADVANCE diffractometer coupled with a Vantec-1 position sensitive detector as shown in figure 4.9 below.

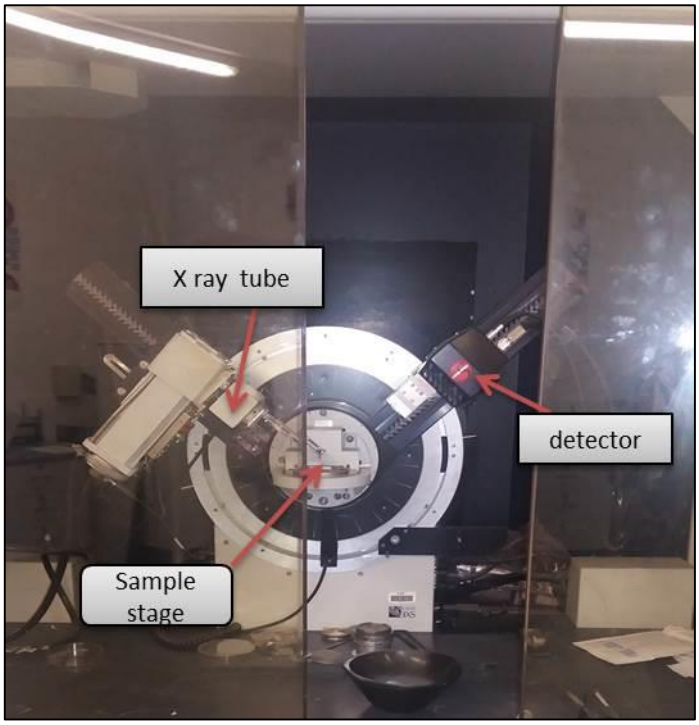

Figure 4.9: A labelled image of the X-ray diffraction machine taken during the experiment duration at iThemba labs.

This technique was predominantly used for the phase identification. Data was collected between 20 and 90 degrees in 2h with 0.0027 step size using Cu Ka radiation. The structural and morphological characterization of the coatings was investigated using X-ray diffractometer Model Bruker AXS D8 Advance using the Cu Kα1 with the wavelength of 1.5406 radiations. The measurements were done at a Θ - 2Θ configuration, with step size of the detector set at 0.01^{0}/sec. The Origin software was used to analyze and draw XRD patterns of the synthesized Gold thin films.

4.2.2.2 Analysis using scanning electron microscope

Scanning electron microscopy (SEM) is one of the main methods to determining topology on the deposited layers. It determines the completeness and uniformity of the deposited layers. In this study, SEM was used to investigate the surface morphology of the thin film layer coating. Generally, thin film growth mechanism and their properties is understood well by characterization using various techniques. The intent of this section was to grow gold thin films and use different analytical techniques that essential to characterize the thin films for SPR applications. In the next section 4.3 gives a narrative of the results obtained.

4.3. Results and Discussion

Thin metals are partially transparent and inductive at the same time. They represent continuous or un-continuous (island) structures. The shape of the island of the metal film increases their transmittance and decreases their conductivity. However, bulk metals are translucent to light, which is due to the high concentration of free charged carriers of metal [9]. In thin films, metals begin to behave in a different way compared to the thick films; their optical and electrical properties depend on the frequency of the incident electromagnetic wave. From literature, it is documented that gold is the material of choice for exciting plasmons for plasmonic applications [9, 11]. When a film is thick and continuous, or when the surface of a bulk metal is rough, this extra absorption band may correspond to the optical excitation of surface plasmons. In this context, it is also important to be able to use conventional metal deposition methods to obtain high-quality films on common transparent substrate materials, such as glass.

4.3.1. Characterization using X-ray diffraction (XRD) Spectroscopy

As previously stated, x-ray diffraction was used to examine the structure of the coated thin films. From the x-ray raw data generated form the XRD machine, gold synthesis showed diffraction intensities by means of peaks at different angles, as depicted in figure 4.10.

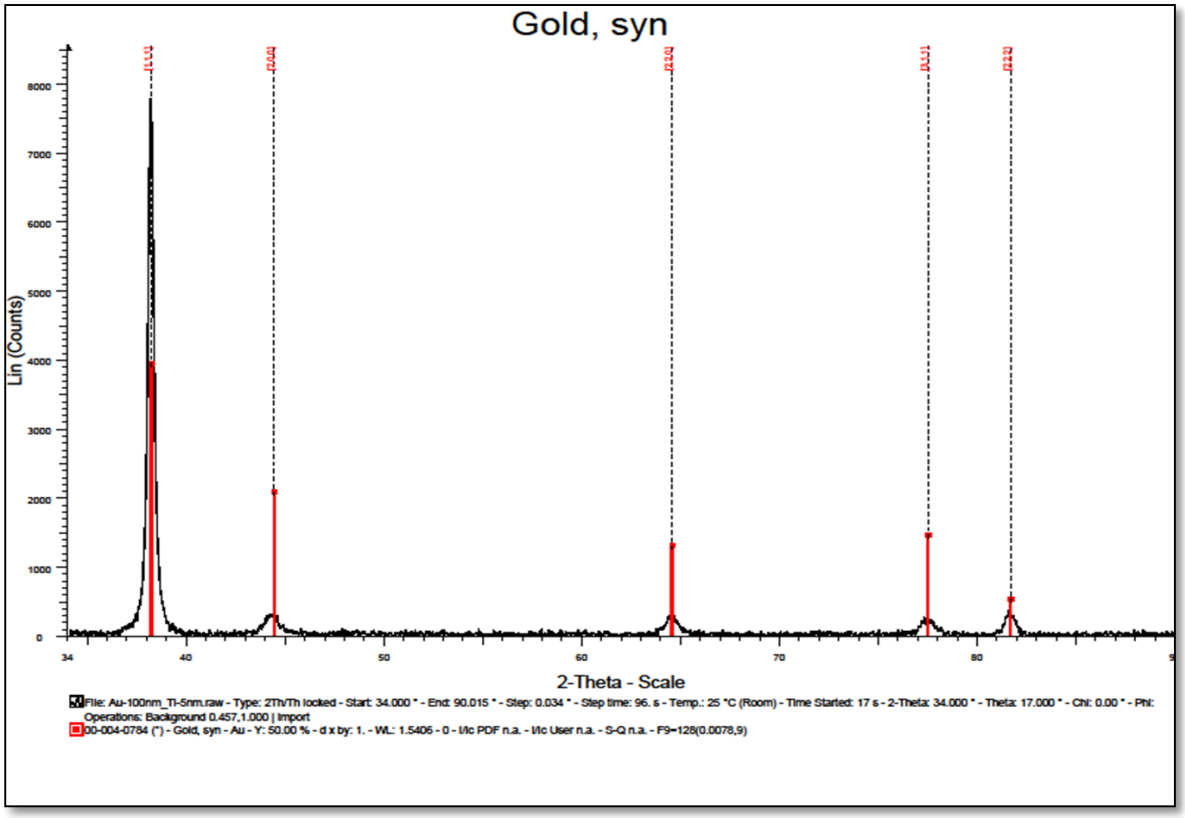

Figure 4.10: Raw data of gold synthesis using the X-ray diffraction for phase identification. XRD peaks was detected between 20° and 90°. Different peaks were detected from the coated slides, which shows and determines the phase identification of the gold.

Since diffraction power of thin films are small, so they maximize on the intensities of the film deposited. As XRD is known for providing phase identification in thin film studies, the identification is done by comparing the measured d-spacing in the different diffraction patterns that were produced from the experiment against their integrated intensities that are known standards given in the joint committee on powder diffraction standards file (JCPDS).

Figure 4.11, shows the x-ray diffraction pattern of the gold coated thin film. It can be seen that the sample exhibited three diffraction peaks from the (111), (200) and (220) planes from the angles 30^0 to 70^0. The first peak was seen in the plane (111) while the second and the third peaks were seen in the planes (200) and (220) on the graph, respectively.

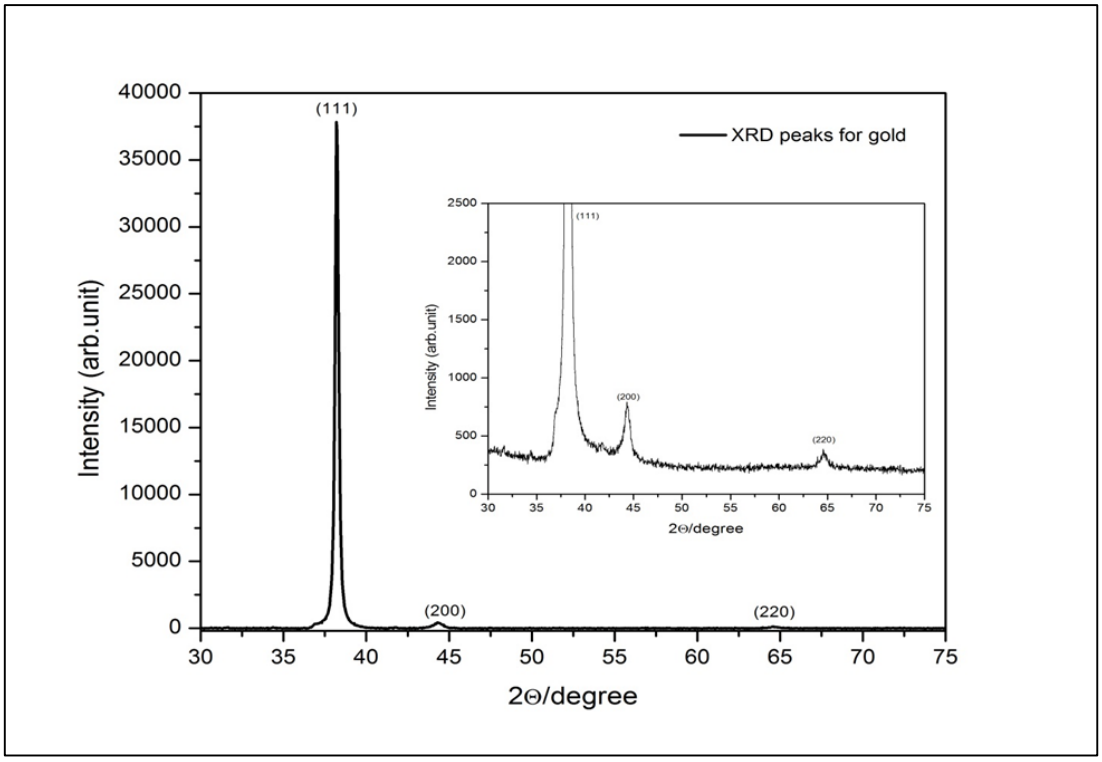

Figure 4.11: X-ray diffraction pattern of the gold coated thin film deposited on glass substrate using the e-beam evaporation system. XRD peaks for gold detectable planes at (111), (200) and (220).

The results obtained were matched with data for bulk gold standard of Joint Committee on Powder Diffraction Standards of the gold structure. The detectable planes (111), (200) and (220) are crystal planes that coincide with the face cubic lattice of crystalline metal of gold [4,

9]. It can be concluded that a pure crystalline of gold has been formed on the substrate surface since there are no appearances of other peaks in the XRD pattern obtained.

4.3.2. Surface morphology using Scanning electron Microscope

Scanning electron microscopy was used to investigate the surface morphology of the thin film layer coating. Figure 4.12 a and b depicts SEM images of the gold coated thin film.

At lower magnification of X5000 (Figure a), the deposited surface exhibited a smooth surface while at closer inspection with a higher magnification of X10 000 (Figure b), showed a homogenous uniformly coated surface.

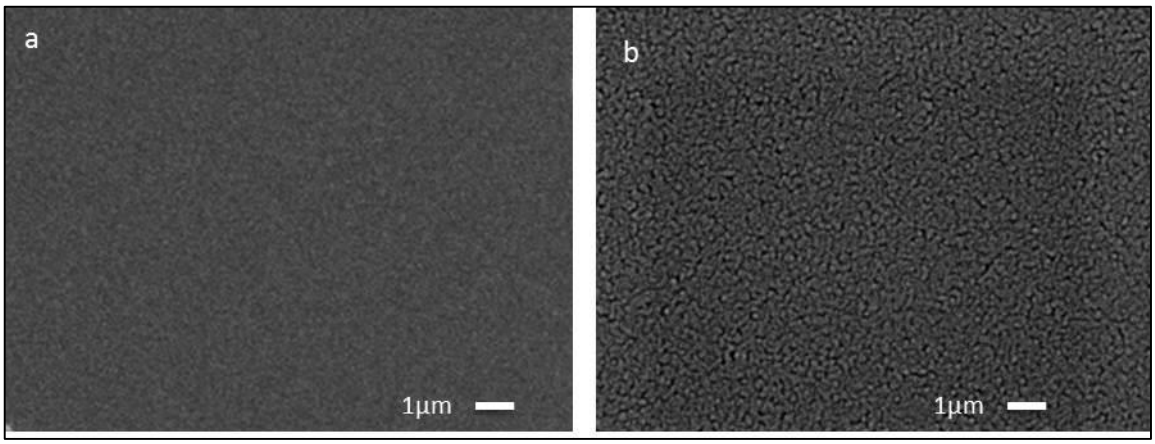

Figure 4.12: Depicts SEM images of the e-beam deposited samples. (a) gold coated thin film at a X5000 lower magnification and (b) gold coated thin film at X10 000 high magnification.

Due to the vacuum nature of deposition, larger atomic continuous structures are observed. This was anticipated since there more layer thickness is deposited the more the atoms cluster together resulting in uniform density and good metal conductivity unlike when using a sputtering method, single atoms are visible and this results in a discontinuous granular island thin film. Given the results shown by the XRD pattern together with the SEM results obtained above, it was clearly demonstrated that the e-beam evaporation system was efficient for gold thin film layer growth and deposition.

4.4.3. UV-Vis Characterization

The optical properties of the gold thin film coated layers were characterized using the UV-Vis spectrometer. Transmittance and absorbance spectroscopy of the different layers coated was performed in order to determine which layer would be the most suitable for SPR applications. Figure 4.13, shows the transmittance spectra at different thickness of the gold thin layers.

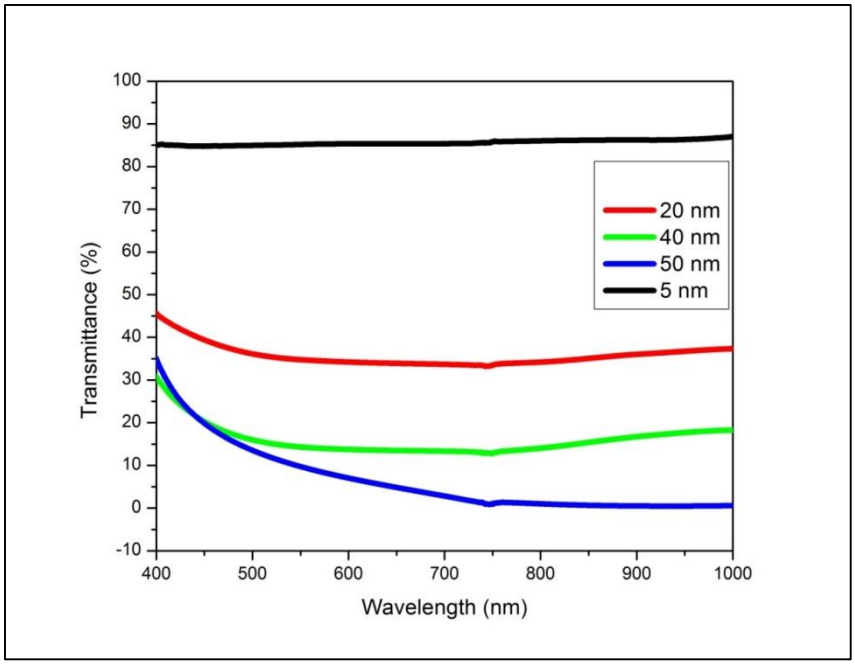

Figure 4.13: A Graph showing the transmittance spectra of different gold thickness (5, 20 40 and 50 nm) of the gold coated thin film.

It was observed that gold coated thin metal films were transparent at the thickness of 5 nm and has a maximum transmittance at the visible range. Usually, the gold thin films have a transmittance maximum peak at ~500 nm, but might behave differently at a longer wavelength [9]. It was also noted that the transmittance minimum also depends on the film thickness. The absorption edge at 400 nm for all thickness is due to absorption of the glass substrate. The absorption spectra are shown on the figure 4.14 below, we observed that 40 nm thickness displayed absorbance peak at ~560 nm this corresponds to the expected transverse surface plasmon resonance peaks [13]. As the thickness becomes greater, the absorption band is broadened due to a wider particle size distribution.

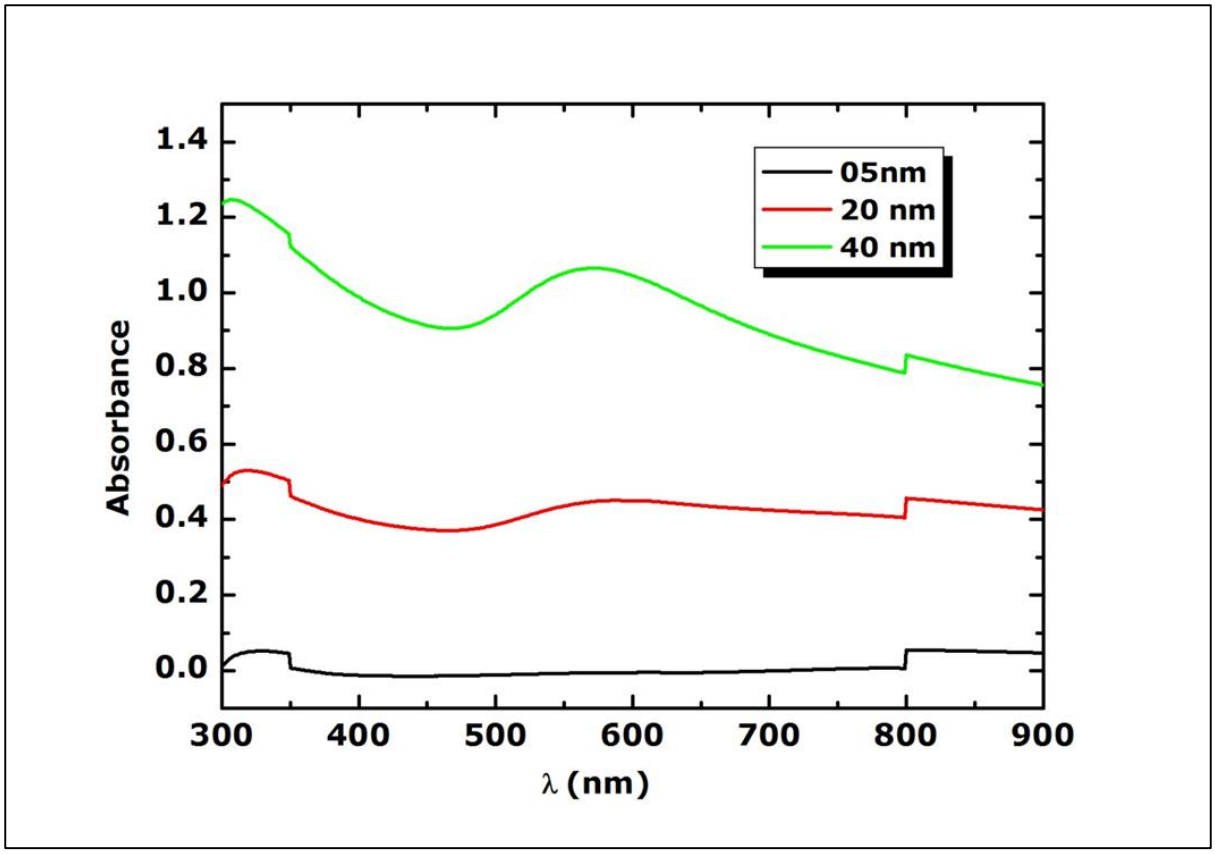

Figure 4.14: A Graph showing the absorption spectra of different thickness (5, 20 and 40nm) of gold coated thin films using the e-beam system**.**

The resonance spectrum is related to the surface density of gold film layers. Metal thickness is one of the most crucial parameter in surface plasmon resonance since it defines the maximum dynamic and shape of the plasmon [14, 20, 21]. The results also indicated that the 40 nm thickness layer was appropriate layer to use for surface plasmon resonance since it portrayed good absorption and transmission spectra. The thickness of the metal film is an important factor that influences the characteristics of SPR transducer. A study by Xinglong *et al*, 2003 [22], demonstrated that gold film thickness should be from 30 to 45 nm, and this plays an important role in increasing the changes in the refractive index. Translating to the thickness of the gold film is, the bigger the curve of the slope in SPR signals [21, 23]. The minimum at 500 nm shows a slightly red shift but with increasing film thickness, it was observed that pronounced absorption increasing at longer wavelength is a direct indication of surface plasmon resonance.

4.4.4. SPR signaling

Using the custom made SPR setup mentioned and illustrated in chapter 3, the same conditions were employed to determine angular measurements using different thickness of the gold thin films in order to determine which thickness will be best suitable to create a Plasmon wave in

our applications for sensing which will be discussed in chapter 5. In figure 4.15 (a) to (e), it was observed that there was angular dip of 55.80 ± 0.1° for the prism, 54.65 ± 0.1°° for the 5 nm gold layer; 55.23 ± 0.1°for 20 nm gold layer; 51.47 ± 0.1° for 40 nm Au layer; 50.71 ± 0.1° for 50 nm Au layer and 49.49 ± 0.1°for 60 nm gold thickness respectively. From these individual plots of each thickness layer versus the prism, it is clearly visible that there was an angular shift in the resonance angular measurements.

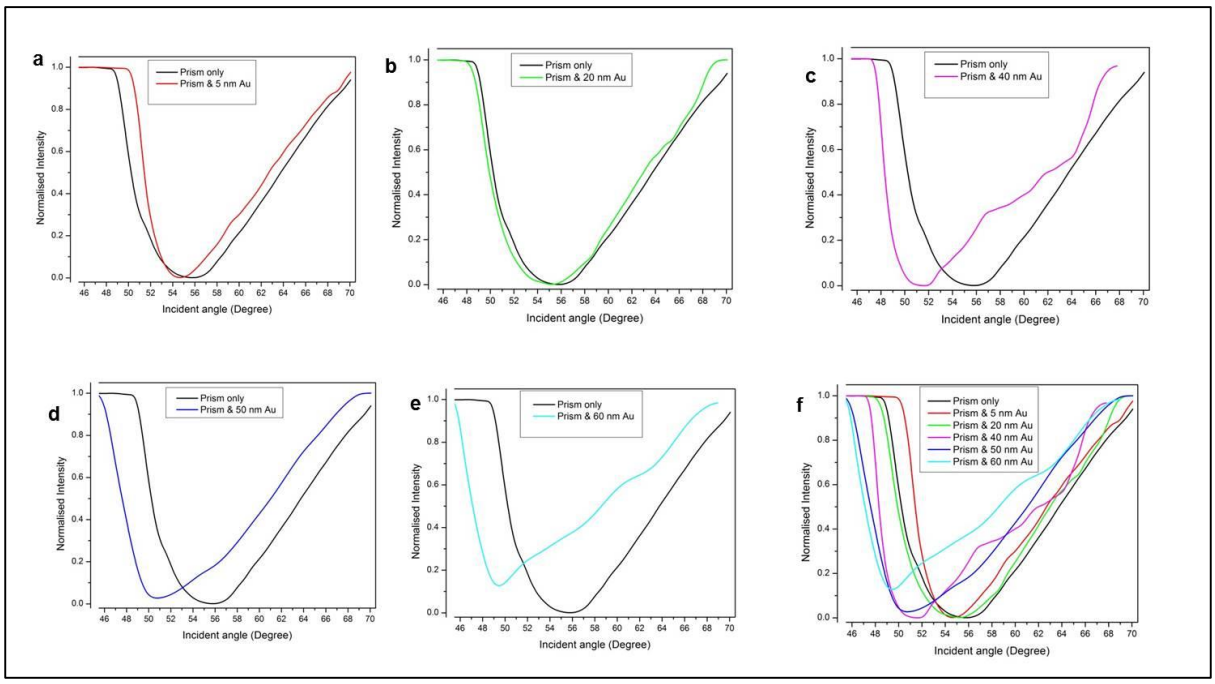

Figure 4.15: Graphs showing shifts of SPR curve of resonance using the prism with different gold (Au) thickness.(a) prism with 5 nm Au and (b) prism with 20 nm Au (c) prism with 40 nm Au; (d) prism with 50 nm and (e) prism with 60nm Au thicknesses, (f) the prism plotted with all the thicknesses of Au from 20 nm to 60 nm.

From the UV-Vis characterisation, we found that the 40nm was the optimal. This is because the 40 nm is able to create a surface plasmon wave that does not have decay faster than when you use the 50 nm. Furthermore, it take more time to create a surface plasmon wave with the 50nm due to that is a bit bulky and absorbs more energy rather than transmitting the energy.

There was an angular shift in the SPR resonance of 1.14° between the prism and the 5 nm Au layer. This is as a result of the thinness of the film coating which shows minimum transmittance as it was documented by Axelevitch *et al*, 2012 [9]. Not only did this shift result due to the thinness (5 nm) it can also be explained by the changes in the refractive index between the

prism and the coated layer. It is known from the SPR phenomenon, which is governed by the total internal reflection law, that light moves from a higher refractive index media to a lower refractive index media [9, 24]. As a result, a shift is expected since the light has moved from a higher refractive index media (prism) to a lower refractive index media (5 nm). However, the other contributing factor of this shift is the discontinuous nature of the 5 nm thickness layer. With the thickness of 20 nm (figure 4.15(b)), a shift of 0.57° compared to the 1.14 ° of the 5 nm Au layer was noticed, this could have been influenced by the size and distribution of the gold of on the surface, it might be that the gold was neither porous nor continuous resulting in less poor conductivity. This is also supported by the absorption results obtained presented in figure 4.14.

A shift of 4.33° was observed for the angular shift between the prism and 40 nm Au thickness layer (figure 4.15 (c)). The drop in the intensity almost to zero at the angular dip was seen as a good sign, as it translates that the excitation beam transferred its energy to the surface plasmon wave which is needed to cause polaritons that are highly efficient for facilitating binding interactions between molecules in bio sensing applications. This behavior conforms to the expected response of surface SPR band, due to the increase of the effective dielectric constants near surface of the gold [21, 23 and 24]. With this evident; it was determined that the ideal thickness needed for pursuing the sensing applications that will be discussed in the next chapter 5 is 40 nm.

For the 50 nm and the 60 nm thicknesses shifts of 4.79° and 6.31°respectively were observed (figure 4.15(d) and (e)). Since both these thicknesses have a continuous nature and metal conductivity they exhibit smooth curves due to distribution of the islands of the gold. At fixed wavelength, a maximum absorption is observed, which corresponds to the nature of the metal film [9, 24]. However the angular shift is broaden at the dip due to the particle aggregation of the metal surface. There are more large atomic clusters confined on the surface that leads to uniform density and leaving the metal bulky and less reflective for the applications in question. However, literature has documented that, the thicker the gold film is the sharper the SPR spectrum peak will dip, corresponding to the thickness of the different thickness layers, it can be seen that the 40 nm spectrum portrayed a dip sharper that the other layers figure 4.17 below.

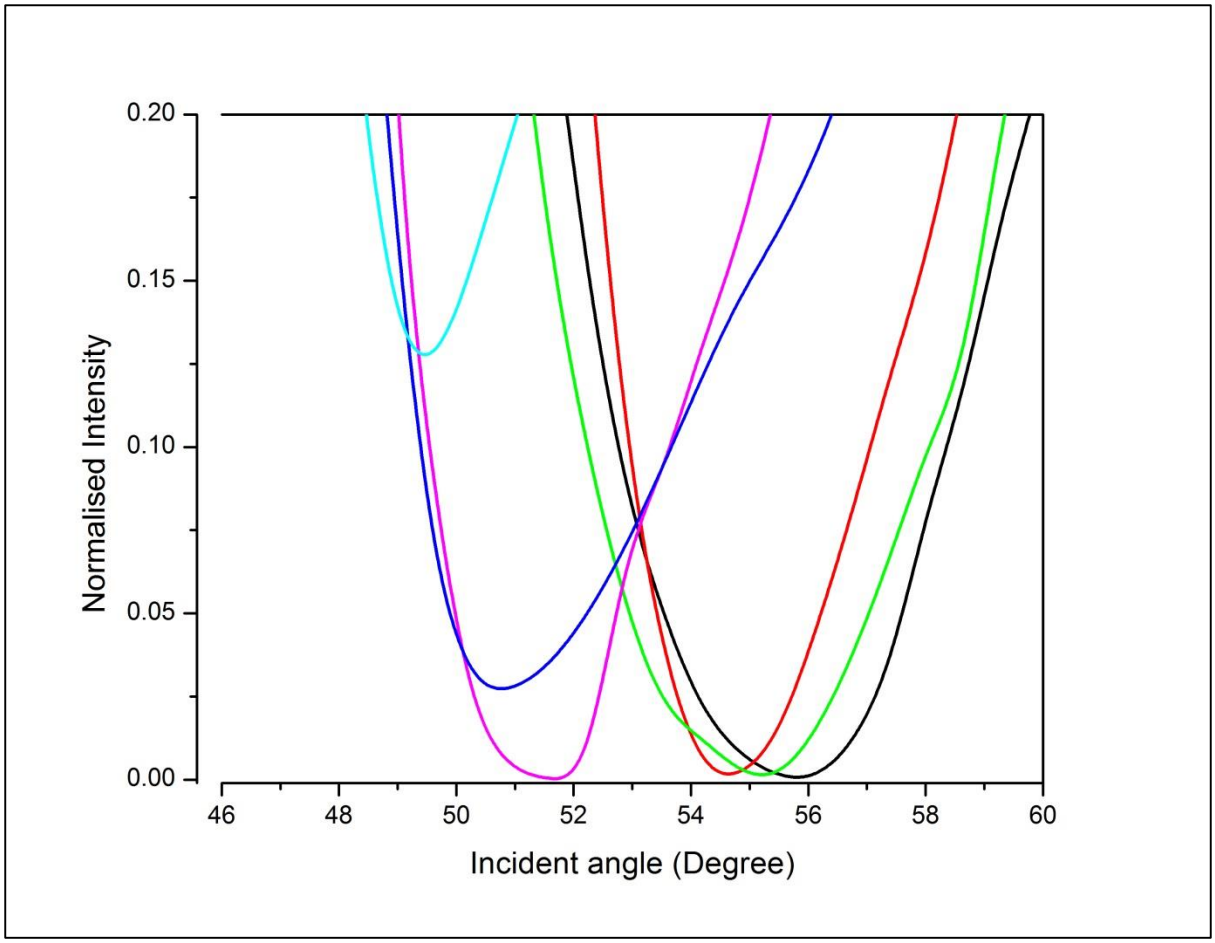

Figure 4.16:.A Graph showing shifts of SPR curve of resonance using the prism with different gold (Au) thickness. Prism (black), 5 nm (red), 20 nm (green), 40 nm (pink),50 nm (blue) and 60 nm (turquoise).

By observing this dip, it became easy to determine that the 40 nm thickness is the best thickness layer to use since it will guarantee a more precise measurement during bio sensing applications. Overall, it was evident that growth of gold thin films with e-beam system is more consistent and more stable and influences the plasmons appearance and their shape.

4.5. Conclusion

In this chapter, structural, morphological and optical properties of gold thin film layer deposited on glass substrates using an electron beam evaporation technique were studied.

From the XRD results, it was confirmed that Gold has a crystalline structure of Au (111) and their grain sizes were structural homogenous, which improves the gold thickness. SEM results correlated with the XRD results with the structural morphology of the thickness. Thin metal films exhibit resonant, SPP-related peaks (dips) at specific wavelength. Gold is a good conductor of electrons that are capable of resonating with light at a suitable wavelength.

Generally, gold is resistant to oxidation and other chemical reactions, which makes it a very eligible candidate for SPR sensing applications. More over gold is compatible and provides stability to self-assembly monolayers that are bound to its surface for a period of time. From the results obtained, it was evident that the metal thickness of the gold plays a vital role in the excitation of surface plasmons, which is very crucial for SPR applications. Through absorption and transmission spectra and SPR signaling using different thickness of gold, it could be clearly determined that the 40 nm thicknesses was the best thickness layer for our SPR application for further research interest to be conducted in chapter 5. In this study, we found that, growth and characterization of gold thin film layer using the e-beam evaporation system was a highly efficient technique for the gold thin film layer coating for SPR applications.

References

1. Kossoy A, Merk V, Simakov D, Leosson K, Kéna-Cohen S, Maier SA. Optical and structural properties of ultra-thin gold films. Advanced Optical Materials. 2015 Jan;3(1):71-7.

2. Wilson DM, Hoyt S, Janata J, Booksh K, Obando L. Chemical sensors for portable, handheld field instruments. IEEE sensors journal. 2001 Dec;1(4):256-74.

3. Moazzez B, O'Brien SM, Merschrod S, Erika F. Improved adhesion of gold thin films evaporated on polymer resin: applications for sensing surfaces and MEMS. Sensors. 2013 Jun;13(6):7021-32

4. Zheng G, Xu L, Zhan Y, Wu Y, Zhang C. Gold nanoparticle embedded titanium dioxide thin film for surface plasmon resonance gas sensing at room temperature. Sensor Letters. 2013 Nov 1;11(11):2038-42.

5. Malabi R, Manoto S, Ombinda-Lemboumba S, Maaza M, Mthunzi-Kufa P. Surface Plasmon Resonance as a biosensing technique for possible development of a point of care diagnostic tool. InLaser Science 2018 Sep 16 (pp. JW4A-108). Optical Society of America.

6. Voss RF, Laibowitz RB, Allessandrini EI. Fractal (scaling) clusters in thin gold films near the percolation threshold. Physical Review Letters. 1982 Nov 8;49(19):1441.

7. Malureanu R, Lavrinenko A. Ultra-thin films for plasmonics: a technology overview. Nanotechnology Reviews. 2015 Jun 1;4(3):259-75.

8. Habteyes TG, Dhuey S, Wood E, Gargas D, Cabrini S, Schuck PJ, Alivisatos AP, Leone SR. Metallic adhesion layer induced plasmon damping and molecular linker as a nondamping alternative. ACS nano. 2012 Jun 26;6(6):5702-9.

9. Axelevitch A, Gorenstein B, Golan G. Investigation of optical transmission in thin metal films. Physics Procedia. 2012 Jan 1;32:1-3.

10. Bishop C. Vacuum deposition onto webs, films and foils. William Andrew; 2011 Jun 21.

11. Matope S, Van der Merwe AF, Nemutudi R, Nkosi M, Maaza M. Micro-material handling employing e-beam generated topographies of copper and aluminium. South African Journal of Industrial Engineering. 2011;22(2):175-88.

12. Lu Z, Levi MD, Salitra G, Gofer Y, Levi E, Aurbach D. Basic electroanalytical characterization of lithium insertion into thin, well-crystallized V2O5 films. Journal of Electroanalytical Chemistry. 2000 Sep 8;491(1-2):211-21

13. Morsin M, Salleh MM, Sahdana MZ, Mahmud F. Investigation on the growth process of gold nanoplates formed by seed mediated growth method. Procedia engineering. 2017 Jan 1;184:637-42.

14. Yuan Y, Dai Y. A revised LRSPR sensor with sharp reflection spectrum. Sensors. 2014 Sep;14(9):16664-71.

15. Zhou W, Wang ZL, editors. Scanning microscopy for nanotechnology: techniques and applications. Springer science & business media; 2007 Mar 9.

16. Buerger MJ. X-ray crystallography: an introduction to the investigation of crystals by their diffraction of monochromatic X-radiation. J. Wiley & Sons, Incorporated; 1942.

17. Klug HP, Alexander L. E.(1954).'X-ray Diffraction Procedures.'.

18. Cullity BD. Elements of X-ray Diffraction. Addison-Wesley Publishing; 1956.

19. Schwartz LH, Cohen JB. Diffraction from materials. Springer Science & Business Media; 2013 Apr 17.

20. Lecaruyer P, Canva M, Rolland J. Metallic film optimization in a surface plasmon resonance biosensor by the extended Rouard method. Applied Optics. 2007 Apr 20;46(12):2361-9.

21. Švorčík V, Zehentner J, Rybka V, Slepička P, Hnatowicz V. Characterization of thin gold layers on polyethyleneterephthalate: transition from discontinuous to continuous, homogenous layer. Appl Phys A. 2002;75:541-4.

22. Xinglong Y, Dingxin W, Zibo Y. Simulation and analysis of surface plasmon resonance biosensor based on phase detection. Sensors and Actuators B: Chemical. 2003 Jun 1;91(1-3):285-90.

23. Slepička P, Kolská Z, Náhlík J, Hnatowicz V, Švorčík V. Properties of Au nanolayers on polyethyleneterephthalate and polytetrafluoroethylene. Surface and Interface Analysis: An International Journal devoted to the development and application of techniques for the analysis of surfaces, interfaces and thin films. 2009 Sep;41(9):741-5.

24. Brust M, Bethell D, Kiely CJ, Schiffrin DJ. Self-assembled gold nanoparticle thin films with nonmetallic optical and electronic properties. Langmuir. 1998 Sep 15;14(19):5425-9.

25. Kalyuzhny G, Vaskevich A, Schneeweiss MA, Rubinstein I. Transmission surface-plasmon resonance (T-SPR) measurements for monitoring adsorption on ultrathin gold island films. Chemistry–A European Journal. 2002 Sep 2;8(17):3849-57

Chapter 5

Detection of biological analytes and HIV-1 using SPR as a biosensing technique for possible development of a POC diagnostics tool.

In this chapter, a brief overview on the SPR sensors, literature and characteristics is looked into. Then, the immobilization of biomolecules and signal amplification of the SPR system using the gold thin layer from chapter 4 is outlined. Briefly, the gold coated slides were functionalized and bioconjugation was achieved by covalently attaching antibodies to gold nanoparticles. Then, sensor chips were used on the SPR sensor system built in Chapter 3 for SPR sensing applications. Following this, angular interrogation and spectral experiment before and after conjugation were performed to successfully demonstrate the bioconjugation of the antibodies to the gold nanoparticles. Throughout the thesis, the Origin software was used to analyse and present the collected data in a form of graphs. Morphological changes of the sensor chips, observed using SEM not only emphasized the novelty in the functionalization protocol used, but also proved that the protocol was efficient for the bioconjugation of antibodies and nanoparticles to the sensor chips. Finally, the detection of HIV-1 using the SPR system through application of the protocol utilized for the bioconjugation of antibodies was performed. The results obtained displayed for the first time, that, bioconjugation of the virus to the HIV specific antibodies was achieved on the sensor chips. Additionally, in this thesis, gold nanoparticles were used to improve the sensitivity of the SPR system. Here, different concentrations of the virus were detected by the shift in the resonance angle, which can be translated to the sensitivity of the SPR system. Thus, the ability to detect different virus concentrations proved for the first time that SPR can facilitate the detection of HIV-1.

5.1. Introduction

Since SPR is a real-time and label-free high sensitive optical method of analysis in biological and chemical sensing applications [1, 2, 3, and 4]. As a powerful tool for high resolution in identifying chemical changes on the metal thin films, SPR has advantages of direct detection of analytes with high sensitivity and a short detection time when performing immunoassays [4].

Although SPR biosensors have been developed for detection and identification of specific analytes, these biosensors use a number of platform designs, biomolecular recognition elements and detection setups [5]. The detection setup for a particular application depends on size of

target analytes molecules, binding characteristics of biomolecular recognition element and the range of analytes concentration to be measured. The SPR technique can also be used in biomolecular binding [6, 7], DNA hybridization [8], antibody-antigen recognition [7, 8], cell based measurements [9] and protein nano-arrays [9], which is feasible by performing fluorescence [10]

On the other hand, viruses are diverse microorganism that comprises of DNA or RNA genome surrounded by capsid proteins, which are associated with an entry to the host cell [11]. Viruses require a host to propagate their lives and many are related to the human pathogens. HIV is a well-known variant that can cause acquired immunodeficiency syndrome (AIDS) which not only leads to a life-threatening infections but also carries the generic symptoms that are difficult to diagnose [12]. Therefore, in HIV infection, rapid detection of the virus has emerged as an important aspect in saving human lives. Of note, currently, SPR detection is performed in fixed high cost systems which are designed for central laboratories. Therefore, there is a growing need for designing a miniaturized SPR biosensing system that will be label-free, highly sensitive, and portable and can be used for point of care diagnostic applications. In the present study, a custom made SPR sensing system was used to detect biological analytes and facilitate the label-free detection of HIV-1 and its various concentrations for possible point of care applications in resource-limited settings. The next subsections 5.1.1. to 5.1.2 elaborates more on the factors and parameters that govern a potential SPR biosensing system.

5.1.1. Applications of SPR sensors

SPR biosensing appears to be one of the most powerful methodologies for monitoring of affinity binding of biomolecules and primary screening of drugged and drug-like molecules [13, 14]. Over the past decades, SPR biosensor, have been characterized by its ability for real-time, label-free detection and high sensitivity. It plays a significant role in studying biomolecular inter-actions in biomedicine, environmental monitoring, and food testing. Literature shows that, SPR-type sensors are increasingly used to study a variety of biological entities, such as DNA, RNA, proteins, carbohydrates, lipids, and cells in the field of biomedical research [15, 16].

There are several examples of biomedical applications of SPR technology including interaction analyses, conformational change studies and mutation detection. SPR has been used as a potent tool to study communications between biomolecules based on affinity binding analysis of a variety of bonds, including antibody-antigen [17], ligand-receptor kinetics [18], enzyme-

substrate reaction [19] and epitope mapping [20]. Real-time monitoring of DNA manipulation such as hybridization kinetics, enzymatic modifications, and DNA strand separation has also been done using SPR biosensors [16]. In conformational change studies, the SPR technique has been used to monitor structural transition in protein-small molecule interactions, proteins under diverse environmental conditions or impacts on apoptosis inducers [16, 21]. For example, when a protein molecule undergoes a structural change, those optical indicators such as optical thickness of the organic mono/bilayers are also affected and can be monitored by SPR biosensors. For physical applications, SPR is capable of investigating physical properties of an extensive range of materials by determining many surface characteristics including dielectric properties, absorption processes and surface degradation or hydration.

5.1.2. Characteristics of SPR sensors

In SPR sensors, refractive index directly modulates characteristics of light wave such as coupling angle, wavelength, intensity, phase and polarization. From literature, there are five main characteristics that best describe the performance of SPR biosensors which include sensitivity, linearity, resolution, limit of detection and limit of quantification. However, with relevance to SPR sensing applications and available literature, sensitivity, resolution and limit of detection are the most crucial characteristics that best describe the performance of SPR biosensors that are based on the Kretschmanns geometry. These characteristics are described in detail within subsections 5.1.2.1 to 5.1.2.3below.

5.1.2.1. Sensitivity

Sensitivity of the SPR sensor is defined as the ratio of the change in sensor output to the change in the quantity (concentration of the analyte) to be measured [5]. The sensitivity of an SPR affinity biosensor depends on sensitivity of the sensor output (this can be either the resonant angle or wavelength) to the refractive index and efficiency of the conversion of the binding to a change in the refractive index [5, 6].

5.1.2.2 Resolution

The resolution of an SPR sensor is defined as the smallest change in the bulk refractive index that produces a detectable change in the sensor output [5]. Resolution is a key performance characteristic of an SPR sensor and its value is equal to the ration of the standard noise deviation to the sensitivity of the SPR sensor. To determine the sensor output, SPR sensors need to measure the intensity of the light coupled to the surface plasmon. This results in their resolution being limited by the noise in the intensity of light detected [6].

5.1.2.3. Limit of detection

The limit of detection is defined as the analytes concentration, which causes a change in the sensor signal equal to three standard deviations of the background signal [5]. The limit of detection is directly dependent on the resolution of the sensor. However, this is also as a result in the properties of the analytes such as molecular weight of the analytes with relevance to its interaction to the receptor [5.6]. Despite its rapid growth and advancement, SPR biosensor biomolecular approaches still need investigation in order to improve sensor performance.

In this chapter, a custom made SPR sensing system was used to detect biological analytes for surface plasmon resonance biosensing applications and subsequently, facilitate the label-free detection of HIV-1 and its various concentrations for possible point of care applications in resource-limited settings.

5.2. Experimental methods

5.2.1. Gold nanoparticle (AuNP)-goat anti mouse IgG conjugation

In a 2 ml eppendorf tube, N-hydroxysuccinimide (sNHS) (Sigma Aldrich, South Africa) and N-ethyl-N'-(3-dimethyiamino-propyl) carbodiimide hydrochloride (EDC) of the same molar ratio were added to a solution of heterobifunctional polyethylene glycol (SH-PEG-COOH) and shaken for an hour. A 10 X phosphate buffer saline was used to adjust the pH of the solution to 7.4 prior the addition of the goat anti-mouse IgG. After the addition of the goat anti-mouse IgG, the solution was incubated for 2 hours before filtering with a 50 kDa filter to remove any residual by-products. The solution mixture now contained the SH-PEG-IgG that were collected after filtration. For the formation of AuNPs-IgG conjugate, 12 µl of AuNPs were added to the SH-PEG-IgG solution and incubated for an hour. UV-vis absorption spectroscopy was performed using the NanoDrop ND 1000 spectrophotometer to record the absorption spectra, where, several spectra were collected before and after conjugation.

5.2.2. Immobilization of primary and secondary antibodies

Gold coated substrates with a thickness of 40 nm were cleaned with absolute ethanol and deep rinsed with distilled water and the substrate was dried under the nitrogen (N_2) flux. The substrate was then immersed in 1 mM poly (ethylene glycol (PEG) 2-mercaptoethyl ether acid (Sigma Aldrich, South Africa)) at room temperature overnight. The substrate was rinsed several times with absolute ethanol and distilled water and the dried with N_2 flux to remove any residual materials. The functionalized substrate was then exposed to the solution mixture of 5 mM *N*-ethyl-*N'*-(3-dimethyiamino-propyl) carbodiimide hydrochloride (EDC) - *N*-

hydroxysuccinimide (sNHS) (Sigma Aldrich, South Africa) pH 6.0 buffer for 15 minutes at room temperature. Prior exposure to the 0.5 µg/ml primary antibody in 500 µl phosphate buffer saline (PBS) buffer solution, the substrates was rinsed several times with absolute ethanol and distilled water. The functionalized substrate was exposed to the primary antibody solution and incubated at room temperature protected from light overnight. The next day, the substrates were rinsed with 1 X PBS, and kept at room temperature while, the different concentrations of the 2 µg/ml secondary antibody solution conjugated to the gold nanoparticles of 10 µl, 20 µl, and 30 µl were prepared.

The functionalized substrates were exposed to the different concentration of the conjugated solutions (gold nanoparticles) at room temperature protected from light. After 2 hours, the substrate was rinsed and dried.

5.2.3. SPR sensing of the functionalized substrates on the custom made SPR system

The SPR measurements were performed using the SPR spectroscopy, where a coherent cube laser with the wavelength of 640 nm and the maximum power output of 60 mW was used as the light source for these experiments as was described in chapter 3. A prepared gold substrate as described in chapter 4 was placed onto a glass with the index matching oil (n = 1.52) and fixed onto a high index equilateral BK7 prism (n = 1.517) as shown in figure 5.1 below).

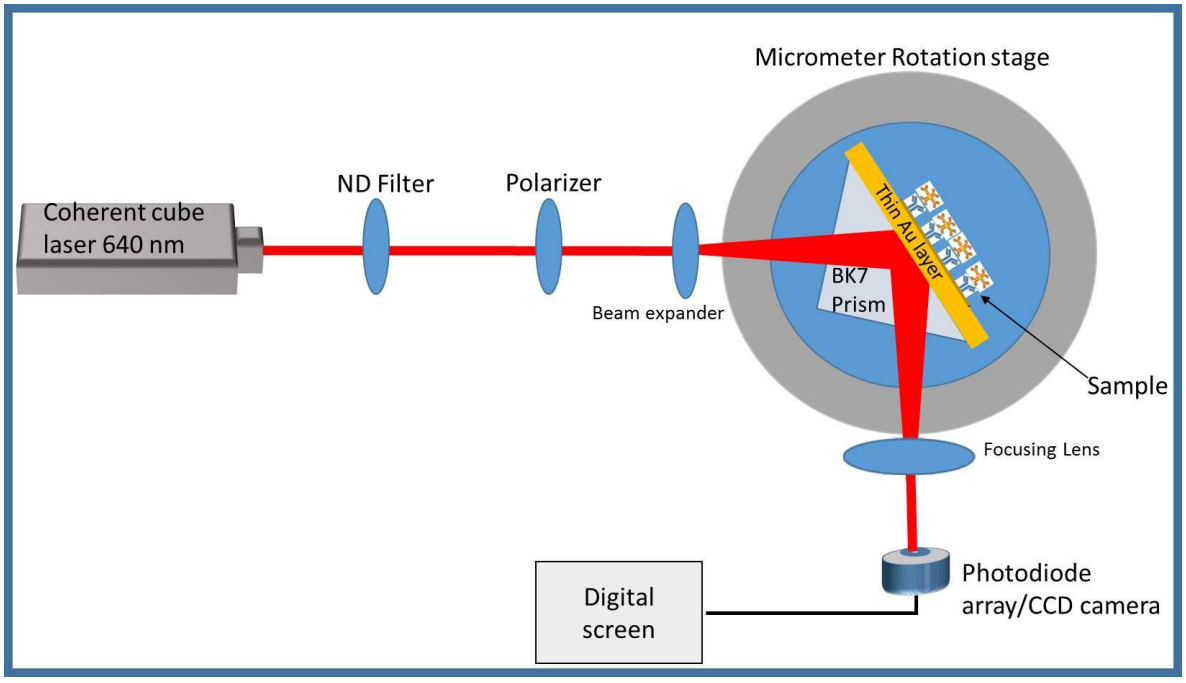

Figure 5.1: Setup of SPR spectroscopy with the sample (40 nm gold coated substrate with antibodies) fixed on the prism.

As previously mention in chapter 3, this setup was designed to SPR sensing applications and in the present chapter, this setup is used to detect biological analytes. The detailed SPR sensing of the analytes are transcribed in detail in Section 5.2.5

5.2.4. Structural analysis of the substrates using scanning electron microscopy (SEM)

The surface morphology of the prepared bare gold and the antibody conjugated with gold nanoparticles glass substrates were obtained using SEM operated at room temperature under air conditioning. This was done to see the structural changes on the surface of the sensor chips and to confirm if there was a self-assembly monolayer formed on the sensor chips before and after conjugation. Lower, higher and back scattering magnification settings on the SEM were used to acquire the images

5.2.5. SPR sensing on the custom made SPR system

An incident light of a 640 nm from coherent cube laser of 60 mW average power was *p*-polarised and then utilized to excite the surface plasmons by approaching the gold film surface of the SPR sensor. A manual micrometer rotation stage with an accuracy of 0.1° was used for measuring the incident angle changes. The intensity of the reflected light after the SRP sensor was detected with a biased photodetector and read with a multimeter, figure 5.2.

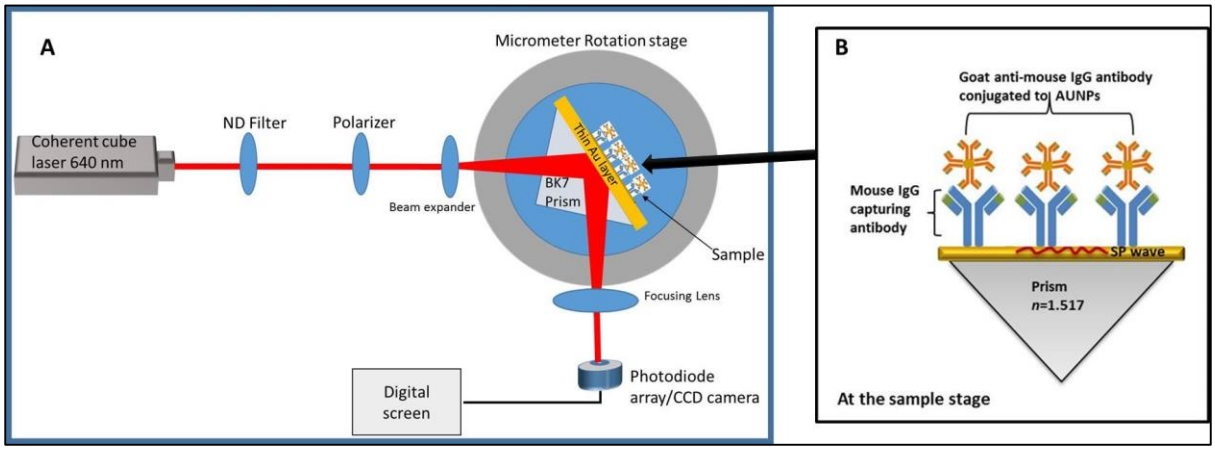

Figure 5.2: Schematic representation of the SPR setup with the 40nm gold substrate functionalised with antibodies (A). At the sample stage after the light hits the metal surface, surface plasmon (SP) wave is formed which facilitated the binding interaction of the primary (mouse IgG capturing) antibody to the Secondary (goat anti-mouse IgG) antibody conjugated to gold nanoparticles (AuNPs) (B).

SPR signals were acquired from the three SPR sensor chips of the 40 nm gold coated substrates contained the bare gold, substrates coated with primary antibody (mouse IgG) and substrate coated with antibody (goat anti-mouse IgG) conjugated to the gold nanoparticles. The angular

measurements were done, and the data collected was analysed and plotted using Origin software.

5.3. Results and Discussion

SPR technique provides sensitive, label-free and real time montioring of reactions of different biomolecular structures such as intertactions of proteins, DNA and viruses. It relies on the binding dynamics between the biomarker in the solution and a linked receptor that is immobilised on the surface of the sensor chip. These has shown potential results that can be very beneficial and suitable for clinical diagnostics. Although these biomarkers exist in small concentrations in clinical samples, this affects the efficiency of the SPR based sensors. These hindereness of the efficiency of the SPR based sensors can be improved by employing metallic nanoparticles such as gold nanoparticles that will enhance the SPR signal. Being known for their excellent properties and role in surface enhancement for sensing and being amplification tags, AUNPs amplifies the signal by inducing an increase in the refractive index on the surface of the SPR sensing chip.

In SPR biosensing, SPR sensors show high senstivity and selectivity towards biological markers. However, to improve the sensitivity of the SPR system, the use of AuNPs that form robust conjugates with biomarkers resulting in an increase in refractive index changes needs to be employed. This chapter, firstly demonstrates the effiective AuNPs covalently conjugated to antibodies on the sensor chips as biological analytes that are detected using our SPR system, then subsequently, use the SPR sensing system to detect HIV-1 and its various concentrations.

5.3.1. UV-Vis spectroscopy

The UV-vis absorption spectroscopy was used to test and verify the conjugation of goat anti-mouse IgG antibody to the AuNPs. A spectra of AuNPs was taken before and after conjugation with the goat anti mouse IgG antibody as presented in figure 5.3.

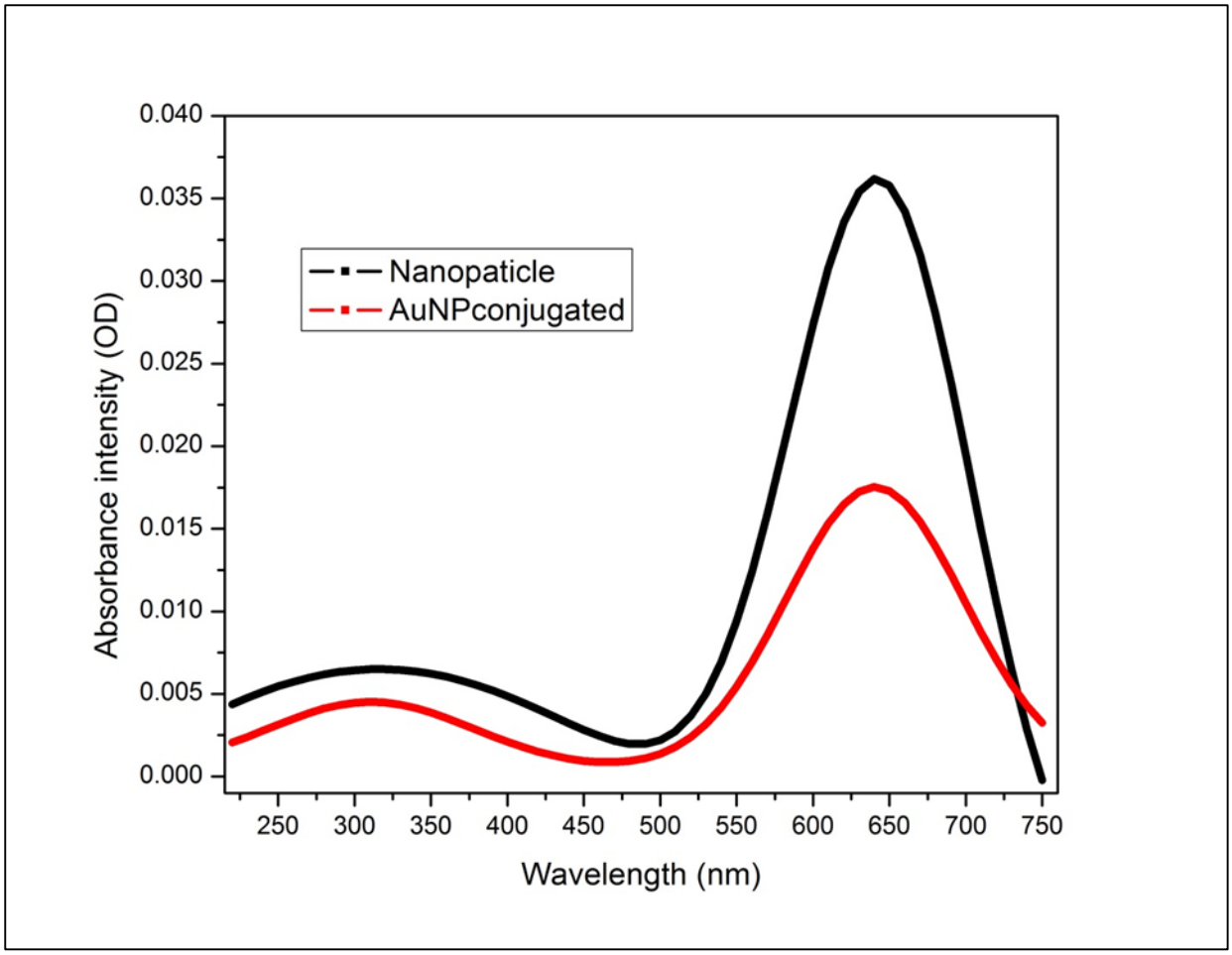

Figure 5.3: UV-Vis absorption spectra of Gold (AuNPs) nanoparticles before (**black**) and after conjugation with goat anti-mouse IgG antibody (**red**).

A red shift and a drop in the absorption intensity in the spectra after the conjugation of AuNPs to the goat anti-mouse IgG antibody were observed. The AuNPs showed absorption at a wavelength of 640 nm. The resonance wavelength and bandwidth of AuNPs are dependent on the shape, particle size and the refractive index of the surrounding medium as well as the temperature. The shift in the spectra after conjugation of AuNPs to the antibody might have resulted due to the changes in the dielectric environment surrounding the AuNPs. These conjugated nanoparticles can act as a transducer in optical sensing devices. The binding of analytes on recognition elements (biomolecules on a particle surface) using a specific biomolecule-biomolecule interaction represents the actual sensing step [22, 23]. The results above were able to demonstrate that AuNPs were covalently conjugated to antibodies successfully.

5.3.2. Immobilisation of antibodies and structural analysis using scanning electron microscopy

Scanning electron microscopy was used to study the structural morphologies of the gold coated substrates, and the functionalized gold coated substrate with secondary antibody conjugated to the gold nanoparticles. As shown in figure 5.4, the bare gold coated substrate displayed a smooth surface structure (fig 5.4a), while in (fig 5.4b) back scattering SEM image of the antibodies conjugated to gold nanoparticles showed a homogenous distribution of gold nanoparticles, this pattern was seen throughout the substrate. On the other hand, figure 5.4c exhibit super resolution scanning electron microscope results of the gold coated substrate functionalized with antibodies conjugated to gold nanoparticles.

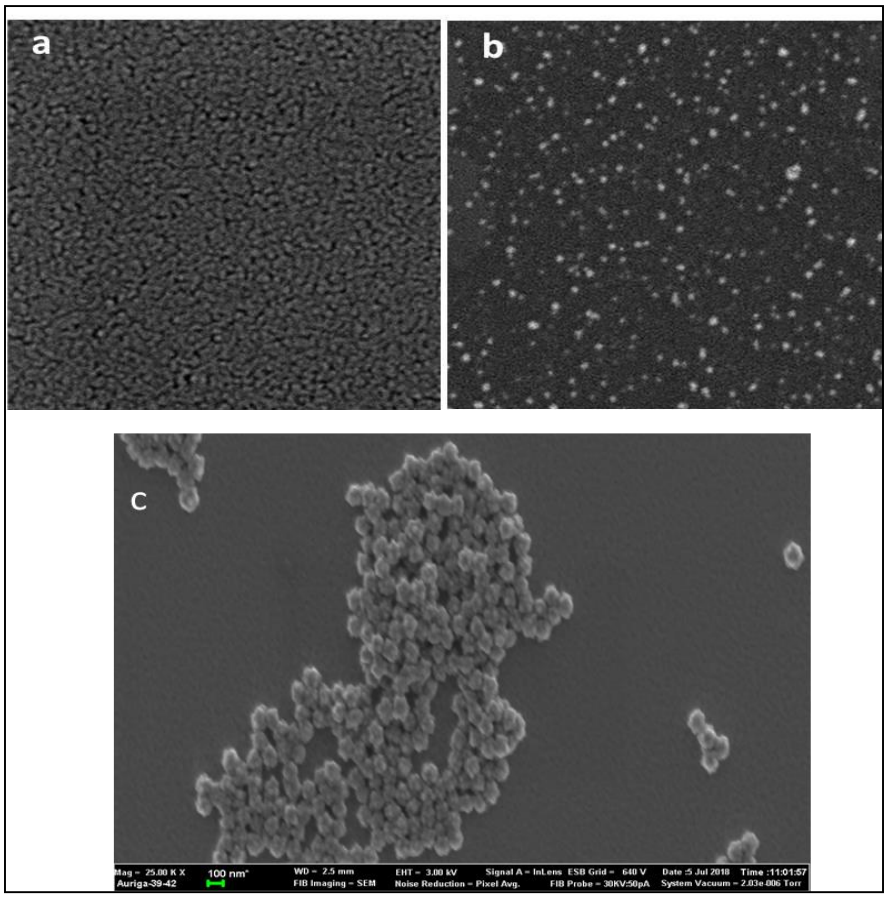

Figure 5.4: SEM images of the bare gold coated substrate (a), low magnification of the gold coated substrate with antibodies conjugated to the gold nanoparticles (b) and super-resolution image of the gold coated substrate with primary and secondary antibodies conjugated to gold nanoparticles (c)**.**

In figure 5.4c, a cluster of the gold nanoparticles (100 nm in size) bound to the surface of our SPR sensor chip was observed. Scanning electron micrographs confirmed that the procedure of functionalization of the gold coated substrates was successful for SPR sensing application.

5.3.3. Detection of biological analytes using SPR sensor

The custom made SPR sensing system was used to detect biological analyte. In Figure 5.5, changes in the SPR curve by absorbing of the primary antibody and the secondary antibodies conjugated to the gold nanoparticles are presented. These changes are due to charge interaction in series on the gold coated substrate. As a result, the SPR angle was appropriately 36.91° for 40 nm gold coated substrate, 36.49° for the functionalized gold coated substrate with primary antibody and 41.71° for the gold coated substrate functionalized with secondary (SEC) antibody conjugated to gold nanoparticles (SEC&AuNP). These results show SPR angle shift of 4.8° between gold coated substrate and gold coated substrate functionalized with secondary antibody conjugated to gold nanoparticles (SEC&AuNP).

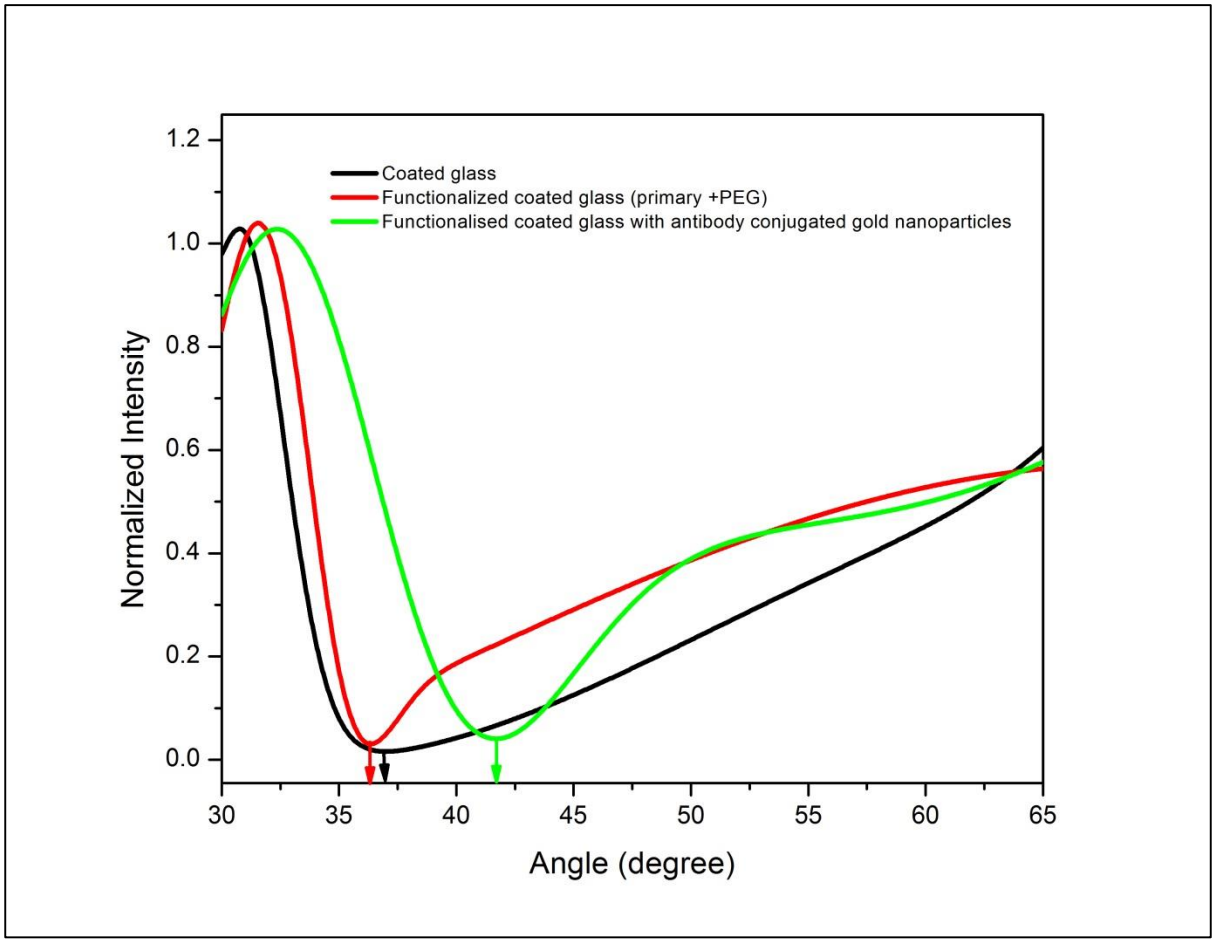

Figure 5.5: A graph showing shifts of SPR curve of resonance of the bare gold coated slide (black) functionalized gold coated substrate that has SH-PEG-IgG (red) and the gold coated substrate functionalized with secondary antibody conjugated to gold nanoparticles (SH-PEG-IgG + AuNPs IgG) (green).

In principle, a surface plasmon is a bound electromagnetic wave propagating at the metal-dielectric interface [11]. The spatial charge distribution creates an electric field which is localized at the metal-dielectric interface [11]. Hence, the plasmon resonance allowing the monitoring of the binding of the biological analyses to the functionalized surface with accuracy and precision. A dip in the measured reflection spectrum was observed where its reflectance spectrum shifts with the increase in refractive index in the gold coated substrate functionalized with secondary antibody conjugated to gold nanoparticles (SEC&AuNP), which can be easily be translated to the sensitivity of the SPR sensing system. Therefore, the shift in the SPR angle verified a thin layer of antibodies conjugated to gold nanoparticles bound to the gold coated substrates.

From literature, SPR biosensors are more sensitive when compared to other transduction principled based biosensor such as radioimmunoassay and calorimetry do not offer real time kinetic data [18]. They can be applied for kinetic measurements of analytical signals allowing the separate constants and thus more accurate characterization of the kinetic reaction of an analyte in the sample of interest [24]. In high-throughput screening applications, SPR biosensors are not only used for ligand-receptor interaction kinetic dynamics analyses, but also for drug discovery and drug development [16].Their different formats such as multichannel unit format and SPR imaging format allows continuous and simultaneous detection to analyze the performance of thousands of affinity binding events on the chip surface [16,25,26]. SPR biosensors have also been useful in proteomics researches, for example, Proteins (e.g., antibodies) and peptides are most frequently immobilized via covalent bonds formed between amino groups of the protein and activated carboxyls on a self-assembly monolayer of alkane thiolates or within a dextran matrix. Oligo-nucleotide can be efficiently immobilized via interaction between avidin or streptavidin immobilized on the sensing surface and biotinylated oligonucleotide [5]. Due to its sensitivity, portability and capability of multiplexed detection SPR has shown to be a useful tool for the detection of biomarkers. This methodology has been used to detect biomarkers for diseases such as cardiac and neurological diseases as well as ovarian and breast cancer [26, 27and 28].

SPR based microscopy has been used to detect the binding of single nanoparticles to functionalized gold sensor surfaces. In a study conducted by Zybin *et al,* 2010 [29], they were

able to visualize the binding of any single particle on the sensor surface using SPR imaging. The study also demonstrated that SPR is highly sensitive, since it was able to show binding events at a relatively big surface area of the sensor [29]. Given that, the SPR sensor platforms can be tailored for the detection of any analytes and allows label-free detection. In this study, it was observed that binding of the biological analytes (secondary antibody conjugated to the gold nanoparticles) to a detecting agent immobilized (functionalized surface with the primary antibody) on the metal surface (gold coated substrate) results in a shift of the resonance dip in the SPR spectrum. Therefore, it can be conclude that the home-built SPR system was able to successfully detect biological analytes (goat anti mouse IgG conjugated to gold nanoparticles) that were immobilized on the SPR sensor chip, thereby paving a way into designing a label-free point of care diagnostic tool.

Subsequently, It was shown successfully that our custom made SPR system described for the first time in chapter 3 has the ability to perform biosensing applications as is evident in the data obtained in subsection 5.3.3 above, going further the same methodology described in section 5.2 above, was applied for the detection of HIV-1 using the SPR sensing system. From the literature to date, there is not much that has been explored nor documented in laser based technologies in HIV-1 diagnostics using surface plasmon resonance. There was a need to explore the detection of HIV-1 using the custom made SPR sensing system as a proof of concept that will pave a way in developing a rapid SPR sensing HIV-1 label-free point of care diagnostic tool.

5.3.4. Immobilization of HIV-1 antibodies and structural analysis using SEM.

The HIV-1 GP41 capturing antibody was coated onto the gold sensor chips before adding the HIV-1 pseudovirus and the GP41 antibody conjugated to the AuNPs. This covalent bioconjugation is illustrated in figure 5.6A while the structural morphology of the bioconjugation process using SEM microscopy is depicted in figure 5.6B. As shown in the illustration, the GP41 capturing antibody were coated on the gold sensor chip using the chips that were coated using the e-beam evaporation system as described in chapter 4 and following the functionalization method described in subsections 5.2.1 and 5.2.2 above.

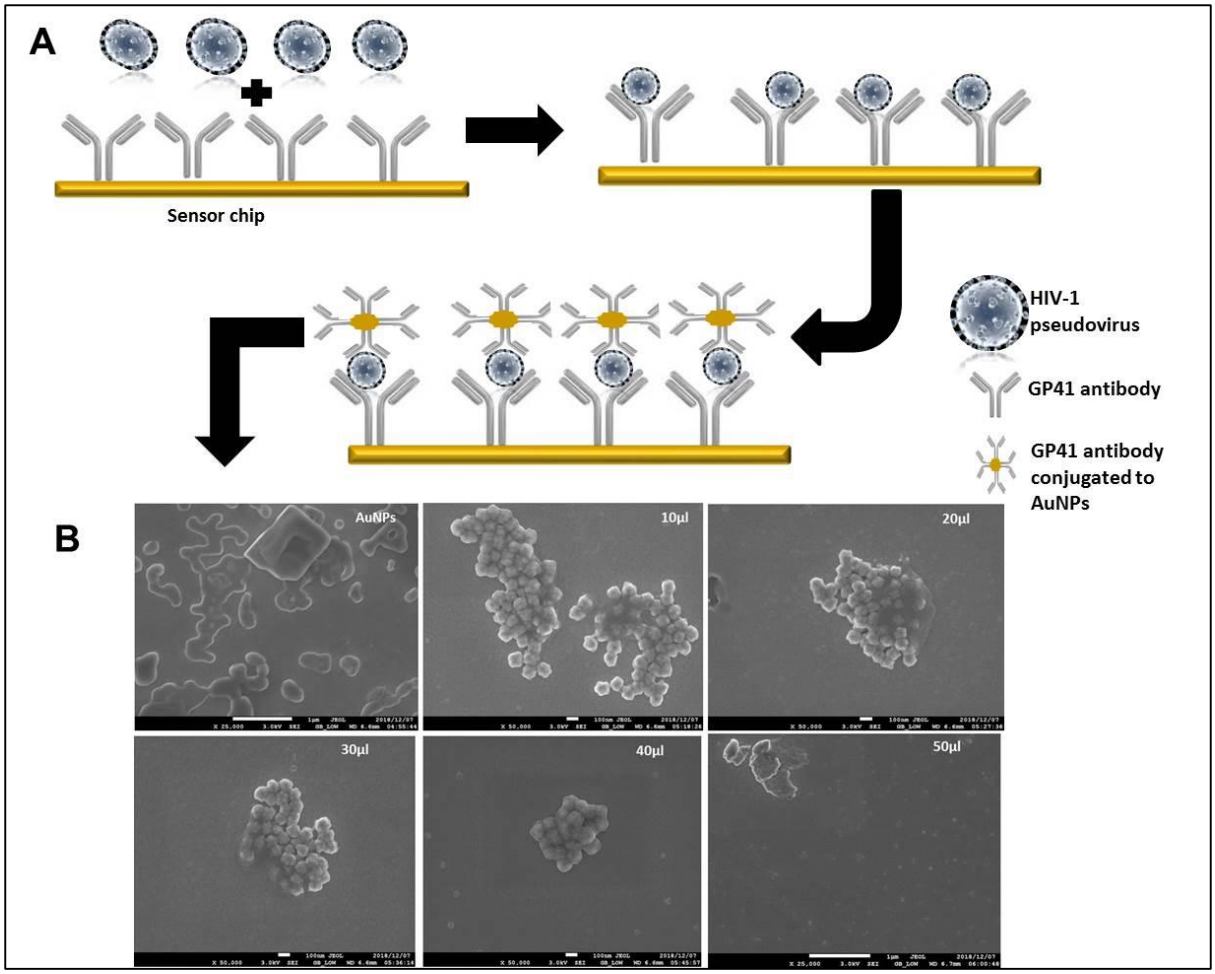

Figure 5.6: (A) Schematic representation of the gold sensor chips coated with GP41 antibodies and HIV-1 pseudovirus for capturing GP41 antibody conjugated to AuNPs. (B) SEM images of the different concentrations of GP41-AuNPs conjugate (10 µl – 50 µl) after binding to the surface of the sensor chip containing the virus.

Addition to the HIV-1 pseudovirus to the sensor chip with the GP41 capturing antibody resulted in the virus binding to the surface of the sensor chip; this is because the virus has a receptor that recognizes the GP41. It was also noticed that the addition of the GP41 antibody conjugated to the AuNPs to the sensor chip resulted in the GP41 capturing antibody bound to the virus binding to the AuNPs conjugates. This is shown by the SEM images in figure 5.6.B with different concentrations of the AuNPs. In this study, AuNPs called nanourchins with a phenotypic feature of spike nanoantenna type shape were utilized. From the SEM images (figure 5.6.B), the spike like AuNPs were seen bound to the surface of the sensor chip depending on their different concentrations.

Furthermore, depending on the concentrations of the AuNPs there is no uniform distribution of the AuNPs on the sensor chips, thus is due to the sporadic aggregation of the AuNPs. It was also observed, as the concentration increases the less the aggregation. Gold Nano urchins are

known to aid in the enhancement of plasmonic extinction resonance effect [30]. Their spiky nature uneven surface causes a red shift in the surface plasmon peak and a larger enhancement of the electromagnetic field [30]. While binding of biomarkers such as proteins to these gold nanourchins surface also causes a larger shift in the surface plasmon resonance peak.

5.3.5. Detection of HIV-1 using the SPR sensing system

The modified sensor chips was employed to measure different concentrations of HIV-1 virus bound to GP41-AuNPs conjugates based on the shift in the resonance angle due to changes in the refractive index changes by the specific binding interactions of the virus particles recognition events. Figure 5.7 shows the results of the changes in the SPR curves by the absorbing HIV-1 virus concentrations binding on the GP41-AuNPs conjugates bound on the surface of the sensor chip. As a result, the SPR angle of 50.91° well 2 (raw virus), 50.26° well 3 (300 pg/ml virus), 52.87° well 4 (150 pg/ml), 52.22° well 5 (75 pg/ml) and 52.22° well 6 (37.5 pg/ml) respectively.

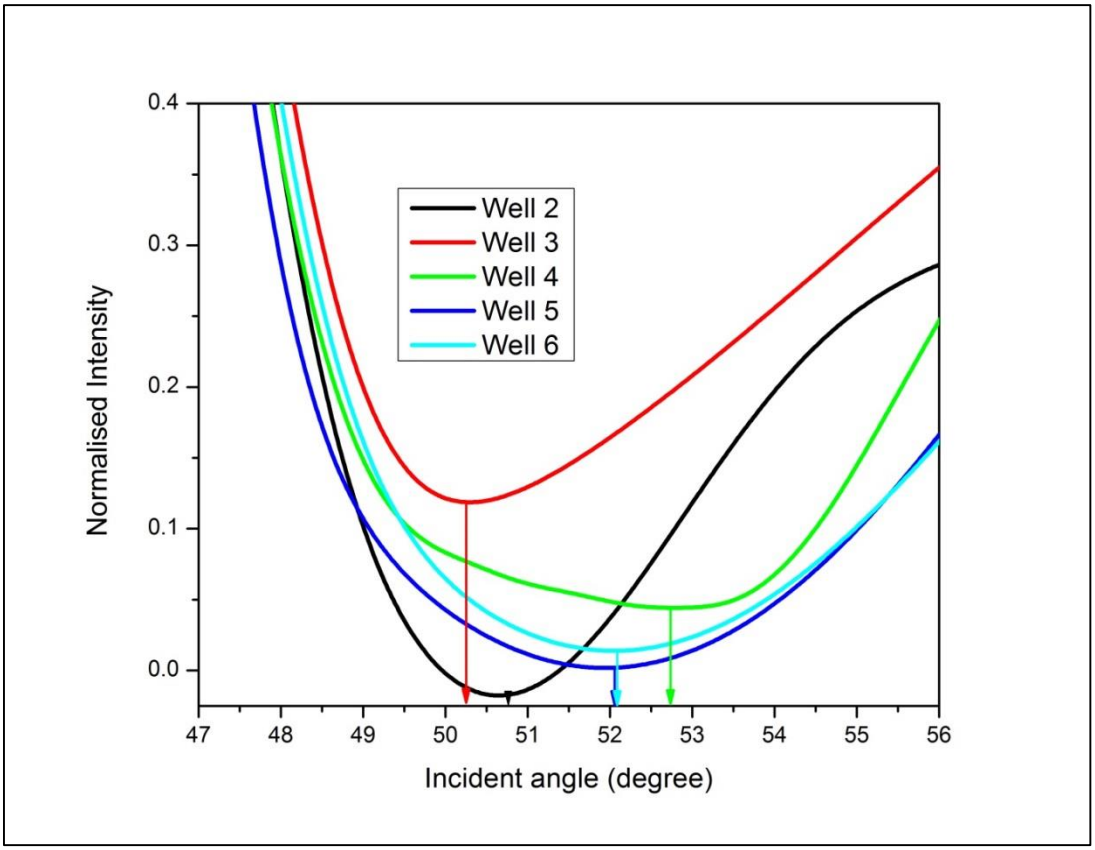

Figure 5.7: A Graph showing shifts of the SPR curve by absorbing HIV-1 virus concentrations binding onto the GP41-AuNPs conjugates bound to the gold sensor chip. With wells containing different virus concentrations: well 2 = raw virus; well 3 = 300 pg/ml; well 4 = 150 pg/ml; well 5 = 75 pg/ml and well 6 = 37.5 pg/ml.

Based on the raw virus, there was a shift in the SPR angle of 0.65° for the 300 pg/ml, 2.16° for the 150 pg/ml, 1.31° for the 75 pg/ml and 1.31° for the 37.5 pg/ml concentrations respectively. The significant changes were observed in the shift of the SPR angle of 2.16 for the 150 pg/ml of HIV-1 virus. The success in this change meant that the modification of the sensor chip for the detection of the virus was successful. Following that, it was observed that there were no significant changes in the SPR angle with the 75 pg/ml and the 37.5 pg/ml. This could have resulted in the non-specific binding reactions or the low concentrations that are bound on the sensor chip. These discrepancy findings were also noted by Lee *et al,* 2013 [31] when conducting a similar study using HIV virus like particles targeting the Gp120. In principle, surface plasmon resonance is a bound electromagnetic wave propagating at the metal dielectric interface.

The laser creates free electron mass of the metal which are in a distinctive mode, as soon as those electron are spatially charged, they create an electric field on the metal surface. This electric field is very sensitive to the interface and once absorption takes place, there will be a shift in the plasmon resonance. This shift allows the monitoring of the analyte to the metal binding interaction with accuracy. It also results in measurements in the refractive index changes.

Due to the changes in the refractive index changes and the resonance shift in the SPR angle, the estimated detection limit of our SPR sensing system for the detection of HIV-1 is at 75 pg/ml which is a better outcome compared to the results documented by studies by Park *et al,* 2012 [32] as well as Chang *et al,* 2010 [33]; when detecting viruses using SPR based sensing technique. Given the results obtained above, it can be concluded that the SPR sensing system used in this study was highly sensitive and selective with concentrations above 75 pg/ml.

When comparing these techniques in this study and what has been documented, Au sensor chips were consistently grown using the e beam deposition method, and the virus bound to the antibody with gold nanoparticle conjugates based on covalent interaction between the gold and the nanoparticles results in enhancement of sensitivity and selectivity of the SPR sensing system. With this favorable outcome, HIV-1 was detected successfully with the custom made SPR sensing system based on changes in the resonance angle shift without any labelling tools.

5.4. Conclusion

In the present study, immobilization of biomolecules was achieved by using the gold thin film of 40 nm described in chapter 4. The results obtained from the spectrograph of the conjugation of antibodies and nanoparticles confirmed that there was self-assembly monolayer on the surface of the sensor chips. By so doing, it showed that bioconjugation was achieved successfully. Angular and spectral measurements before and after conjugation showed that the protocol used for conjugation was efficient for bioconjugation of antibodies to nanoparticles structural morphology using the SEM demonstrated that there was successful bioconjugation of antibodies and nanoparticles supporting the results obtained during UV-vis spectroscopy. Furthermore, it also supported the results obtained in chapter 4 that 40 nm gold thin film metal layer was the ideal thickness layer to use for SPR sensing applications. This was evident by the SPR shift curves that were observed during angular measurement confirming that there was surface plasmon excitation on the sensor surface. Given all this results, it can be concluded that the protocol used was efficient for covalently attaching antibodies to nanoparticles, known as bioconjugation. Moreover, that the SPR sensing system was able to detect biological analytes (antibodies conjugated to nanoparticles).

Following this, the employment of the bioconjugation protocol also successfully demonstrated the for the first time conjugation of HIV-1 virus with nanoparticles on the sensor chips. Gold nanoparticles enhances the SPR signal, this is translated as the sensitivity of the SPR system. The observed changes in the resonance SPR shift curves when using different concentrations of the virus portrayed that the SPR system was sensitive and was able to detect HIV-1. The lowest concentration detected was 75 pg/ml, based on what was observed in the structural morphology using SEM and the changes in the resonance by shifts in the SPR curves; it was evident that the SPR system can detect HIV-1. Therefore, it can be concluded that the custom made SPR sensing system in this study was able to detect biological analytes for SPR biosensing applications and also facilitate the label free detection of HIV-1 and its various concentrations for possible of point of care applications.

References

1. Nguyen HH, Park J, Kang S, Kim M. Surface plasmon resonance: a versatile technique for biosensor applications.Sensors (Basel). 2015; 15(5):10481-510.
2. Homola, J.; Yee, S.S.; Gauglitz, G. Surface plasmon resonance sensors: Review. Sens. Actuators B 1999, 54, 3–15.
3. Yuan, W.; Ho, H.P.; Wong, C.L.; Wu, S.Y.; Suen, Y.K.; Kong, S.K.; Lin, C. Surface Plasmon Resonance Biosensor Incorporated in a Michelson InterferometerWith Enhanced Sensitivity. IEEE Sens. J. 2007, 7, 70–73.
4. Yuan, W.; Ho, H.P.; Wong, C.L.; Wu, S.Y.; Suen, Y.K.; Kong, S.K.; Lin, C. Sensitivity enhancement based onapplication of multi-pass interferometry in phase-sensitive surface plasmon resonance biosensor. Opt. Commun. 2007,275, 491–496.
5. Homola, J. 2008. Surface plasmon resonance sensors for detection of chemical and biological species.Chemical Reviews 108:462–93.
6. Homola, J. Surface Plasmon Resonance Based Sensors; Homola, J., Ed.; Springer: Berlin/Heidelberg, Germany, 2006; ISBN 9783540339182.
7. Baek, S. H., Y. B. Shin, M. G. Kim, H. S. Ro, E. K. Kim, and B. H. Chung. 2004. Surface plasmon resonance imaging analysis of hexahistidine-tagged protein on the gold thin film coated with a calix crown derivative. Biotechnol.Bioprocess Eng. 9: 143-146.
8. Lee, J. Y., H. J. Ko, S. H. Lee, and T. H. Park. 2006. Cell-based measurement of odorant molecules using surface plasmon resonance. Enzyme Microb. Technol. 39: 375-380.
9. Lee, W., B. K. Oh, Y. M. Bae, S. H. Paek, W. H. Lee, and J. W.Choi. 2003. Fabrication of self-assembled protein A monolayer and its application as an immunosensor. Biosens. Bioelectron.19: 185-192.
10. Oh, B. K., W. Lee, B. S. Chun, Y. M. Bae, W. H. Lee, and J.W. Choi. 2005. The fabrication of protein chip base on surface plasmon resonance for detection of pathogens. Biosens. Bioelectron. 20: 1847-1850.
11. Lee S, Sim S.J, Park C, Gu M.B, Hwang U.Y, Yi J, Oh BK, Lee J. Development of surface plasmon resonance immunosensor through metal ion affinity and mixed self-assembly monolayer. J.Microbiol.Biotechnol (2008), 18 (10), 1695-1700.
12. Lee J-H, et al, Highly sensitive localized surface plasmon resonance immunosensor for label-free detection of HIV-1.Nanomedicine: NBM2013;9:1018-1026

13. Pepin KM, Domsic J, McKenna R. Genomic evolution in a virus underspecific selection for host recognition.Infect Genet Evol2008;8:825-34.

14. Masson JF. Surface plasmon resonance clinical biosensors for medical diagnostics. ACS sensors. 2017 Jan 6;2(1):16-30

15. Wang SH, Yu J. Data for peptide-binding assay with oriented immobilization of GRP78 in Biacore. Data Brief. 2016 May 4;7:1696-1699

16. Nguyen HH, Park J, Kang S, Kim M. Surface plasmon resonance: a versatile technique for biosensor applications. Sensors (Basel). 2015 May5;15(5):10481-510.

17. Evans, S.V.; Roger MacKenzie, C. Characterization of protein-glycolipid recognition at the membrane bilayer. J. Mol. Recognit. 1999, 12, 155–168.

18. Pattnaik P. Surface plasmon resonance: applications in understanding receptor-ligand interaction. Appl Biochem Biotechnol. 2005 Aug;126(2):79-92.Review

19. Wegner GJ, Wark AW, Lee HJ, Codner E, Saeki T, Fang S, Corn RM. Real-time surface plasmon resonance imaging measurements for the multiplexed determination of protein adsorption/desorption kinetics and surface enzymatic reactions on peptide microarrays. Anal Chem. 2004 Oct 1;76(19):5677-84

20. Sibille, P.; Strosberg, A.D. A FIV epitope defined by a phage peptide library screened with a monoclonal anti-FIV antibody. Immunol. Lett. 1997, 59, 133–137

21. Kim, M.; Jung, S.O.; Park, K.; Jeong, E.-J.; Joung, H.-A.; Kim, T.-H.; Seol, D.-W.; Chung, B.H.Detection of Bax protein conformational change using a surface plasmon resonance imaging-based antibody chip. Biochem. Biophys. Res. Commun. 2005, 338, 1834–1838.

22. Cs´aki, A., Schr¨oder,K.,Willsch, R., Bartelt,H. et al., Plasmonic nanoparticles for optical biosensing, SPIE Photonics, Prague 2011.

23. Cs´aki, A., Berg, S., Jahr, N., Leiterer, C. et al., Plasmonic nanoparticles—Noble material for sensoric applications, in:Chow, P. E. (Ed.), Gold Nanoparticles: Properties, Characterization and Fabrication, Nova Science Publishers, Hauppauge,NY, 2010, pp. 245–261.

24. Canovi M, Lucchetti J, Stravalaci M, Re F, Moscatelli D, Bigini P, Salmona M, Gobbi M. Applications of surface plasmon resonance (SPR) for the characterization of

nanoparticles developed for biomedical purposes. Sensors (Basel). 2012 Nov 27; 12(12):16420-32.

25. Smith EA, Corn RM. Surface plasmon resonance imaging as a tool to monitor biomolecular interactions in an array based format. Appl Spectrosc. 2003 Nov; 57(11):320A-332A. Review.

26. Steiner G. Surface plasmon resonance imaging. Anal Bioanal Chem. 2004 Jun;379(3):328-31

27. Hiragun T, Yanase Y, Kose K, Kawaguchi T, Uchida K, Tanaka S, Hide M. Surface plasmon resonance-biosensor detects the diversity of responses against epidermal growth factor in various carcinoma cell lines. Biosens Bioelectron. 2012 Feb15; 32(1):202-7.

28. Liu C, Lei T, Ino K, Matsue T, Tao N, Li CZ. Real-time monitoring biomarker expression of carcinoma cells by surface plasmon resonance biosensors. Chem Commun (Camb). 2012 Oct 28;48(84):10389-9

29. Zybin A, Kuritsyn YA, Gurevich EL, Temchura VV, Überla K, et al. (2010) Real-time detection of single immobilized nanoparticles by surface plasmon resonance imaging. Plasmonics 5: 31-35.

30. http://www.cytodiagnostics.com/store/pc/Gold-NanoUrchins-c214.html.

31. Park TJ, Lee SJ, Kim D-K, Heo NS, Park JY, Lee SY. Development of label-free optical diagnosis for sensitive detection of influenza virus with genetically engineered fusion protein.Talanta2012; 89:246-52.

32. Chang Y-F, Wang S-F, Huang JC, Su L-C, Yao L, Li Y-C, et al. Detection of swine-origin influenza A (H1N1) viruses using a localized surface Plasmon coupled fluorescence fiber-optic sensor.BiosensBioelectron2010;26:1068-73

Chapter 6

Conclusion

This contention presented six chapters that fully transcribe what the study entailed, with chapter one giving a brief introduction of the study by stating the problem in HIV-1 diagnosis and treatment challenges and reasons why the study needs to be explored. Furthermore, it also introduced the two major laser based technologies namely: surface plasmon resonance (SPR) and laser enhanced drug delivery using femtosecond laser pulses; used in the study by giving a brief overview of each technique and displaying their potential that can possibly assist in addressing HIV-1 diagnosis and treatment challenges.

Chapter 2 focused on displaying the laser light properties with the emphasises towards its employment on tissue interactions which is relevant to the current study. This interaction of lasers and tissues was outlined using the concept of photoporation in section 2.2.6. An optical setup was built using a 800 nm Titanium Sapphire laser with an optical train that takes the beam with peak powers that can precisely disrupt the cell plasma membrane, in order to allow immediate transportation and expression of exogenous matter into live mammalian cells, in this case the cells were already infected with HIV-1 and the exogenous matter was the ARVs. To avoid damage to the cells, minimal powers of 4µW with 10 ms laser cell exposure time were used to porate the cells. After laser treatment of the cells, the employment of the biological assays to evaluate cellular responses such as cell viability, toxicity and viral inhibition were explored. Finally, the exploration results from cellular responses gave a certainty that there was potential in the use of fs laser pulses in promoting targeted optical drug delivery of ARVs into HIV-1 infected TZM-bl cells and that laser enhanced drug delivery system efficiently reduces HIV-1 viral infectivity in-vitro. With the absence of a cure and a known active potential vaccine with feasible outcomes, not much has been documented on laser based drug delivery of HIV-1. However from the exploration of this study, it was demonstrated and can be concluded for the first time that laser enhance drug delivery using ARVs that target all the life stages of the HIV-1 cycle is efficient in the significant reduction of HIV-1 infection. Further efforts will involve the integration of an endoscope-like optical fibre to this optical drug delivery system for *in vivo* applications.

In chapter 3, the aim of the study was to develop and characterise the surface plasmon resonance system. A brief history of SPR was outlined as to give insight and understanding to where the technique originated. Following that, the principles that govern the SPR technique were transcribed together with its different sensor configuration methodologies. Subsequently, governed by the different geometry and applications described in section 3.4., a SPR system was built according to the Kretschmanns configuration with a 640 nm continuous wave coherent cube laser with an output power of 60 mW and portrayed. All the basic essential components that are needed to have a performing SPR sensor system were described in detail and incorporated in the custom made SPR system according to their specific functions. To get excitation of plasmons on the metal surface in order to create surface plasmon waves, a 640 nm continuous wave laser was used specifically with the knowledge of its capability of being able to create these plasmon waves with gold as the metal surface of choice. To test the performance of the SPR system, three materials namely: the prism, the uncoated glass slide and the gold coated slide were explored. Due to the fact that the three materials have different refractive indexes, angular measurements were explored. To avoid discrepancies in the angular measurements, the three materials were cleaned thoroughly before measurements were performed. The results obtained showed that each material had its own refractive index changes per angle measured and the shift in the resonance of the three materials was not the same. The noticed, drops in the resonance dips to nearly zero that signals excitation beam energy transfers to surface plasmon waves proved that there was plasmon excitation and highlighted that the angular measurements taken were indeed accurate. Nonetheless, it was also noted that using the gold coated slide, there was reflections shifts; this means that the gold was neither damaged nor rough, and also indicated that there were wave propagation on the metal surface. Given these observation, it could be concluded that the system could accurately determine angular position of the prism, the uncoated glass slide and gold coated slide and that the plasmon excitation is highly dependent on the material of excitation. Coupling of the surface plasmon wave with the gold metal surface as metal of choice, showed a strong resonance shift in the visible region. Lastly, the study demonstrated that the custom made SPR system based on the Kretchmanns configuration could excite plasmon resonance for sensing applications that were explored in chapters 4 and 5.

Chapter 4 focused on the growth and characterisation of gold thin film layers for SPR setup using the electron beam evaporation system. Structural, morphological and optical properties of gold thin film layer deposited on glass substrates using an electron beam evaporation

technique were explored. Firstly, a brief summary of gold and its properties were outlined. Then, a detailed description of the e-beam as the deposition growth technique was portrayed followed by the characterisation techniques that are used to characterise growth of thin films. To avoid uneven surface and roughness on the slides, the slides were thoroughly cleaned out using ethanol and nitrogen gas was used to blow dry and remove any excess dirt left. Following deposition using the e-beam, first the 5 nm layer of titanium was deposited, in order to enhance the attachment of the gold on the glass slide. This layer allows for smoother and waveguides passing through without changing the characteristics of the structure. Following this, the deposition of gold was added done onto the adhesion layer. X-ray diffraction was used to explore the structural morphology in a form of phase identification. This was also done to confirm the purity of the gold coated on the films. The acquired data confirmed that gold was deposited on the surface of the film, this was given by the crystalline structure of a peak diffraction pattern of (111), determining the face cubic lattice of crystalline metal of gold. Without further delays, the same coated films were explored using scanning electron microscope (SEM) to study the uniform homogenous distribution of the gold on the film surface. Depending on the different magnification employed on the film, there was a smooth uniform homogenous distribution of gold with continuous structures. Since the vacuum nature provides an environment of free impurities and contamination, the films portrayed continuous structures with more atoms clustering together depending on the layer thickness. Finally, to determine which thickness layer to use for sensing applications, the optical properties of the films were explored using absorption and transmission spectroscopy. With transmittance, it was validated that the more the thickness of the film the less transmittance of will be noted at the visible range. In addition, it was evident that peak transmittance was at approximately 500 nm. Meanwhile the exploration of the absorption spectroscopy portrayed that the 40 nm thickness layer had absorption peaks at 560 nm. This observation corresponded with what has been documented in literature. However, it is known that as the thickness becomes greater, the absorption band becomes broad. Thus, wider size particle distribution. As metal thickness is the most important objective that characterise a performing SPR transducer, gold thickness film plays a crucial role in increasing the changes in the refractive index. The SPR sensing system was used to explore signalling using the different thickness layers.

With the 5 nm, the size and distribution of the gold on the surface of the film showed it to be less effective and translated it as less conductive for the applications the study had aimed to achieve. The same was observed with the 20 nm thickness layer. While with the thickness of 40 nm, the drop in the intensity to almost zero supports what was obtained in chapter 3 that

there is a good indicator that there is excitation of plasmons on the metal surface that causes plasmon waves. These waves on the surface are considered enough to facilitate the interaction between molecules that bound on the surface of the metal. Given this observations it was evident to determine that 40 nm is ideal thickness layer for conducting sensing applications. Therefore, it was concluded that, thin metal films exhibit resonant, SPP-related peaks (dips) at specific wavelength. In addition, that gold is a good conductor of electrons that are capable of resonating with light at a suitable wavelength. Generally, gold is resistant to oxidation and other chemical reactions, which makes it a very eligible candidate for SPR sensing applications. Furthermore, the metal thickness of the gold plays a vital role in the excitation of surface plasmons, which is very crucial for SPR applications.

Lastly, in chapter 5, immobilization of biomolecules was achieved by using the gold thin film of 40 nm described in chapter 4. Firstly, bioconjugation of nanoparticle to antibodies was explored following an optimised protocol described in appendix A. Following this protocol with different steps altered to suit these applications different from the protocol of functionalisation described by Zuppella *et al.,* 2015 [1]. Structural morphology was explored using SEM, while UV-vis absorption spectrograph was explored to confirm the bioconjugation of the antibodies to nanoparticles. The results obtained of the conjugation of antibodies and nanoparticles confirmed that there was self-assembly monolayer on the surface of the sensor chips. Angular and spectral measurements before and after conjugation showed that the protocol used for conjugation was efficient for bioconjugation of antibodies to nanoparticles structural morphology using the SEM demonstrated that there was successful bioconjugation of antibodies and nanoparticles supporting the results obtained during UV-vis spectroscopy. Furthermore, the ideal thickness of 40 nm layer to use for SPR sensing applications was supported by the data obtained in a form of SPR shift curves that were observed during angular measurement confirming that there was surface plasmon excitation on the sensor surface. Given all this results, it can be concluded that the protocol used was efficient for covalently attaching antibodies to nanoparticles, known as bioconjugation. Additionally, that the SPR sensing system was able to detect biological analytes (antibodies conjugated to nanoparticles)

Following this, the employment of the altered bioconjugation protocol also successfully demonstrated for the first time in the conjugation of HIV-1 virus with nanoparticles on the sensor chips. Different concentrations of the virus bound to the metal surface were explored. The data obtained showed that there were changes in shifts in the resonance angle due to the

changes in the refractive index. These changes are cause by the specific binding interactions between the virus and the recognition event which is the antibody bound on the surface of the metal surface. Gold nanoparticles enhances the SPR signal, this is translated as the sensitivity of the SPR system. The observed changes in the resonance SPR shift curves, when using different concentrations of the virus portrayed that the SPR system was sensitive and was able to detect HIV-1 and the lowest concentration detected was 75 pg/ml. Based on what was observed in the structural morphology using SEM and the changes in the resonance by shifts in the SPR curves, it was evident that the SPR system can detect HIV-1. AuNP have great optical properties and allows improved detection of biological interactions. With SPR, the size and the metal thickness play a crucial role at the metal surface. Therefore, it can be concluded that the custom made SPR sensing system in this study was able to detect biological analytes for SPR biosensing applications and also for the first time facilitate the label free detection of HV-1 and its various concentrations for possible point of care applications.

Future aspects for this study will involve incorporating an imaging techniques that will display the label-free detection of the HIV-1 and its various concentrations in real-time. It will also focus on fibres nanoplasmonics that will involve a flow cell to facilitate a multiplex channel for the binding interactions in real time. And finally, lead to a compactible HIV-1 viral load detection laser based device using smartphones, which will help in treatment monitoring of the disease in poor resource limited settings.

Finally, as stated in the beginning of the thesis, there is growing need for developing an HIV point of care (POC) diagnostic tool that is label-free, highly specific and sensitive as well as therapeutic modification therapies which can be used to address the HIV-1 pandemic. The exploration of laser-based technologies such as the treatment of cells using light and the detections of diseases has shown great potential in attempting to address these challenges. Therefore , there's a need to further engage in these laser based technologies to give an insight into the therapeutic healing of the cells by minimising the side effects of orally administered ARVs and by designing and developing an HIV POC detection diagnostic tool that can be applied in resource limited settings.

Appendix

The modified Functionalisation method used for bioconjugation of biological analytes on the gold sensor chips **.**

- Glass substrates coated with 5nm titanium adhesion layer and 40nm gold (Au) by electron beam evaporation were used a sensor chips.
- The chips were cleaned by rinsing in ethanol and ultrapure water and dried under nitrogen flux.
- The chips were functionalized with poly (ethylene glycol) (PEG) 2-mercaptoethyl ether acid by 24 hour immersion.

  ***PEG acts a polymer to antibodies to improve binding efficiency.**
- After 24 hour immersion the chips were rinsed with ultrapure water and blow dried with nitrogen flux.

  ***Nitrogen gas is used to displace oxygen.**
- Prior adding the primary antibody, N-hydroxy succinimide (NHS) and 1-Ethyl-3-(3-Dimethylaminopropyl) carbodiimide (EDC) with the same molar ratio was added to activate the surface of the chip for 10 minutes.

  ***NHS-EDC covalently couples the amine group of the molecule to the surface by binding the amid ether antibodies to the surface of the chip.**
- The surface was rinsed with ultrapure water and blow dries with nitrogen flux, then primary antibody (Mouse IgG antibody) diluted in phosphate buffer saline was added to the surface and incubated for 18hours.
- A cocktail mixture containing (NHS-EDC-SH-PEG-COOH-NAOH-DH_2O) adjusted to pH 7.4 using 10X phosphate buffer saline was added in a 2ml Eppendorf tube and shaken for 1 hour protected from light.
- After 1 hour incubation the secondary antibody (anti-Goat IgG) was added to the mixture cocktail and shaken for 2 hours protected from light.
- After 2 hours, the solution was filtered with a 50kDA filter following manufactures instructions, to remove any by-products. Briefly: the solution was transferred into the filter and spin down for 10minutes at 14000g. The liquid was discarded in the tube. The antibody is bound to the filter. The filters was washed twice with 1XPBS and spin down

for 10mins.after the second wash, the filter was inverted in a clean collection tube and spin down for 10 minutes.

- After filtration, 12µl of the solution (SH-PEG-IgG) was added to gold nanoparticles (AuNPs)(urchins) and incubated in a shaker for 1 hour protected from light to form AuNP-IgG conjugate.
- After 18 hours, the chip functionalised with the primary antibody (mouse IgG antibody) was rinsed and blow dried with nitrogen.
- The AuNP-IgG conjugate was added to the chip functionalised with the primary antibody (mouse IgG antibody) and incubated for 1 hour before characterisation with SEM and SPR.